Upgrading of crude lipid pyrolysis liquid product into drop-in hydrocarbon fuel

by

Samuel Koranteng

A thesis submitted in partial fulfillment of the requirements for the degree of

Master of Science

in

Bioresource Technology

Department of Agricultural, Food and Nutritional Science

University of Alberta

Abstract

The use of fatty acid feedstock to produce renewable fuel and value-added chemicals has recently gained a lot of attention. Pyrolysis has been used in fatty acids conversion to yield products with fuel characteristics like fossil fuel equivalent. However, the conventional heating at commercial scale is done through the walls of the reactor, placing limits on how fast the commercial reactors can heat up, in the fatty acids pyrolysis conversion process. In addition, the crude pyrolysis liquid product generated may contain residual fatty acids, which may require some level of upgrading process to make it compatible with the existing fossil fuel infrastructure, hence impacting the operational cost.

The first objective of this thesis involved incorporation of microwave-assisted heating to pyrolyze model fatty acid, focusing on the heating rate and deoxygenation reaction. Stearic and oleic acid were pyrolyzed with silicon carbide (SiC) as heating aid in a microwave reactor at 430 ˚C for 1 hour under N_2 at an initial pressure of 100 psi (689 kPa). The results showed that the set reaction temperature was successfully achieved within one minute in the stearic acid run, while in the case of the oleic acid run, the set temperature was not reached throughout the reaction time. The gas product consisted of deoxygenation products as well as light hydrocarbons, predominantly C_1-C_3. On the other hand, the liquid product consisted of aromatic compounds as the main product, although the conversion was low. The predominance of aromatic compounds pointed to the presence of hotspots or a lack of uniform heating, which was confirmed using a thermal paper.

The second study investigated the catalytic effect of a stainless-steel mesh on oleic acid pyrolysis, focusing on liquid product yield and composition. Oleic acid pyrolysis was conducted in a 15 mL microreactor at 430 ˚C for 2 hours under N_2, starting at atmospheric pressure. The stainless-steel mesh was thermally and chemically treated. The gas, liquid, and solid product yield

varied between 9.2 – 11.7 wt. %, 82.4 – 85.5 wt.%, and 5.3 – 5.9 wt. % respectively. The liquid analysis revealed alkanes with carbon numbers ranging from C_6 to C_{19} and residual fatty acids with carbon numbers C_6 - C_{18}. The results revealed no significant catalytic effect of the stainless-steel mesh and the microreactor material on the liquid yield and composition.

The third study focused on incorporating deoxygenation catalysts to remove residual fatty acids in crude pyrolysis liquid product. The crude pyrolysis liquid product was treated with 65 wt.% loading of nickel on silica-alumina, 1 wt.% loading of platinum on silica, silica support, and silica-alumina support catalysts in a 15 mL microreactor at 350 ˚C for 0.5 – 2 hours under N_2 at atmospheric pressure. The results revealed that the nickel on silica-alumina catalyst at 2 hours treatment resulted in complete deoxygenation of residual fatty acids in the crude pyrolysis liquid product, whereas the other catalyst and supports tested still contained acids under similar conditions.

The final study focused on the scale-up of the catalytic deoxygenation using the nickel on silica-alumina catalyst in a continuously stirred 1 L batch reactor at 300 ˚C and 350 ˚C for 1.5 hours under N_2 at atmospheric pressure. Deoxygenation was complete in the fresh nickel catalyst at 300 ˚C and 350 ˚C treatment, whereas the regenerated nickel catalyst at 300 ˚C treatment did not result in complete deoxygenation of residual fatty acid. This study demonstrated the feasibility of scaling up the deoxygenation work using nickel on silica-alumina catalyst.

Overall, the preliminary data from the microwave study revealed some critical concerns of the microwave technology as the fatty acids feedstock did not absorb the microwave energy and the heating aid used to absorb the microwave generated hotspot in the reactor thus, influencing the formation of aromatic compounds and incomplete fatty acids conversion. Nevertheless, further investigations are required to improve the uniformity of heating in the reactor to successfully

incorporate microwave-assisted heating into the existing fatty acid conversion technology. Secondly, the thesis revealed the successful incorporation of a less expensive deoxygenation catalyst to remove residual fatty acids in the crude pyrolysis liquid product to yield liquid hydrocarbon fuel.

Preface

This dissertation is an original work by Samuel Koranteng. No part of this dissertation has been published. The experimental methodologies spelt out in this thesis were discussed in detail and approved by Dr. David C. Bressler, Dr. Justice Asomaning, and Dr. Michael Chae. The experiments were conducted in Dr. Bressler's Biorefining Conversions and Fermentation laboratory at the Department of Agriculture, Food and Nutritional Science at the University of Alberta. Brunauer-Emmet-Teller (BET) analysis for the catalyst's physical characterization was conducted at the NanoFab laboratory of the Faculty of Engineering. Dr. Justice Asomaning contributed to the thesis revisions and edits.

Acknowledgements

With a heart full of gratitude, I would like to say a big thanks to my supervisor, Dr. David C. Bressler, for this great opportunity to further my studies under his supervision and mentorship. Thanks, Dave, for your support in making me a better researcher and improving my presentation skills. I also want to thank Dr. Roopesh Mohandas Syamaladevi for being part of my supervisory committee and his valuable feedback and advice during my Master's degree program. A special thanks to Dr. Samir H. Mushrif for being my external examiner and Dr. Jonathan Curtis for accepting to be my exams chair.

My sincere appreciation goes to the two program managers in the Bressler laboratory, Dr. Justice Asomaning and Dr. Michael Chae, for their support, feedback, and thesis editing. Thank you, Dr. Justice Asomaning, for training me on the microwave project. I would also thank Dr. Nancy Zhang of the NanoFab facility for her technical assistance on the catalyst's characterization analysis.

This project was successful because of the able support from our funders, Forge Hydrocarbon Inc., Alberta Innovates, and the Natural Sciences and Engineering Research Council of Canada (NSERC). I would like to say a big thank you for your support in making this project possible.

My appreciation goes to Mr. Jingui Lan for his assistance in training on the use of analytical instruments. I want to say thank you to the wonderful lab mates in the 2-38 graduate office for their support and encouragement to help me get to this stage of my academic ladder.

Thanks to my parents, siblings and friends for their love and support throughout my master's degree program. I love you.

Table of Contents

List of Tables

List of Figures

List of abbreviations

ANOVA = Analysis of Variance

BET = Brunauer-Emmet-Teller

BJH = Barret-Joyner- Halenda

CO_2 = Carbon dioxide

CO = Carbon monoxide

EIA = U.S. Energy Information Administration

EI = Electron ionization

FID = Flame ionization detector

FTIR = Fourier transform infrared spectrometry

g = grams

GC-FID = gas chromatography coupled with Flame ionization detector

GC-TCD = gas chromatography coupled with Thermal conductivity detector

GC-MS = gas chromatography coupled with mass spectrometry detector

h = Hour

min = Minutes

mL = Milliliters

$Ni/SiO_2/AL_2O_3$ = Nickel on silica-alumina

SiO_2/AL_2O_3 = Silica-alumina

SiO_2 = Silica

Pt/SiO_2 = Platinum on silica

µL = Micro liter

Chapter 1

1.0 Introduction

The increase in industrialization and expansion of human habitation have resulted in higher global energy demand. The majority of the world's energy demand is derived from fossil fuels such as crude oil, coal, and natural gas (EIA, 2020). Crude oil is the most utilized energy source in the transportation sector to power automobiles, heating buildings, and generating electricity (EIA, 2020). Coal is used as an energy source to generate electricity for domestic and industrial applications (World Coal Association, 2016). Natural gas has been an energy source for generating heat and electricity for commercial and residential purposes (EIA, 2020). However, these resources are finite reserves, and their continuous use will result in ongoing depletion, thereby making them unable to meet the growing energy demand globally. Also, the utilization of fossil fuel resources has been linked to environmental concerns such as the global warming effect (Taufiqurrahmi and Bhatia, 2011). As a result of these issues associated with fossil fuel use, substantial research and development to utilize renewable alternatives have been made over the last decades.

Several alternatives and renewable energy sources, such as solar, hydro, wind, and biomass energy, are continuously undergoing development to substitute and augment the use of fossil fuels (Ong et al., 2011; Sorrell et al., 2010). Among the various sources of alternative energies, biomass has been considered the only renewable energy source for generating liquid, gaseous, and solid fuels (Bridgwater 2003; K. D. Maher and Bressler 2007; Xu et al., 2018a). A report released by IEA in 2018 noted that 9.3 % of the world's primary energy supply is derived from biomass, which has a significant contribution across the energy systems, particularly in the heat and the transport sector. The report also revealed that about 4.5 % of the world's primary energy supply is obtained from other renewable energy sources such as hydro, solar, and wind.

Biomass is a term broadly used to describe materials with organic origin and can be derived from living or recently living organisms (K. D. Maher and Bressler 2007; Pande and Bhaskarwar 2012; Xu et al., 2018b). As an energy source, biomass can be either utilized directly by burning to produce heat or indirectly undergo a biorefining conversion to generate various fuels and other valuable co-products. Additionally, biomass as an energy source can improve the economic value for the agricultural and forestry sectors as products from this industry will play a vital role in generating renewable energy (Asomaning et al., 2014b).

In biorefinery systems, several conversion processes have been employed to convert biomass feedstock into marketable products such as fuels, chemicals, other high-value co-product. The biomass conversion processes can broadly be classified as thermochemical and biochemical processes (Balat et al., 2009; Sharma et al., 2015; Cherubini et al., 2009).

1.1 Biomass conversion technologies

Biochemical conversion processes involve utilizing microorganisms and/or enzymes to convert biomass into products that can be utilized for energy generation and other valuable co-products. Examples of biochemical conversion processes include fermentation, anaerobic digestion, anaerobic conversion, and enzymatic processes (Cherubini et al., 2009; IEA, 2011). Among the numerous biochemical conversion processes, fermentation has been used to produce bioethanol to serve as an automotive fuel. In this process, lignocellulosic biomass is hydrolyzed to release simple sugars using acids or enzymes, or the direct utilization of starch and sugar-based feedstock such as corn and sugarcane, and with the incorporation of yeast, the sugar generated gets converted into bioethanol and other co-products (IEA 2011; Wang et al., 2020).

Thermochemical conversion processes are considered some of the most common and accessible methods employed in harnessing energy from biomass. In these processes, the biomass

feedstock is treated at high temperature and pressure, with or without catalysts, to yield solid, liquid, and gaseous products. There are several thermochemical conversion processes employed in biomass conversion to generate fuel and other co-products: this includes combustion, pyrolysis, gasification, and hydrothermal liquefaction (IEA, 2011; Balat et al., 2009).

Among the various thermochemical conversion processes to convert biomass feedstock into fuel and intermediates, this thesis dealt with pyrolysis as a promising conversion process to convert biomass into solid, liquid, and gas products. There are several process parameters such as heating rate, residence time, and nature of the biomass feed that may affect the yield and quality of the pyrolysis products (Asomaning et al., 2014a; Dunn, 2010; Maher et al., 2007; McKendry, 2002; Snare et al., 2005). Biomass conversion via pyrolysis process occurs at elevated temperatures under an inert atmosphere, with or without a catalyst to yield different pyrolysis products, as shown in **Figure 1**. The pyrolysis conversion process can be classified as slow and fast pyrolysis. The reaction temperature and heating rate are the key parameters that can be used to differentiate slow and fast pyrolysis. In the slow pyrolysis process, the biomass conversion occurs at a lower temperature between 300 ˚C to 700 ˚C, for long residence time (mostly minutes to hours) and at a lower heating rate of 0.1 to 10 ˚C (Ng et al., 2020). In the literature, slow pyrolysis process has widely been employed in converting lignocellulosic biomass to maximize the yield of biochar compared to the gaseous and liquid product yield (S and P, 2019; Bridgwater, 2003).

Several efforts in research and development have employed fast pyrolysis to increase the liquid product from the biomass conversion. In this process, the biomass is rapidly heated at 600 - 1000 ˚C, for short residence time (0.5 -5 seconds), and at a faster heating rate >10 ˚C/min, which

favors the yield of liquid product compared to other products (Bridgwater, 2012; Ng et al., 2020; Greenhalf et al., 2013; Mullen & Boateng, 2011).

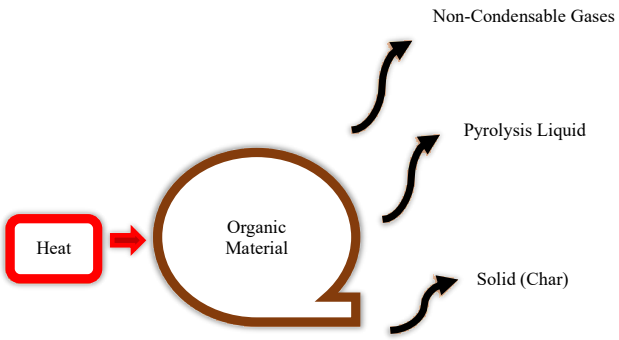

Figure 1. Pyrolysis reaction conversion. Pyrolysis of biomass (organic) materials to yield different pyrolysis products.

Previous work at the Bressler laboratory has demonstrated the pyrolytic conversion of model fatty acids such as stearic acid and oleic acid to yield hydrocarbon fuel precursors. A complex sequence of reactions that involves deoxygenation and cracking at certain conditions have been reported in the literature (Asomaning et al., 2014b; Maher et al., 2008; Omidghane et al., 2017a). However, the liquid product generated from the pyrolysis of fatty acids may have high acid numbers because of the presence of residual fatty acids. If not removed, these can corrode metal parts in storage tanks and transportation equipment, leading to low compatibility with conventional petroleum infrastructures (Asomaning et al., 2014b; Azuara et al., 2016; Huang et al., 2010). In order to improve the liquid product compatibility, it is necessary to upgrade or remove acids to enhance its direct utilization in automobiles.

Several upgrading techniques have been explored in literature, such as caustic wash to neutralize the residual fatty acids in the crude pyrolytic liquid product (Kumar et al., 2014) and the use of deoxygenation catalysts to convert residual fatty acid in the crude pyrolysis liquid to

hydrocarbons (Cheng, 2017; Crawford et al., 2020; Santillan-Jimenez et al., 2014; Shimada et al., 2017). Both techniques improve the chemical and physical properties of the crude pyrolytic product that in turn serves as a drop-in hydrocarbon fuel. Among the upgrading methods mentioned above, the application of catalysts has proven to be a promising technique for improving the liquid fuel quality generated from pyrolysis (Crawford et al., 2020). The caustic wash tends to generate large volumes of wastewater, and form an emulsion that can result in incomplete separation (Wu et al., 2019).

In this thesis, two methods are proposed to improve the crude pyrolysis product generated from fatty acids: (1) incorporating microwave-assisted heating to increase the heating rate in the pyrolysis of fatty acids into hydrocarbon fuel; (2) using catalysts to deoxygenate residual fatty acid in the crude pyrolysis liquid product to yield hydrocarbons.

1.2 Microwave technology mechanism and its advantages

Microwave radiation an example of electromagnetic wave, positioned between the radio and infrared frequencies in the electromagnetic spectrum. Microwave is characterized by a frequency range of 300 MHz to 300 GHz and a wavelength of 0.001 to 1 m^{-1}. The two components of microwave radiation are the electric and the magnetic fields. According to the Federal Communication Commission (FCC), specific frequencies (0.433, 0.915, 2.54, 4.0, and 5.8 GHz) have been allocated specifically for industrial, scientific, and medical (ISM) purposes as they do not interfere with the communication frequencies (Thostenson & Chou, 1999; Hossan and Dutta, 2012).

Depending on the electrodynamic properties, materials behave differently under microwave radiation. Three categories of materials have been classified based on their interaction with microwave (Thostenson & Chou, 1999; Hossan & Dutta, 2012; Mutyala et al., 2010).

(1) Absorptive materials directly absorb microwave energy to generate heat, e.g., water, silicon carbide, methanol.

(2) Transparent materials do not absorb microwave but allow the wave to pass through it. e.g., glass, Teflon®

(3) Reflective materials bounce off the microwave as they interact. e.g., metals.

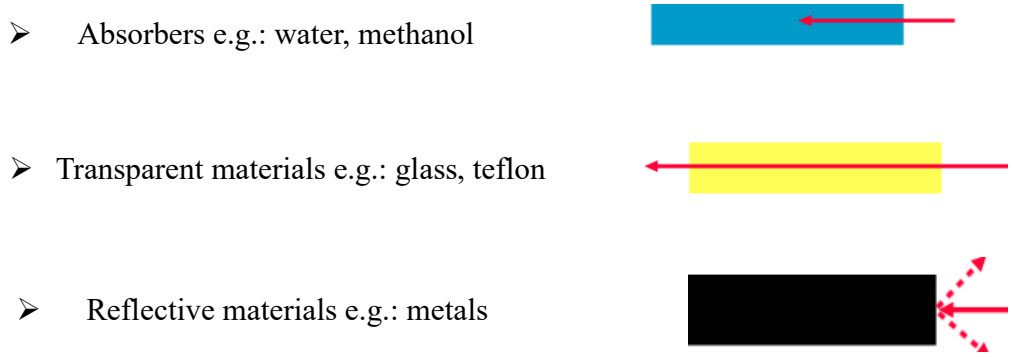

Figure 1.1. Microwave – material interaction. Different microwave and material interactions.

Microwaves have traditionally been employed in the rapid heating of polar solutions. This application has allowed microwave-assisted heating to be widely investigated in the pyrolysis of lignocellulosic and fatty acids with microwave absorbers as heating aids, yielding renewable fuel, and finding success (Mohamed, Kim, Ellis, & Bi, 2016; Pianroj, Jumrat, Werapun, Karrila, & Tongurai, 2016). Microwave dielectric heating possesses several advantages over conventional heating. These include (1) rapid response to start and shut down of the magnetron, (2) selective form of heating, (3) volumetric heating (Asomaning et al., 2018; Haque, 1999). With all the merits associated with the use of microwave, incorporating it as an alternative source of heating in the pyrolysis of lipids can improve the heating rate to enhance the fatty acid conversion to generate hydrocarbon fuel.

1.3 Catalytic upgrading of crude pyrolysis liquid product

Residual fatty acids in crude pyrolysis liquid product may limit its direct usage in petroleum infrastructures. One way of improving product compatibility with petroleum is to remove these residues. Thus, incorporating deoxygenation catalysts will remove residual fatty acids in crude pyrolysis liquid product to yield liquid hydrocarbon fuel.

Different catalytic metals such as nickel (Ni), nickel-molybdenum (Ni/Mo), ruthenium (Ru), palladium (Pd), palladium-platinum (Pd/Pt), platinum (Pt), iridium (Ir), osmium (Os), and rhodium (Rh), supported on several types of catalytic supports, have been widely studied in various catalytic deoxygenation reactions of fatty acids to yield liquid hydrocarbons (Oi et al., 2020; Santillan-Jimenez et al., 2014; Yang et al., 2015). The nature of the metal catalyst and the support play a significant role in the deoxygenation of fatty acids. For instance, it is reported that metal catalysts such as Rh, Ru, and Ni have a higher affinity toward the production of alkanes; this observation is due to the cleavage of C-O bond rather than C-C bond (Alonso et al., 2010; Naik et al., 2014). The utilization of acidic catalytic support, such as SiO_2/Al_2O_3, has been reported to enhance dehydration and hydrogenation, which increases alkanes (Davda et al., 2005). Therefore, the catalyst support's acidic nature can influence its selectivity for the cleavage of the C-O bond by a dehydration reaction (Wang et al., 2019).

In addition to the nature of catalysts and supports, the reaction gas atmosphere can influence the conversion and the selectivity of the catalyst employed in the deoxygenation reaction. The presence of reactive gas atmospheres such as hydrogen has been reported to enhance decarboxylation at 330 ˚C using heterogeneous Pd and Ni catalysts (Santillan-Jimenez and Crocker, 2012). On the contrary, when an inert gas atmosphere was used, no reaction occurred (Maier et al., 1982). These studies provided evidence on utilizing a reactive gas atmosphere in the

catalytic decarboxylation of fatty acids into hydrocarbons. In addition, the thesis looked at understanding the inert nature of the stainless-steel materials used in making the reactors for fatty acids pyrolysis process.

1.4 Hypotheses

1. Incorporating silicon carbide (SiC) as a heating aid in the reactor cavity will increase the microwave absorption at a given microwave power, thereby speeding up the heating rate to influence the pyrolysis of model fatty acids into liquid hydrocarbon fuel.
2. The use of stainless-steel mesh in the thermal pyrolysis of oleic acid will catalytically influence the product distribution and liquid product composition.
3. Increasing reaction time in the incorporation of platinum on silica and nickel on silica-alumina catalysts will influence the remove residual fatty acid in a crude liquid product to yield liquid hydrocarbon fuel.

1.5 Objectives

The overall objective of this research seeks to develop an efficient method to improve the conversion of fatty acids into drop-in hydrocarbon fuel and potential platform chemicals. The thesis specific objectives are as follows:

1. To study the incorporation of microwave-assisted heating to speed up the heating rate in the pyrolysis of fatty acids into hydrocarbon fuel.
2. To study the catalytic effect of a stainless-steel mesh on the oleic acid pyrolysis focusing on product distribution and liquid composition.
3. To investigate the effect of incorporating catalysts in the upgrading process of a crude pyrolysis liquid product to yield liquid hydrocarbon fuel.

Chapter 2

2.0 Literature review

2.1 The push for renewable alternative fuel

The world's energy demand since the industrial revolution era has seen an increasing trend and is projected to rise in the coming years, which is mainly due to the rising standards of living and population growth in the world (Arend et al., 2011; IEA, 2020; Taufiqurrahmi & Bhatia, 2011). Notably, most of the world's energy demands for economic activities such as transportation, producing chemicals, and other valuable products are derived from non-renewable resources in the form of petroleum, natural gas, and coal (EIA, 2016).

The petroleum fraction derived from fossil reserves supplies about 95 % as fuel source used in the transportation sector (Abbaszaadeh et al., 2012; Brown and Huntington, 2013; Khalili et al., 2019; EIA, 2020). It is also used in the chemical industries as raw material to produce valuable products such as solvents, plastics, and polymers (K. D. Maher and Bressler, 2007). A report released by British Petroleum energy in 2019 estimated that global energy demand would increase by 25-35 % in 2040 (BP, 2019). The report pointed out that the demand for renewable energy utilization would increase, as shown in **Figure 2-1,** which will provide a lot of prospects in the renewable energy space.

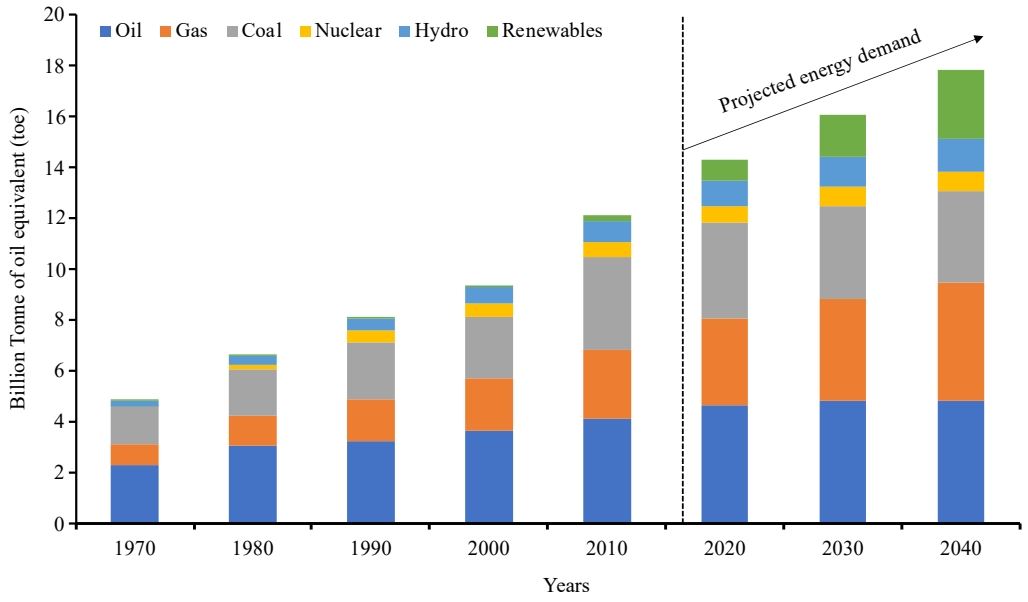

Figure 2-1. The primary energy demand in terms of fuel. The primary energy demand in terms of fuel usage by the year 2040. *Renewable includes solar, wind, hydro, geothermal, and biomass. This figure was produced using data from BP Energy Outlook, 2019.

Despite the benefits of utilizing fossil fuel resources as an energy source, there have been rising concerns about utilizing these resources recently. One of the major issues linked with fossil fuel's constant utilization is that it is a non-renewable reserve, and the continuous usage of these energy sources can lead to the total depletion of these resources (EIA, 2016; Van Gerpen, 2005; Spring, 2014). Also, the combustion of petroleum fuel has been linked to emitting greenhouse gases such as CO_2, CO, and CH_4, creating a greenhouse effect that can result in global warming and climate change (EIA, 2016).

Considering these issues related to the use of petroleum fuel, selecting a fuel source that is renewable and sustainable for socio-economic activities is essential to meet the ever-increasing energy demand. These include solar power, wind, hydropower, geothermal energy, and bioenergy (Asomaning et al., 2014b; Maher et al., 2008; Motasemi & Ani, 2012; K. D. Maher & Bressler,

2007). Among the numerous forms of alternative and renewable energies, bioenergy has generated much interest as it can produce fuel with similar characteristics as fossil-derived fuels (Taufiqurrahmi & Bhatia, 2011).

2.2.1 Biomass feedstock

Biomass feedstock possesses advantages, such as carbon-neutral, renewable, and distributed worldwide, making it suitable for generating fuel and valuable chemicals (Asomaning et al., 2014b; K. D. Maher and Bressler, 2007; Xu et al., 2018b). There are different forms of biomass used in energy generation. For the purpose of this review, biomass can broadly be grouped into three classes, namely: sugars and starches, lignocellulosic, and lipids (fats and oils). These biomass materials can directly be used to generate heat and electricity or indirectly through biorefining conversions to generate different types of fuels. However, using edible crops such as palm oil, soyabean oil, etc., to generate fuel has generated some concerns.

A current solution for this concern is the use of waste feedstock such as yellow and brown grease and crop residues such as lignocellulosic materials to prevent competition with food and land use. (K. D. Maher & Bressler, 2007; Syamsiro et al., 2014; Velghe, Carleer, Yperman, & Schreurs, 2011). The use of lignocellulosic materials, lipids (oils and fats), sugars, and starch as feedstock for fuel generation have widely been documented (Asomaning et al., 2014b; Bridgwater, 2012; Canakci and Van Gerpen, 2001; Christian, 2000; Zhang et al., 2007). Specifically, the utilization of lipids (vegetable oils or animal fats) has shown to be a potential feedstock for fuel production under the right reaction conditions. Hereon, the review focuses on using lipid (fats and oils) feedstock.

2.2.2 Biomass conversion technologies

Several conversion processes, such as biochemical and thermochemical, have been employed in transforming biomass into a value-added product (Sharma et al., 2015). It is worth mentioning that the conversion processes employed are dependent on various factors, one of the most important is the type of biomass used. **Figure 2-2** shows a simplified summary of conversion processes used for converting biomass into valuable products. For the purpose of this review, thermochemical biomass conversion processes will be discussed further in this review.

There are two basic approaches involved in the thermochemical conversion processes of biomass to generate a value-added product. In the first basic approach, the biomass is gasified to produce syngas (CO and H_2), which are subsequently converted to hydrocarbons through Fisher-Tropsch synthesis. The second approach involves the direct conversion of the biomass via pyrolysis and liquefaction to maximize the yield of liquid product. Selecting any of the thermochemical conversion processes depends on the type and quantity of biomass and the desired form of energy needed (Goyal et al., 2008). Pyrolysis is discussed further in this review.

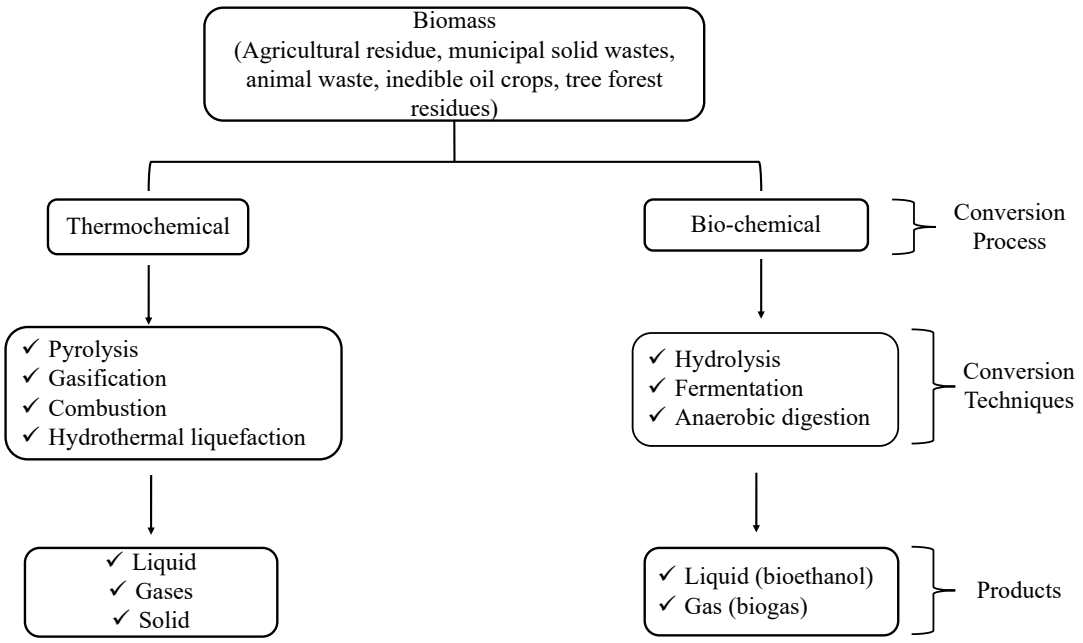

Figure 2-2. Biomass conversion and products. Summary of biomass conversion and the corresponding bio-based products. Reproduced with permission from (Sharma et al., 2015)**.** Minor modification was made.

2.2.3 Pyrolysis of lipid (fats and oils) biomass

The utilization of lipids (fats and oils) as potential feedstock to generate renewable hydrocarbon liquid fuels and other platform chemicals has gained considerable attention. This is mainly attributed to the high energy density, high carbon to hydrogen ratio, high heat content, and the liquid nature of oil, it possesses over other forms of biomass (Maher et al., 2007; Maher et al., 2008; Van Gerpen, 2005).

Triacylglycerols (TAG), the predominant components of lipids, can be directly pyrolyzed to generate gas, solid, and liquid product as fuel sources (Dupain et al., 2007; Lestari et al., 2009; Suarez et al., 2009; Yakub et al., 2015). On the other hand, the TAG can undergo hydrolysis to liberate free fatty acids from the glycerol backbone (Espinosa-Gonzalez et al., 2014). The fatty acids recovered are subsequently pyrolyzed to yield the liquid hydrocarbons (Asomaning et al., 2014c; Hengst et al., 2015; Omidghane et al., 2017; Wang et al., 2012).

2.2.4 Pyrolysis reaction mechanisms

Free radical reactions have been reported as the main reaction mechanism in the pyrolysis of fatty acids to yield liquid hydrocarbons (Maher et al., 2008). The free-radical reaction mechanism consists of initiation, propagation, and termination reactions (Poutsma, 2000). In the initiation reaction, the reactants break into two radicals. These radicals generated are highly reactive and proceed into the propagation step. The propagation step is temperature-dependent and can occur through β-scission or hydrogen abstraction. β-scission is favored at a higher temperature, resulting in breaking the C-C bond to generate radicals, while hydrogen abstraction results in

substrate activation and new radicals. The termination step involves the recombination of two radicals to form stable molecules (Poutsma, 2000).

Deoxygenation is another major reaction pathway involved in fatty acid pyrolysis conversion to yield hydrocarbon fuel. Many researchers have studied the thermal deoxygenation reaction mechanism of fatty acids without the use of a catalyst (Asomaning et al., 2014c; Maher et al., 2008) and with the incorporation of a catalyst (Chang & Wan, 1947; Idem et al., 1997; Lovás et al., 2015; Shimada et al., 2017).

Several approaches have been employed to upgrade pyrolysis liquid products to enhance their utilization in petroleum infrastructures. A notable one is hydrodeoxygenation (HDO), which requires hydrogen utilization to remove oxygen as H_2O. The use of an inert reaction atmosphere in catalytic deoxygenation of lipids has been explored to yield liquid hydrocarbon fuel. For instance, an acidic catalyst such as zeolite has been used in catalytic pyrolysis, to deoxygenate triglycerides to yield carbon monoxide (CO), carbon dioxide (CO_2), H_2O, and hydrocarbon liquid fuel (Kabir & Hameed, 2017).

Shimada et al. (2017) summarized the reaction mechanisms involved in converting triglyceride into hydrocarbon fuel via non-catalytic cracking and catalytic cracking using metal oxide catalyst. As shown in **Figure 2-4,** the triglycerides feedstock initially undergoes thermal conversion through β-elimination to yield two fatty acids, acrolein, and ketene as shown in the reaction path (R1). The ketene generated is unstable and rapidly gets converted via decarbonylation to yield olefins seen in the reaction path (R2). The acrolein product from the reaction path (R1) decomposes to yield propylene in the reaction path (R3). In addition, the acrolein further undergoes Diel-Alder reaction to generate aromatics as seen in the reaction path (R4) and polymerizes to yield coke as seen in the reaction path (5).

As shown in reaction path (R6), the fatty acids produced in the reaction path (R1) undergoes deoxygenation reaction via decarboxylation, yielding hydrocarbons and CO_2. The fatty acids further undergo decarbonylation, generating H_2O, CO, and unsaturated hydrocarbon compounds as seen in the reaction path (R7), similar to findings reported by the following researchers (Asomaning et al., 2014; K. D. Maher & Bressler, 2007). Long-chain hydrocarbon paraffins and olefins generated from reaction path R2, R6, and R7 further get cracked into shorter chain hydrocarbons constituting the liquid fuel observed in reaction path (R11) - (R13), which fall in the gasoline fuel range. Furthermore, cracking of longer-chain hydrocarbons into shorter fractions has been reported in the literature (Asomaning et al., 2014; Dupain et al., 2007; K. D. Maher & Bressler, 2007; Santillan-Jimenez et al., 2013).

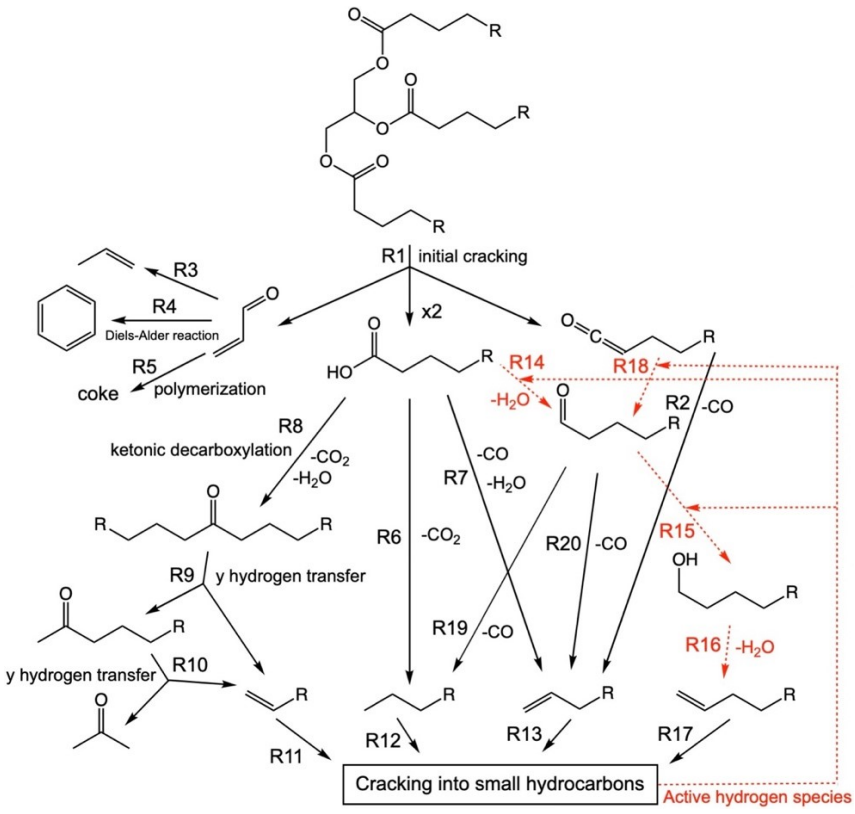

Figure 2-4. Catalytic deoxygenation reaction mechanism of triglycerides. Reused with permission from (Shimada et al., 2017).

The use of conventional heating employed in fatty acids pyrolysis to generate hydrocarbon fuel has widely been studied and has achieved much success. However, the conventional heating at commercial scale is done through the walls of the reactor, placing limits on how fast the commercial reactors can heat up, which, tends to impact the operational process in the pyrolysis of fatty acids to yield hydrocarbon fuel. As a result of this, the use of microwave-assisted heating and heating aid has recently been studied to convert fatty acids into hydrocarbon fuels due to the enormous advantages of microwave heating over conventional heating (Macquarrie et al., 2012). Therefore, this thesis research looked at using microwave-assisted heating in fatty acids pyrolysis to yield hydrocarbon fuel.

2.3 Microwave technology and heating mechanism

Microwave energy is an electromagnetic, which has two components: the electric field and the magnetic field. The electric field plays a fundamental role in heating the sample under microwave irradiation. Materials that have the tendency to absorb and convert microwave energy into heat are termed dielectrics. Hence, microwave heating can be classified as dielectric heating (Khaghanikavkani, 2013; Wang et al., 2016). Dielectric heating of the sample is dependent on the electromagnetic field characteristics and the sample material properties. The main principles involved in dielectric heating are dipole reorientation and conduction (Lam & Chase, 2012). As the microwave energy is continuously emitted into the system, molecules that are microwave absorbing align themselves in the electric field's direction, causing molecules to rotate, collide, and create friction, thus generating heat in the entire material.

In the dielectric reorientation, the electric field from the microwave transmission causes shifting of the π-electrons and atomic nuclei from the equilibrium position, resulting in an induced

dipole. The positive and negative charges within the materials travels in different directions in the electric field created. The dipole molecules continuously rotate and realign in the alternating electric field, which causes an energy transfer from the electric field to the material. As a result, molecular friction occurs, which converts the absorbed electric energy into thermal energy (Nüchter et al., 2004). For proper heat generation in the material under microwave interaction, the following extremes must be avoided: dipoles realigning too rapidly or not have sufficient time to realign in the electric field created. For this reason, 2.45 GHz frequency has been used in commercially available systems, as this frequency allows the dipole molecule enough time to align in the electric field. Also, it lies between these extremes mentioned (Mingos & Baghurst, 1991).

In the conduction mechanism, the transmitting electromagnetic wave generates electric current within electrically conductive material. During this microwave-material interaction, the electrons or ions within the material oscillate as the microwave radiation transmits through the material. As a result, the charged particle in the field collides with neighboring molecules or atoms to generate heat and is transferred to other molecules via conduction. Depending on the material's electrical resistivity, more or less thermal energy can be generated, thus influencing the heat dissipation as the current flows through the material. Kappe et al. (2012) reported that the conductivity principle has a much stronger effect on heat generation capacity than the dipolar rotation mechanism.

2.3.1 Microwave-assisted pyrolysis of biomass to yield hydrocarbon fuel

The application of microwave-assisted heating has been reported in biomass conversion to yield hydrocarbon fuel and other valuable chemical products. A significant number of studies have investigated reaction conditions to convert biomass into value-added products. Feedstocks such as

lipids and lignocellulosic biomass from agricultural and forest residues, and waste origin such as tires, rubbers, etc., have been investigated in microwave-assisted pyrolysis process.

Ravikumar et al. (2017) investigated the used a modified domestic microwave oven to convert different types of biomass into bio-oil. The reaction parameters employed were a frequency of 2.45 GHz, at a power of 0.800 kW, and a temperature range of 400 to 500 ˚C for 10 min. Different feedstocks such as corn cob, corn stover, rice straw, and sawdust were employed in this study. They reported that the bio-oil yield from the corn cob feedstock was the highest, whereas the rice straw was the lowest. The bio-oil yield for all the different feedstocks used was between 15.3–42.1 wt.%. The different compound compositions observed in the liquid products were alkanes, alkenes, and aromatics. The most prevailing compound category was oxygenated compounds such as carboxylic acids and phenols. This data suggests that corn cob is a promising feedstock for the microwave-assisted pyrolysis process to yield more liquid products. However, the oxygenated compound in the liquid product limits the direct utilization of the crude liquid product obtained from microwave-assisted pyrolysis.

To understand the utilization of waste materials as a potential feedstock for microwave-assisted pyrolysis to yield liquid hydrocarbon products, Lin et al. (2012) investigated the utilization of sewage sludges to yield bio-oil. They reported 30.4 % as the maximum liquid product yield from microwave-assisted pyrolysis of sewage sludge. The study revealed the importance of incorporating microwave-assisted heating to convert sewage sludge into liquid hydrocarbon fuel. Capodaglio et al. (2016) employed post anaerobic digestion sewage sludge as feedstock for microwave-assisted pyrolysis in a 3 kW mono-modal microwave and a temperature range of 180 to 650 ˚C for 1-28 min. A biodiesel-like oil product was formed from the microwave-assisted pyrolysis of feed. However, the yield of the product was dependent on the operating conditions

used. Also, this study showed that proper tuning to minimize reflected power in the reactor and the use of a good microwave absorber could improve microwave absorption to generate heat for feedstock conversion into fuels.

Many studies have investigated the use of different heating aids such as solids and liquid to enhance microwave adsorption to generate heat in microwave-assisted pyrolysis. As a result of this, Wang et al. (2016) studied the effect of using glycerol as a heating aid in microwave-assisted pyrolysis of sodium salts of fatty acids. The reaction was carried out using a 2.45 GHz frequency at 2 kW microwave power and a reaction temperature of 500 ˚C. The liquid yield was between 55-70 %, the variation in the liquid yield was attributed to the degree of unsaturation of the feedstock. The main constituent of the bio-oil obtained was deoxygenated hydrocarbons. In addition, the study showed that the bio-oil properties, such as the kinematic viscosity, calorific values, and density, were comparable to fossil-derived diesel.

In a follow-up study, Lam et al. (2017) investigated the effect of using different solid heating aids in microwave-assisted pyrolysis of used frying oil. The heating aids used were activated carbon (AC), particulate carbon (PC), and mesoporous aluminosilicate (MCM-41), mixed separately with the feed at a ratio of 1:1.5. The reaction was carried out on a 2.450 GHz frequency at 800 W microwave power and a reaction temperature range of 350 – 550 ˚C. Among the various heating aid used in the study, the aluminosilicate had a slower heating rate, which required 50–100 min to attain the set temperature. In the carbon-based heating aids, the heating rate was fast, and the time needed to reach the set temperature was less than 35 min. The slower heating rate of aluminosilicate is attributed to lower loss tangent, which indicates the aluminosilicate's low ability to absorb and convert electromagnetic energy into heat. In the case of the PC and AC heating aid, the loss tangent values were high, influencing the microwave

adsorption to attain the set temperature rapidly. The composition of the liquid product was mainly hydrocarbons and with a lower oxygenated compound. The liquid's calorific value was 46 MJ/kg, which is comparable to petroleum-based fuel (Lam et al., 2016). Therefore, this study revealed the importance of knowing the loss tangent value of the heating aid used in the microwave-assisted pyrolysis process.

2.3.2 Pyrolysis Product

Regardless, of the heating source (conventional or microwave) employed in fatty acid pyrolysis process, the following product distributions such as gas, liquid and solid can be obtained. It is important to note that the product distribution is dependent on the reaction or operating conditions. The gas product obtained from pyrolysis is mainly composed of permanent gases, including H_2, CO_2, CO, CH_4, and other light end hydrocarbon gases (Asomaning et al., 2014; Motasemi and Ani, 2012). The solid product obtained from pyrolysis is formed from the polymerization of aromatic compounds to yield polycyclic aromatic hydrocarbons acting as precursors for coke (solid) (Asomaning et al., 2014).

2.3.3 Composition of crude pyrolysis liquid product

The liquid product composition is dependent on the nature of the starting biomass and reaction condition employed. The liquid product obtained from fatty acid pyrolysis is a mixture of different compounds. These include hydrocarbons such as linear and branched alkanes and alkenes, cyclics, and aromatics, as well as oxygenated hydrocarbons such as; acids, ketones, aldehydes, phenolics, and oxygenates existing in the aqueous phase - mostly water (Bridgwater, 2003; Kelly D. Maher et al. 2008; Murnieks et al. 2016). The oxygenated compounds in the liquid product result in negative properties such as corrosion of metal parts, miscibility issues with existing hydrocarbon fuels, low oxidative stability during storage and transportation, high

viscosity, and a high cloud point, thus, limiting the direct utilization of pyrolysis liquid product in existing petroleum infrastructures (Bezergianni et al., 2010; Karim et al., 2011; Mohan et al., 2006; Wan et al., 2009).

Improving the qualities of the crude pyrolysis liquid product through further upgrading or acid removal will enhance the direct utilization of liquid product obtained from fatty acid pyrolysis.

2.4. Catalytic upgrading of pyrolysis liquid product

Catalytic pyrolysis is one of the approaches employed in upgrading pyrolysis crude liquid products. The application of deoxygenation catalysts in the upgrading process results in oxygen removal and improving the quality of the resulting liquid product. The incorporation of deoxygenation catalyst can be done in two ways, including in-situ and ex-situ processes. The in-situ catalyst upgrading process involves the direct mixing of the feedstock with the catalyst in the same reactor. In the ex-situ catalytic pyrolysis process, the feedstock is first pyrolyzed to generate volatile vapour and subsequently passes through a catalyst bed in a different reactor before condensed to liquid product, as shown in **Figure 2-5** (Imran et al., 2018). During catalytic upgrading of pyrolysis liquid product, the reaction occurs on the catalyst's active site to remove oxygen as CO, CO_2, and H_2O.

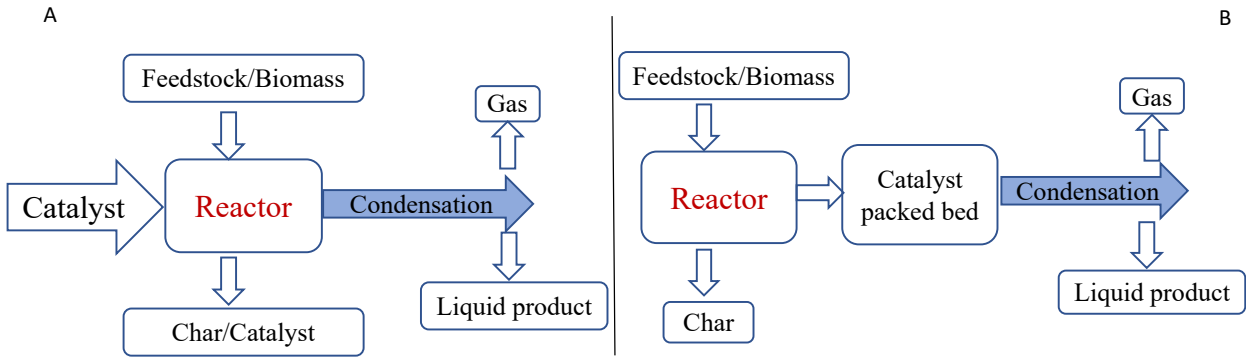

Figure 2-5. Application of catalyst to biomass conversion. The two catalytic pyrolysis reaction pathways employed in the conversion of biomass into liquid hydrocarbon product. (A) the in-situ

catalytic pyrolysis process; (B) ex-situ catalytic pyrolysis process. Reproduced with permission from (Imran et al., 2018). Minor modification was made.

2.4.1 Types of catalyst and application

A catalyst is a chemical compound that changes the reaction pathway and lowers the activation energy, thus accelerating the reaction rate and improving the selectivity of desirable products, as shown in **Figure 2-6**. Catalysts can be classified into a homogeneous and heterogeneous catalysts. In the case of homogeneous catalysis, the reactant and the catalyst are in the same phase. On the other hand, in heterogeneous catalysis, the reactant and the catalyst are in different phases. This type of catalytic reaction only occurs on the interface between the catalyst and the reactants. The heterogeneous catalyst can easily be separated from the product stream, resulting in a continuous chemical reaction. The mechanism of heterogeneous catalysis involves the adsorption of reactants onto the catalyst's active sites, surface reaction of the adsorbed species, and the desorption of product into the reaction atmosphere (Schlögl, 2015). Hereon heterogeneous catalyst is discussed.

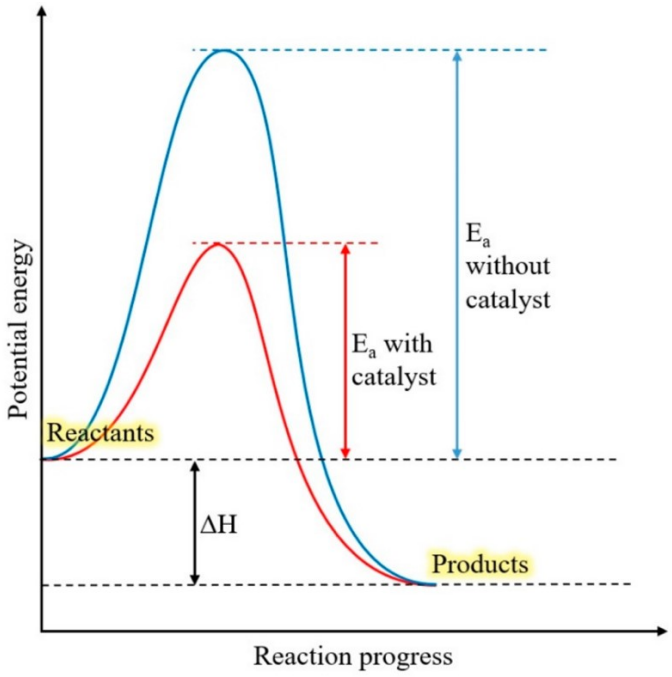

Figure 2-6. Generic energy diagram with and without catalyst. Reused with permission from (Mashuri et al., 2020).

Heterogeneous catalyst has been demonstrated to be a promising catalyst used in upgrading crude pyrolysis liquid products to yield liquid hydrocarbon fuel. The heterogeneous catalyst can be grouped as acid catalysts, including micropore zeolites, mesoporous aluminosilicates, and metal-modified zeolites and base catalysts including MgO, CaO, basic zeolites (Gómez et al., 2013; Tajuddin et al., 2016; Stefanidis et al., 2016). Both acidic and base catalysts have been employed to upgrade crude pyrolysis liquid into hydrocarbon fuels. Different deoxygenation reaction pathways were obtained when either a base or an acid catalyst is used in the upgrading process. In cases where a base catalyst is employed, a higher yield of CO_2 and a lower acid content in the liquid product were observed (Stefanidis et al., 2011).

The use of acid catalysts in fatty acids pyrolysis has been reported to favour dehydration, decarbonylation, cracking, and aromatization reactions (Lappas et al., 2012; Serrano-Ruiz and Dumesic, 2011). The catalyst's acidic nature promotes the rupturing of C-C and C-O bonds (Aho et al., 2013). The silica (SiO_2) catalyst possesses a lower acidity level and medium porosity properties, which removes oxygen and inhibits coke formation on the surface of the catalyst. Acid catalysts have been reported to promote monoaromatic hydrocarbons compound formation such as benzene, toluene, ethylbenzene, and xylene (BTEX) (Liu et al. 2014).

The deposition of a carbonaceous compound on the catalyst surface during the pyrolysis process deactivates the catalyst and lowers the activity and selectivity, resulting in poor performance (Du et al., 2013). The utilization of an acidic catalyst zeolite type ZSM-5 has been reported to result in a high yield of monocyclic aromatic hydrocarbons. However, the catalyst's deactivation was suppressed because the zeolite catalyst had a unique micropore structure and had Bronsted acid

sites (Jae et al., 2011). In addition, employing large surface area catalysts can reduce the deactivation of immediate active acidic sites of the catalyst. As a result of this, Kabir and Hameed (2017) reported that increasing the pressure of hydrogen as the reaction atmosphere gas resulted in saturation of alkene acting as precursors for coke, thus inhibiting coke formation on the surface of the catalyst. Therefore, it is essential to understand the nature of the catalysts and the reaction conditions employed during catalytic deoxygenation of fatty acids to yield hydrocarbon fuel.

2.5 Reaction condition for catalytic upgrading of pyrolysis oil

2.5.1 Effect of temperature on the upgrading of pyrolysis product

As one of the reaction parameters, temperature can influence the catalyst performance, affecting the catalyst's activity and selectivity in the conversion of fatty acids to yield liquid hydrocarbon fuel (Kubičková et al., 2005; Madsen et al., 2011; Snåre et al., 2008). For better activity of a catalyst in a catalytic decarboxylation of fatty acids, the temperature range of 290-380 ˚C has been widely studied in the literature (Popov and Kumar, 2015; Srifa et al., 2014; Zhang et al., 2014).

Temperature alters the catalyst's selectivity by influencing long-chain hydrocarbons cracking and initiating secondary reactions such as cyclization and aromatization (Simakova et al., 2009). These secondary reactions resulting from increasing reaction temperature can reduce the yield of desired products. In addition, Simakova et al. (2009) studied the deoxygenation of palmitic acid over supported Pd catalysts at varying temperatures. They reported a complete conversion of palmitic acid to pentadecane as the main product when the temperature was 300 ˚C and at a reaction time of 110 mins. They also observed a 50 % conversion when the temperature was 260 ˚C at the same reaction time. Despite the complete conversion in the catalytic treatment at a higher temperature, they reported that the conversion of fatty acid was not complete at the same reaction

temperatures in the absence of the catalyst. Therefore, the complete conversion of the fatty acid can be attributed to the presence of the catalyst.

Furthermore, to ascertain the importance of temperature in the catalytic reaction, Yang et al. (2015) studied the deoxygenation of oleic acid over Pt supported on zeolite 5A beads catalyst to yield heptadecane. They reported that reaction temperature influenced the selectivity of catalysts to yield heptadecane as the main product. At 320 ˚C, the catalyst's selectivity to yield heptadecane from oleic acid was 81 %. In a follow-up work, the effect of reaction temperature was studied to understand the yield of heptadecane from oleic acid using a temperature range of 290-335 ˚C (Yang and Carreon, 2017b). The results showed that when the temperature was 290 ˚C, the product observed was in a solid state. Whereas at temperatures above 290 ˚C, liquid product was formed. Among the high temperatures tested, 320 ˚C yielded the highest amount of heptadecane. Interestingly, at high temperatures, the amount of short-chain hydrocarbon increased. This observation can be attributed to cracking being favored as reaction temperature increases.

Therefore, selecting a suitable temperature range can improve the catalytic selectivity and conversion of fatty acids into hydrocarbon fuel. This step is important as it can limit the initiation of further secondary reactions and coke formation that can deactivate the catalyst.

2.5.2 Effect of pressure on the upgrading of pyrolysis product

The gas pressure used in catalytic pyrolysis of fatty acids can influence the yield and quality of the liquid product. For example, hydrogen pressure has been reported to affect deoxygenation, isomerization, and cracking reactions (Yang and Carreon 2017; Pattanaik and Misra, 2017; Madsen et al., 2011). As a result of this, Yang and Carreon (2015) studied the effect of hydrogen pressure at 20 bar (290 psi) on oleic acid's catalytic decarboxylation using two different catalysts, Pt/ zeolite 5A and Pt/ZIF-67/zeolite 5A. The authors reported approximately 98.7 % conversion

of the oleic acid to heptadecane in the two catalysts used. This observation was attributed to the hydrogen pressure promoting the saturation of oleic acid to stearic acid that subsequently underwent decarboxylation to yield heptadecane. The heptadecane selectivity percentage for the two catalysts, Pt/ zeolite 5A and Pt/ZIF-67/zeolite 5A, were 72.6 % and 81.5 %, respectively. The variation in the selectivity for heptadecane in the two catalysts was attributed to the microporous ZIF-67 crystalline layer on the zeolite 5A beads, which improved the heptadecane selectivity.

In a follow-up study, Yang and Carreon (2017) investigated the effect of pressure ranging from 10 to 30 bar (435 psi) at a reaction temperature of 320 ˚C in the decarboxylation of oleic acid over Pt/ZIF-67/zeolite catalyst. At 10 to 20 bar (290 psi), the heptadecane yield was similar to the finding of Yang et al. (2015). Nevertheless, when the pressure increased to 30 bar (435 psi), the heptadecane yield decreased to 69 %. This unexpected observation is attributed to the fact that at higher hydrogen pressure, water gas shift reaction pushes towards CO formation. The CO generated preferentially adsorbs on the catalyst's active site, decreasing the catalyst's selectivity to yield heptadecane due to the catalyst's deactivation (Madsen et al., 2011).

In addition, the increase in hydrogen pressure can concentrate the hydrogen on the surface of the catalyst, which will cause cracking of the heptadecane and octadecane into short-chain hydrocarbon compound, thus reducing the yield of heptadecane.

2.5.3 Effect of reaction time on the upgrading of pyrolysis product

Reaction time has been reported as one of the parameters that can influence the catalytic conversion of fatty acids into hydrocarbons (Asikin-Mijan et al., 2017; Yang & Carreon, 2017). Immer et al. (2010) investigated the effect of reaction time between 1- 5 hours in catalytic deoxygenation of stearic acids to yield liquid hydrocarbon fuel under inert He flow and at 300 ˚C reaction temperature using Pd/C catalyst. As the reaction time increased, the authors reported a

complete conversion of stearic acid with 98% selectivity for *n*-heptadecane was observed at 5 hours. The possible explanation for this observation is that as reaction time increases, the reactant and active site of the catalyst efficiently interact to yield desired products.

In another study, Yang & Carreon (2017) investigated the effect of reaction time ranging from 0.5 – 8 hours on the decarboxylation of oleic acid over Pt/ZIF-67/zeolite 5A bead catalysts. The results showed a complete oleic acid conversion under all the reaction times (0.5 to 8 hours), indicating that the decarboxylation rate was approximately 99 %. However, the selectivity of heptadecane varied as the reaction time increased. Between 0.5 to 4 hours, the heptadecane selectivity was 78-80% and remained constant. Whereas, at 8 hours, the heptadecane decreased to 65 %. This observation is because increasing reaction time to 8 hours favored further cracking of the heptadecane into short-chain hydrocarbon compound.

Zhang et al. (2020) studied the effect of reaction time on catalytic conversion of *Swida wilsoniana* fruit oil to yield hydrocarbon fuel using a 1 wt.% Ni-ZSM-5 catalyst. The reaction conditions employed in this study were reaction temperature of 170 ˚C, hydrogen pressure of 2.0 MPa (290 Psi), and the reaction time between 60 minutes to 180 minutes. As the reaction time increased, the authors reported that the hydrogenation of unsaturated compounds to saturated compounds increased significantly. At reaction times above 150 minutes, the conversion of the unsaturated compounds to yield saturated compound remained the same. This observation indicates that at 150 minutes, the reaction reached its equilibrium point.

Therefore, the study reveals the importance of knowing the suitable reaction time required to achieve higher conversion and selectivity of the desired compound.

2.5.4 Effect of catalytic support on upgrading of pyrolysis liquid product

Many studies have investigated the effect of catalytic support employed in the deoxygenation of fatty acids into hydrocarbon fuels (Kubička & Kaluža, 2010; Kubičková et al., 2005; Madsen et al., 2011; Mäki-Arvela, Kubickova et al., 2007; Mathias Snåre et al., 2006; Veriansyah et al., 2012). The high surface area of the support can enhance the distribution of metal catalysts as active sites for deoxygenation of fatty acid to yield hydrocarbon (Yang and Carreon 2017). Furthermore, the support used in catalyst synthesis provides the active metal phase with a higher attrition resistance and inhibits metal agglomeration (Lup et al., 2017). A variety of supports have been utilized in catalytic deoxygenation of fatty acids into liquid hydrocarbon fuels. Some of these supports include carbon, metal oxides (Al_2O_3, TiO_2, SiO_2, CeO_2, ZrO_2), zeolites (HY, HBeta, HZSM-5), and silica (SBA-15, MCM-41, Al-SBA-15, Al-MCM-41) (Arun et al., 2015; Chen et al., 2014). These supports can be utilized alone in the deoxygenation process and with metal loading (Pd, Pt, Ni, Mo, Rh, Ir, Ru, and Os) on its surface (Mäki-Arvela et al., 2007; Snåre et al., 2006). Supports with acid sites favors the hydrogenolysis of C-O bonds, and the most commonly used acidic supports in this type of reaction pathway are Al_2O_3 and zeolites (Elvan Sari, 2013; Furimsky, 2000; Zanuttini et al., 2013).

The order of acidity of most supports employed in catalytic pyrolysis of fatty acid to yield hydrocarbon fuel are as follows: H- ZSM-5 > H-Beta > HY > Al_2O_3> TiO_2> ZrO_2> CeO_2> SiO_2, the zeolite support has higher acidity than metal oxides (Alotaibi et al., 2012; He and Wang, 2013; Mortensen et al., 2016). The acidic and basic sites on catalytic support can influence the activity and selectivity. Besides the acid sites of the support, the pore volume, pore size, and the porosity of the catalytic support play an essential role in the deoxygenation of the fatty acids with diffusion

limitations of larger molecules. The difference in the porosity and pore sizes of supports tend to enhance specific reaction pathways, such as isomerization (Lup et al., 2017).

Qian et al. (2014) reported that smaller pore size of the catalyst support could influence the isomerization of methyl stearate. The authors reported that the use of Al-SBS-15 support showed isomerization of the compounds in the liquid product, attributing it to the smaller pore size of 0.6 nm, which influenced radical addition. Whereas, in the case of the SAPO-11 support, no isomerization was observed in the SAPO-11 support, as the larger pore size of 3.3 nm inhibited radical addition.

In addition to the metal support, activated carbon has been considered a potential support for catalytic metal loading due to its large surface area, pore size, and inert nature (Wu et al., 2016). Based on this, several metals such as nickel, platinum, and palladium have been loaded on activated carbon as the active site. These catalysts have shown to have higher selectivity in the deoxygenation of stearic acid into hydrocarbon fuel (Mäki-Arvela et al., 2007). A study conducted by Kubičková et al. (2005) showed the effect of using activated carbon support with different metal loadings to deoxygenate stearic acid. When palladium was loaded on the activated carbon support, the decarboxylation reaction pathway was favored over decarbonylation. In the case of loading platinum on the activated carbon, decarbonylation was the most dominant reaction pathway.

2.5.5 Effect of metal loading on the upgrading of pyrolysis product

Metals loaded on catalytic support play a significant role in converting fatty acids and increasing the selectivity for the desired hydrocarbon compound. The effect of metals loaded on catalytic support for deoxygenation of fatty acid into liquid hydrocarbons has widely been studied. Wu et al. (2016b) studied the effect of different weight percentages of nickel (10 %, 20 %, and 30 %) as active sites on a carbon support. The reaction conditions used in the study were reaction

temperature (330 ˚C), residence time (5 hours), amount of catalyst (30 mg), and stearic acid as the feedstock. The outcome of their study indicated that increasing the metal load on the carbon support had a significant increase in the conversion, but the selectivity decreased at higher metal loading. Besides the varying metal loading percent on the support used in this study, 20 % metal loading on carbon was found to be the optimal value that increased conversion and selectivity for alkane heptadecane.

Given these, many researchers have looked at different amounts of metal loading as active sites on catalytic supports. Yang & Carreon (2017b) studied different levels of platinum metal loading on the zeolite 5A bead catalyst support. They looked at different metal loadings (0.25, 0.5, 1.0, and 1.5 wt.%) on zeolites 5A beads used in oleic acid pyrolysis to yield hydrocarbon fuel. The conversion was the same for all the metal loading levels on the zeolites 5A beads, with a decarboxylation reaching approximately 99 %. However, the catalyst's selectivity for heptadecane was not the same in all the metal loading levels studied in this experiment. They found that by increasing the metal loading above 0.25 wt.%, the selectivity for heptadecane yield was 80 % and was the same for the other metal loading levels. This observation was attributed to catalyst deactivating strongly at lower Pt loading of 0.25 wt%, and at higher metal loading, the catalyst was stable.

Chen et al. (2013) reported an increase in catalytic performance when the metal loading of platinum (Pt) on the support increased. However, increasing the metal loading can result in metal aggregation on the catalytic support, hence increasing the catalyst's particle size (Santillan-Jimenez et al., 2014). It is worth mentioning that metal aggregation is not only affected by metal loading but influenced by experimental factors such as the catalyst preparation method and the reaction's thermodynamic condition (Zanuttini et al., 2013). The presence of metal aggregates on

the support reduces catalytic surface area and lowers the active metal dispersions, thus reducing the catalytic selectivity and activity.

Knowing the suitable metals loaded on the catalyst can significantly influence the catalyst's performance in terms of the activity, selectivity, and conversion to the feedstocks used in the deoxygenation reactions.

2.5.6 Effect of monometallic catalyst on decarboxylation of fatty acids into hydrocarbon fuel

Transition metal catalysts have widely been employed in fatty acids pyrolysis to generate renewable fuels and platform chemicals (Idem et al., 1997; Kay Lup et al., 2017; Krobkrong et al., 2018; K. D. Maher & Bressler, 2007). Metals such as Pd, Pt, and Ru have been reported to have a higher affinity to hydrogen on the active metal sites, which results in C-O hydrogenolysis to yield hydrocarbons (Pestman et al., 1997). The removal of oxygen in fatty acids over the following transition metals such as palladium (Pd), platinum (Pt), rhodium (Rh), ruthenium (Ru), and nickel (Ni) have widely been studied. The catalytic performance of these transition metals in terms of their activity and selectivity has been reported in this order: Pd > Ru > Pt > Rh > Ni (Lugo-José et al., 2014). The role of transition metal catalyst in deoxygenation reaction tends to increase the rate of decarboxylation of the fatty acids, thus, increasing the desired alkane hydrocarbon compound yields. For this reason, He and Wang (2013) investigated the effect of using Ru metal catalysts to deoxygenate carboxylic acids such as butyric, isobutyric, propionic, and acetic acids, which occurred via C-C bond cleavage, decarbonylation, and hydrogenolysis to yield hydrocarbons.

Nickel (Ni) metal has been used as an active site on many catalytic supports and demonstrated the deoxygenation and cracking of fatty acids into shorter hydrocarbons. Nickel catalyst has been reported to possess a high hydrogenation activity, which resulted in the saturation of alkene and aromatic rings (Jin et al., 2014). Also, nickel-based catalysts tend to promote the

dissociation of the C-C bond (Tran et al., 2016) and methanation reaction at elevated temperatures (Chen et al., 2015). Furthermore, the nickel-based catalyst promotes hydrogenation, decarbonylation, and decarboxylation reaction pathways while minimizing C-O bond scission (Srifa et al., 2015). This observation is attributed to the nickel-based catalysts possessing lower electrophilicity, resulting in the minimal scission of C=O and C-O bonds (Shi et al., 2017). However, to improve the deoxygenation process, the nickel-based catalyst can be modified with other metals with higher electrophilic properties (Pan et al., 2015).

Platinum (Pt) metal catalyst promotes hydrogenation reaction to deoxygenate fatty acids into liquid hydrocarbon fuel. The Pt-based catalyst has been employed in oxygen removal from glycerol and methyl palmitate (Fu et al., 2010; Mäki-Arvela et al., 2007). The reaction mechanism of the Pt metal catalyst favors hydrogenation of the C=C bond and aromatic rings before removing oxygen (Zanuttini et al., 2013). Furthermore, Pt metal-based catalyst favors the C-C bond cleavage. It has a high potential to adsorb hydrogen to remove oxygen from the fatty acids to yield liquid hydrocarbon fuel (Kay Lup et al., 2017).

Pallidum (Pd) metal catalyst has been reported to favour the decarboxylation reaction pathway in the deoxygenation reaction of fatty acid, to yield liquid hydrocarbons with similar characteristics as that of fossil-based fuel (Fischer et al., 2011; Immer et al., 2010; Immer and Lamb, 2010; Simakova et al., 2010; M. Snåre et al., 2008; Mathias Snåre et al., 2006). They reported a higher Pd catalyst selectivity of above 90 % for heptadecane during the decarboxylation reaction of stearic acid. On the other hand, the Pd catalyst's continuous usage results in deactivation, decreasing the catalyst's selectivity (Fischer et al., 2011; Simakova et al., 2010; Mathias Snåre et al., 2006). Another study conducted by the following group of researchers

(Simakova et al., 2010; Snåre et al., 2007) demonstrated that a monometallic catalytic Pt on carbon support enhanced removal of oxygen atoms from palmitic and stearic acids.

2.5.7 Influence of reaction atmosphere

Regardless of the catalyst employed in the reaction, catalytic deoxygenation can be enhanced by the reaction atmosphere, either inert or reactive gas-phase atmosphere (Santillan-Jimenez and Crocker, 2012; Mathias Snåre et al., 2006; Yang et al., 2015). Depending on the reaction atmosphere used in catalytic deoxygenation reactions, some reaction routes can be more dominant than the others. For instance, using hydrogen as a reactive gas atmosphere can switch to hydrodeoxygenation reaction yielding H_2O and paraffin with the same carbon number as the starting fatty acid.

To understand the effect of the inert atmosphere in catalytic decarboxylation of fatty acids into hydrocarbon, Bernas et al. (2010), investigated the deoxygenation of dodecanoic acid under an inert atmosphere. The reaction was conducted at a temperature range of 300-360 ˚C, pressure (5-20 bar), and under an argon gas atmosphere. The authors reported an increase in the reactant conversion when an argon gas was co-currently flowed with the reactant at higher temperatures. But when the flow of the argon gas stopped, the conversion of dodecanoic acid slowly decreased. The explanation of this observation is that as argon gas flows through the reactor, the CO and CO_2 that could preferentially adsorb on the surface of the catalyst to cause deactivation is removed, thus improving the catalyst performance. Similarly, a higher conversion of about 80 % and an increase in selectivity of a desired C17 hydrocarbon compound were reported when oleic acids were treated with NiMo oxide/ γ-Al_2O_3 inert N_2 gas atmosphere (Krobkrong et al., 2018).

In summary, there has been significant interest in converting lipids via pyrolysis to generate hydrocarbon liquid fuels. The liquid product may contain oxygenated compounds that may

contribute to the liquid product's low heating content and high acid content. These drawbacks limit its direct utilization in petroleum infrastructures.

The caustic neutralization reaction of residual fatty acids in crude pyrolysis liquid product has been elucidated for acid removal. However, this approach generates large volumes of wastewater, and through emulsification, the separation of the hydrocarbon fraction and the aqueous phase becomes incomplete. Therefore, understanding the mechanism of using catalysts in fatty acids pyrolysis to yield hydrocarbon fuel is key in assessing the feasibility of incorporating deoxygenation catalyst to remove residual fatty acids in crude pyrolysis yielding liquid hydrocarbon fuel.

Chapter 3

3.0 Experimental Methodology

This chapter explains the experimental methodologies and analytical techniques involved in (1) using microwave-assisted heating to improve the heating rate fatty acid conversion and (2) catalytic removal of residual fatty acid in crude pyrolysis liquid product.

3.1 Materials and Chemicals

Oleic acid (≥ 99 %) and stearic acid (≥ 95 %) were used as feedstocks. Chemicals and catalysts applied in this thesis research including, nonadecanoic acid methyl ester (≥ 99 %), pentane (≥ 99 %), carbon monoxide standard (≥ 99 %), 65 wt.% nickel on silica-alumina catalyst, 1 wt.% platinum on silica catalyst, silica-alumina support grade 135, diazomethane were purchased from Sigma-Aldrich (St. Louis, MO, USA). The silica catalyst support was obtained from Silicycle (Silicycle, Quebec, Canada). External gas samples such as carbon dioxide (≥ 99 %), hydrogen (≥ 99 %), methane (≥ 99 %), nitrogen (≥ 99 %) were purchase from Praxair Canada Inc. (Mississauga, Ontario, Canada). The crude pyrolysis liquid product and stainless-steel mesh were obtained from an industrial partner. The thermal paper used was obtained from Staples (Edmonton, AB, Canada). Microreactor stainless-steel parts were purchased from Swagelok Edmonton AB, Canada. The microwave unit was from Gerling applied engineering (GAE). All the chemical materials purchased were used without any purification.

3.2 Preliminary study of microwave-assisted pyrolysis for deoxygenation of model fatty acids

The first part of the thesis looked an approach to improve the heating capacity of the existing fatty acid pyrolysis conversion process, microwave-assisted heating, was incorporated in the deoxygenation reaction of model fatty acids (oleic and stearic acid). Due to the low microwave

absorption capacity of fatty acids, a heating aid was employed to increase microwave absorption. In this study, approximately 50 g of stearic acid was mixed with 180 g of silicon carbide (SiC) grits and transferred to the reactor vessel, heaped in the middle to completely cover the K-type thermocouple. The vessel was assembled and purged with N_2 at 500 psi (3445 kPa). The reactor's initial pressure was 100 psi (689.5 kPa) N_2. The pyrolysis reaction was carried out on the 2.45 GHz system at 50 % power (1000 W) for 60 min with a set temperature of 430 ˚C. Reflected power was monitored and dialed to a minimum during the run. At the end of 60 min, the microwave was turned off, and the reactor was cooled to room temperature. The test was repeated with 500 g silicon carbide and 100 g oleic acid following a similar protocol. The liquid and gas product was sampled and analyzed on GC-TCD and GC-FID instruments and methods described in **sessions 3.6** and **3.6.1**. The experimental approach can thus be seen in **Figure 3-1**.

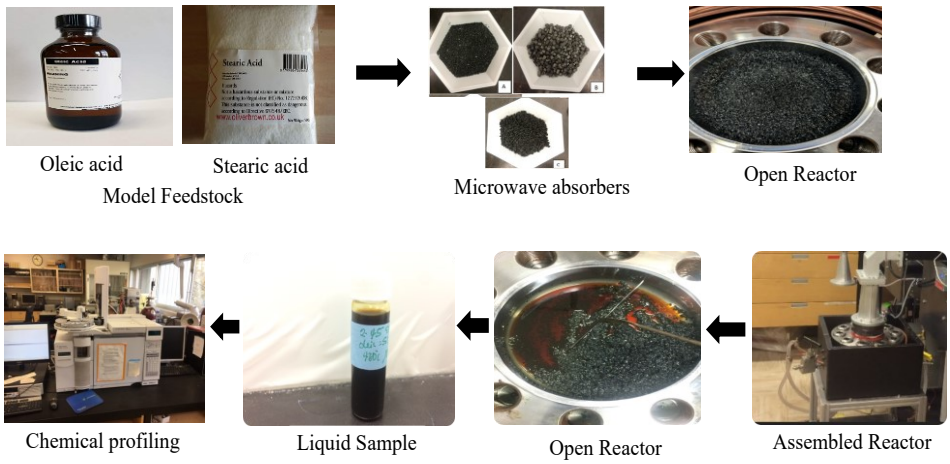

Figure 3-1. Experimental approach used for the preliminary study on microwave pyrolysis of model fatty acid feedstock (oleic acid and stearic acid). The stepwise process used in preliminary study of microwave-assisted pyrolysis of model fatty acid feedstock (oleic acid and stearic acid) in the presence of a 2.45 GHz microwave frequency at a 50 % microwave power level and at a set temperature of 430 ˚C for reaction time of 60 minutes.

3.2.1 Microwave heat distribution determination using wet thermal paper

Based on the evaluation of different chemical compound distribution in the liquid product obtained from **session 3.2**, this experiment was conducted to understand the uniformity of microwave distribution in the reactor cavity using wet thermal paper. The thermal paper used is a specialized type of paper sensitive to heat and primarily used in the printing industry, as shown in **Figure 3-2.**

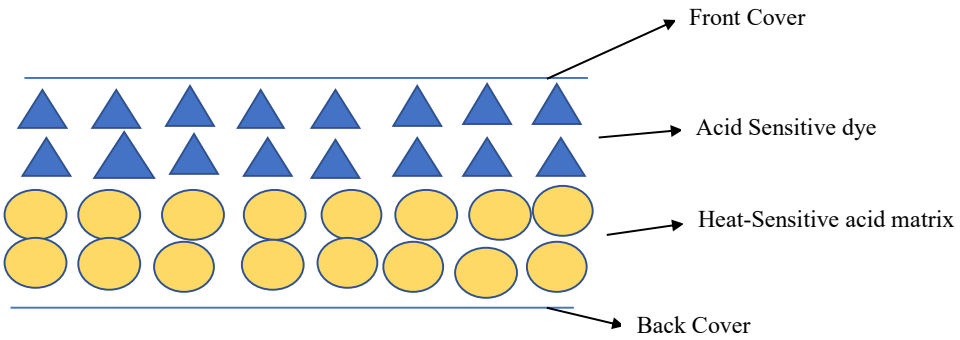

Figure 3-2. Schematic diagram of a thermal paper. The schematic diagram of a thermal paper used in the heating distribution of the microwave in the microwave reactor cavity experiment (modified from (Epa & for the Environment, 2015)).

In this experiment, the thermal paper was designed into a disc shape to fit well in the reactor cavity and was submerged in a beaker of distilled water. The presence of water molecules on the thermal paper's surface acts as a microwave absorber to enhance microwave absorption. The test was carried out on the 2.45 GHz system at full power (2000 W) for 8 minutes, as shown in **Figure 3-3.**

Open reactor with wet thermal paper

Assembled reactor vessel to the 2.45 GHz microwave unit

Figure 3-3. Experimental set-up for the wet thermal paper study. The step approach for the wet thermal paper to indicate the heating distributions in the microwave reactor cavity. Microwave frequency of 2.45GHz, power 2000 W and residence time of 8 minutes.

3.3 Pyrolysis reactions

Unless otherwise indicated, all pyrolysis reactions were carried in a 15 mL volume batch microreactor built in-house. The microreactors were heated in a Techne Model SBS-4 fluidized sand bath (Burlington, NJ), as is shown in **Figure 3-4.** The microreactor set-up used was similar to what is previously used in the Bressler laboratory group (Asomaning et al., 2014c; Maher et al., 2008; Omidghane et al., 2017b).

Figure 3-4. Fluidized sandbath.

3.3.1 Reactor preparation

The 15 mL microreactors were built in-house in the Bressler laboratory of the Department of Agricultural, Food and Nutritional Science (AFNS). The microreactor used in this thesis research can be classified into two parts: the reactor bottom and the reactor head. **Figure 3-5** shows the respective parts of the microreactors used in the study.

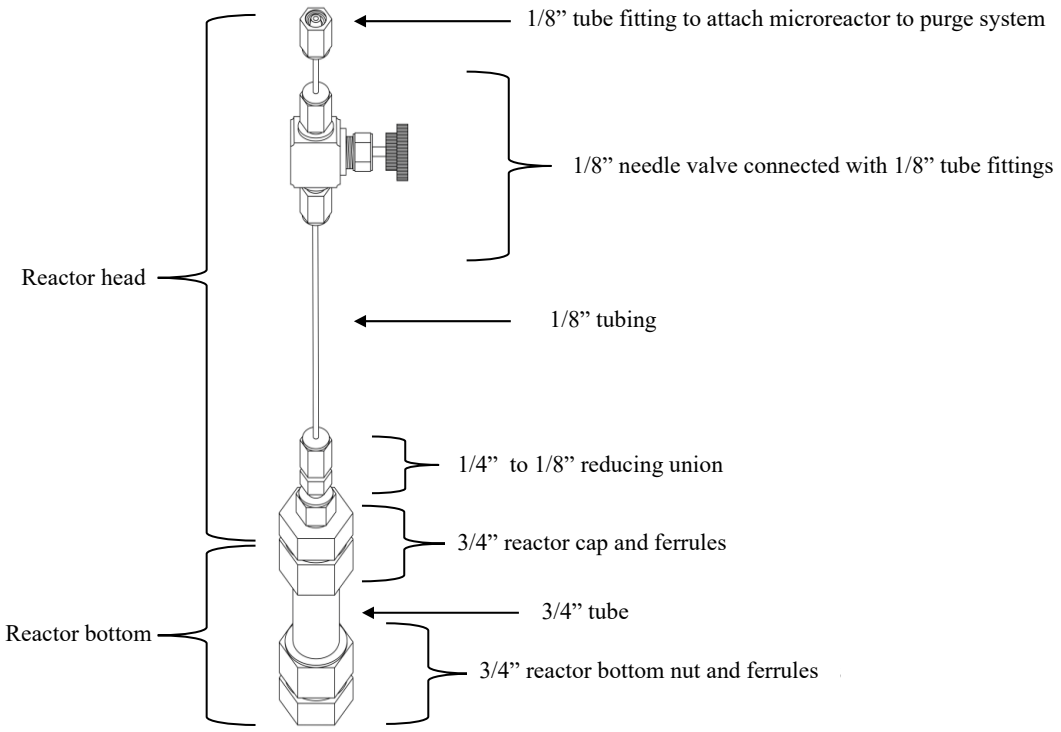

Figure 3-5. The 15 mL microreactor Schematic diagram of a closed microreactor used in the study.

3.3.2 Sample loading and microreactor preparation

Approximately a gram of the feedstock mentioned in **session 3.1** was weighed into the microreactors using Precisa XT220A analytical balance (Switzerland). The microreactors were assembled and purged with nitrogen gas at a pressure of 500 psi (3447 kPa) to create an inert atmosphere in the microreactors. Leak check on the microreactor was conducted at 500 psi (3447

kPa) using Snoop® leak detector or by submerging it into a beaker of water. Continuous bubbles seen from any part of the microreactors indicate leaking, and retightening of the microreactors is done to avert the leaks. The internal pressure is released before assembling the microreactors unto the holding bar, as shown in **Figure 3-4**. When the set temperature is attained, the microreactors are gently lowered into the fluidized sand bath. The mixing of the content in the microreactors is enhanced by constant agitation throughout the reaction time. The reaction is quenched in water at room temperature, approximately 22 ˚C, when the set time for the pyrolysis reaction is reached. All the experiments in this thesis were performed in triplicate.

3.3.3 Pyrolysis of oleic acid in the presence of a stainless-steel mesh

To determine the catalytic effect of a stainless-steel mesh on the liquid product composition, a stainless-steel mesh was incorporated in the pyrolysis of oleic acid. The stainless-steel mesh was formed into a disc shape, which weighed 0.30 grams, as shown in **Figure 3-6.** The disc-shaped mesh was chemically or thermally treated to remove any residues on the mesh. In the chemical treatment, approximately 10 mL of each of methanol, acetone, and dichloromethane (DCM) were used one after the other as listed to wash the stainless-steel mesh. These chemical solvents were selected on the principle of their polarity index. Methanol and acetone solvent dissolved polar residues on the mesh, and the DCM was used to dissolve the non-polar compounds. The solvent was continuously stirred at 150 rpm for 10 minutes to ensure the maximum removal of any residues. After this step, the washed mesh was dried in the fumehood. A different set of the disc-shaped meshes was thermally treated at 500 ˚C for 2 hours in a muffle furnace. The thermally treated mesh was kept in a desiccator, allowing it to cool to room temperature.

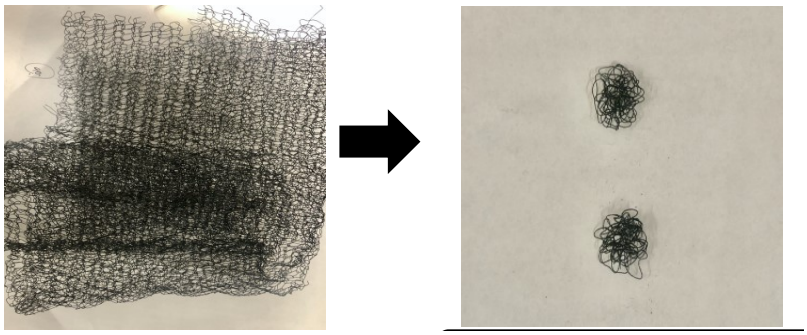

Used stainless-steel mesh Disc shaped stainless-steel mesh

Figure 3-6. Industrial stainless-steel mesh. Stainless-steel mesh cut into disc shaped.

Microreactors were prepared following the procedure mentioned in **section 3.3.2** with either treated or untreated stainless-steel mesh. The untreated refers to direct use of the mesh without chemical or thermal treatment. An experiment without the addition of stainless-steel mesh was performed as the control. To incorporate the mesh, it was positioned inside the microreactor to ensure continuous contact with the oleic acid. The reaction was carried out at 430 ˚C for 2 hours, with atmospheric initial pressure. This reaction condition was selected from previous work to decarboxylate oleic acid (Asomaning et al., 2014b). The experimental approach is shown in **Figure 3-7.**

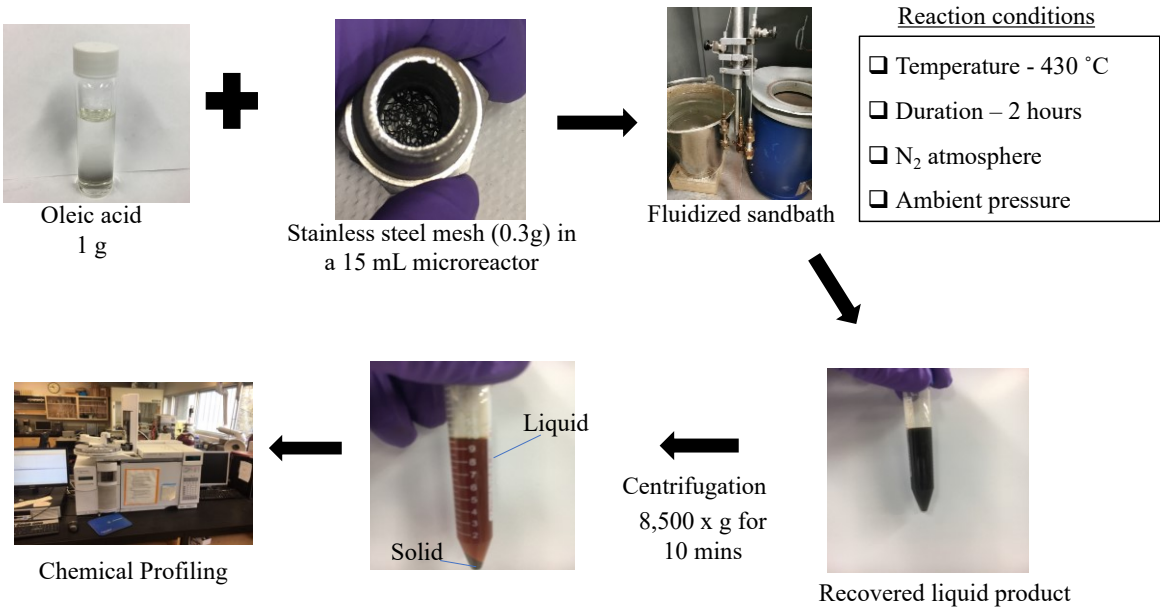

Figure 3-7. The experimental approach used in the pyrolysis reaction oleic acid in the presence of a stainless-steel mesh. A step-by-step process employed in the pyrolysis of oleic acid in the presence of stainless-steel mesh at a reaction condition of 430 ˚C and a reaction time of 2 hours.

3.4 Catalytic deoxygenation of residual fatty acid in crude pyrolysis liquid product using a 15 mL microreactor

The experimental results obtained from **session 3.3.3.** showed the inert nature of the stainless-steel mesh on the product distribution and liquid product composition. However, the residual fatty acids in the crude liquid product could limit the direct utilization in petroleum infrastructures. Therefore, catalytic deoxygenation was evaluated to remove residual fatty acids in crude pyrolysis liquid product to yield liquid hydrocarbon fuel. The following commercially available catalysts, 65 wt.% nickel on silica-alumina, 1 wt.% platinum on silica and their respective supports, were purchased and used in this study.

3.4.1 Catalyst characterization

The purchased catalysts were physically characterized to determine the surface area, pore diameter, and pore volume. The characterization analysis was done at the NanoFab facility (University of Alberta, Edmonton). Before characterizing the catalysts, they were grounded into a fine powder using a pestle and mortar. The BET-specific surface areas for each catalyst were collected on Autosorb-1MP, suitable for mesopore analysis using nitrogen gas, as shown in **Table 3-1**. It is worth mentioning that the catalyst support used in this study was not the exact support used in the catalyst synthesis, as the manufacturers provided limited information on the support used. Based on the BET results obtained, an informed decision was made to select the support that is approximately close to the support used in the loaded catalysts.

Table 3-1 Physicochemical properties of metal loaded catalysts and supports

Catalyst	Properties		
	Surface area (m^2/g)	Pore Diameter (Å)	Total pore volume (cc/g)
*Silica only (SiO_2)	218	164	0.9
Platinum on silica (Pt/SiO_2)	150.9	186.2	0.702
*Silica-Alumina only (SiO_2/Al_2O_3)	382.6	150	N/A
Nickel on silica-alumina ($Ni/SiO_2/AL_2O_3$)	209.6	66.2	0.347

*Silica only properties were obtained from manufacturers (Silicycle, Quebec, Canada), silica-alumina catalyst support data were obtained from the literature (Asikin-Mijan, Lee, Marliza, & Taufiq-Yap, 2018).

Following the sample preparation procedure mentioned in **section 3.3.2**, the feedstock used in this study was a crude pyrolysis liquid product. Approximately 0.2 grams of a catalyst was weighed into the microreactors before adding a gram of feedstock. 0.5, 1, and 2 hours were studied to understand the effect of reaction time on catalytic deoxygenation of residual fatty acids in crude liquid product to yield liquid hydrocarbon. The reaction was carried out at 350 ˚C with nitrogen gas starting at atmosphere pressure. The controls were the crude pyrolysis liquid without any catalyst treatment, silica-alumina support, and silica support only. The experimental approach can thus be seen in **Figure 3-8.**

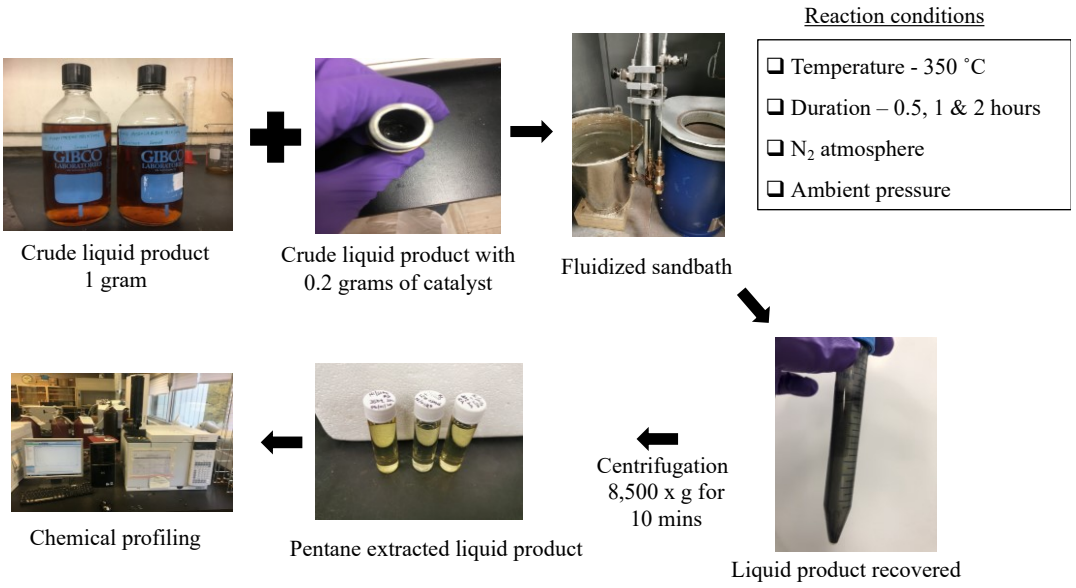

Figure 3-8. Experimental approach for the catalytic deoxygenation of crude pyrolysis liquid product. The various steps used in the catalytic experiment with a reaction temperature of 350 ˚C, the residence time of 0.5, 1, and 2 hours and nitrogen gas were used as reaction atmosphere at atmospheric pressure.

3.5 Scale-Up of nickel silica-alumina catalyst to deoxygenate residual fatty acids in pyrolysis liquid product using 1L reactor

Given the outcome in **session 3.4**, the nickel on silica-alumina catalyst treatment at 2 hours showed a complete deoxygenation of residual fatty acids in crude pyrolysis liquid product. Due to this effect a 1 L batch scale-up experiment was conducted to understand the catalyst's deoxygenation activity on a large scale and the mass balance of the pyrolysis product obtained from the study. Also, this experiment sought to understand the regeneration and reuse of the spent nickel on silica-alumina catalyst. This study provided the needed understanding in the direct transition of the catalytic upgrading method from the bench experiment to a large-scale experiment. It is worth mentioning that the experimental set-up was different from what was describe in **session 3.4**.

3.5.1 Reaction procedure

The removal of residual fatty acids in the crude liquid product was conducted in a 1 L continuously stirred tank reactor operated in batch mode (Parr Instrument Co., Moline IL, USA). An electrical heating element was used as the heat source for the reactor. Approximately, 20 grams of 65 wt.% nickel on silica-alumina catalyst was weighed into a clean 1 L reactor, and 100 grams of crude pyrolysis liquid product was added into the reactor. The selected amount of catalyst and feedstock used was 100 times the amount mentioned in **session 3.4** to maintain the same feed to catalyst ratio. The reactor was checked for leaks and purged with nitrogen gas (N_2) at 200 psi. Lower pressure was used to avoid flushing the pyrolyzed liquid product, which could impact the mass balance. The reactor was heated at the set temperatures of 300 ˚C and 350 ˚C under constant stirring at 150 rpm to ensure uniform mixing for the desired time of 1.5 hours. It should be noted that the initial pressure in the reactor before the start of the deoxygenation reaction was kept at

atmospheric pressure. However, the internal pressure in the reactor increased throughout the reaction.

The above temperatures were selected to understand the effect of temperature on product distribution and the difference in catalytic deoxygenation activity. A desired run time of 1.5 hours was selected to make up for the exact run time used in **session 3.4** because it took 30 minutes to reach the set temperature. The heater was turned off, and the heating mantle was removed from the reactor to quench the reactor and allow cooling of the reactor to room temperature (approximately 22 ˚C). The experimental approach can be seen in **Figure 3-9.**

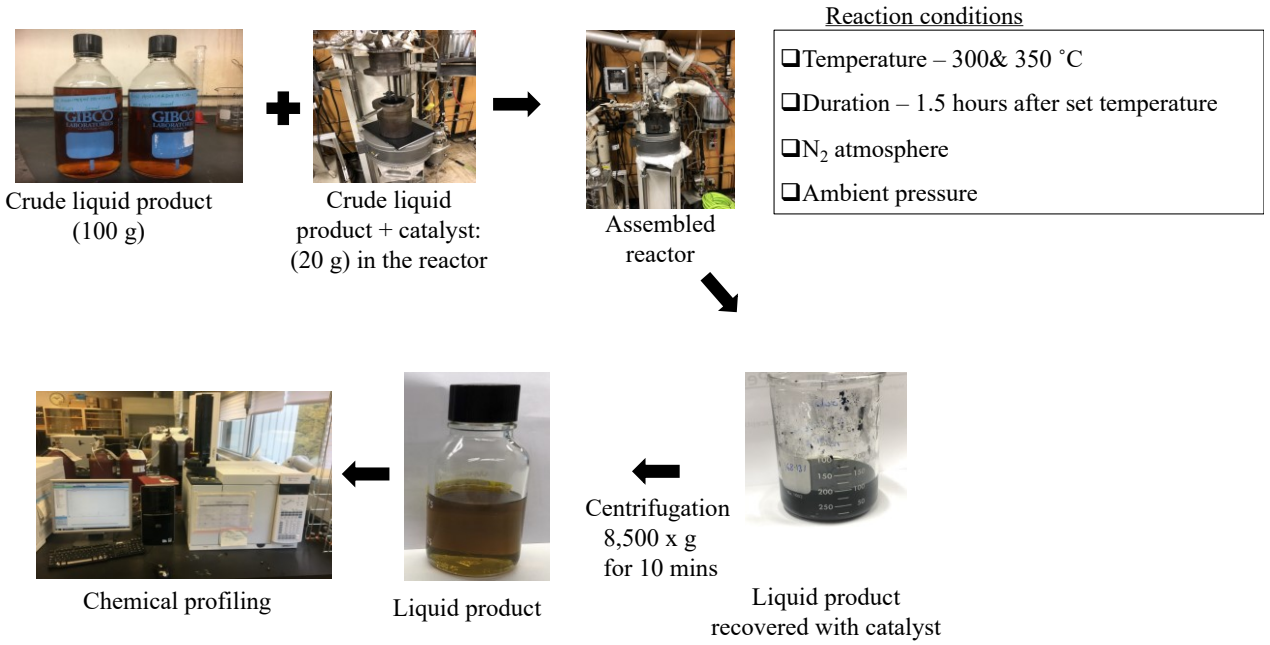

Figure 3-9. Experimental approach for the scale – up catalytic deoxygenation of crude pyrolysis liquid product. A step-by-step process used in the scale - up of the catalytic deoxygenation reaction of the residual fatty acids in crude pyrolyzed liquid product, with reaction temperatures of 300 & 350 ˚C for a residence time of 1.5 hours.

3.5.2 Regeneration of spent catalyst

The liquid product yield obtained from the fresh nickel on silica-alumina catalyst at 300 ˚C treatment was 81.2 %, whereas that from the 350 ˚C treatment was 73.8 %. Due to the higher amount of liquid product obtained from the 300 ˚C treatment, the corresponding recovered spent catalyst was considered for the regeneration study, as shown in **Figure 3-10**. A solvent washing approach was considered as a method to regenerate the spent catalyst. The solvent regeneration approach was selected to reverse the adsorption of organic compounds and carbonaceous materials on the catalyst's active sites (Guo et al., 2011), thus regenerating the catalyst. In this study, pentane was added to the spent nickel catalyst in a beaker. The content was continuously stirred using a spatula for about 5-10 minutes to ensure uniform mixing. The mixture was transferred into Falcon tubes and centrifuged at 8500 x g for 10 minutes to sediment the catalyst. The wet catalyst was dried overnight in a fumehood. It is worth mentioning that the amount of the catalyst recovered was not the same as the initial amount of catalyst used, as shown in **Table 3-2.**

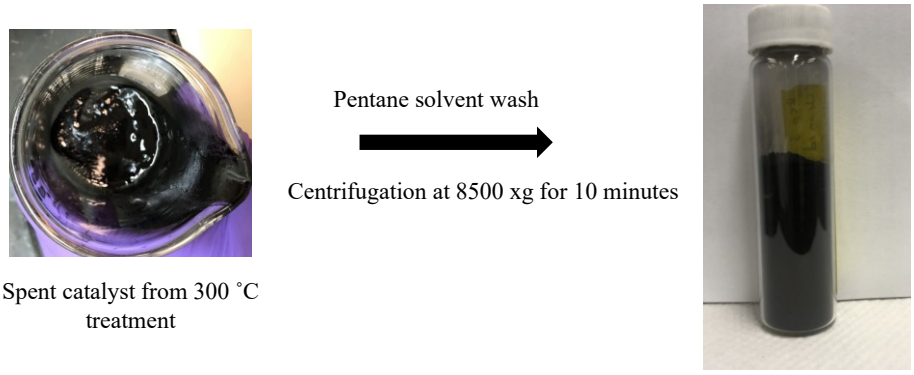

Figure 3-10. Solvent wash regeneration approach.

Table 3-2. The amount of catalyst used in the catalytic deoxygenation reaction.

	Replicate 1	Replicate 2	Replicate 3
Initial amount of fresh catalyst (grams)	20	20	20
Pentane solvent cleaned catalyst for 350 ˚C treatment	18.3	18.8	19.5
Pentane solvent cleaned catalyst for 300 ˚C treatment	17.6	18.9	19.2

3.5.3 Mass balance for products obtained in the scale-up experiment

Since the experimental set-up was different from the bench scale described in **session 3.4**, a different approach was used in the mass balance calculation. Before disassembling the reactor, the gas product was vented into a 1L gas bag. The reactor's content composed of the liquid product, and the nickel on silica-alumina catalyst was poured into a pre-weighed beaker, and by difference, the mass of the content was determined. The mass difference of the reactor before and after cleaning was added to the content's initial mass. The fine powder nature of the catalyst made isolating the liquid product from the catalyst challenging. A best-case scenario was used to simplify the mass balance by assuming no solids were formed. The liquid product was determined by finding the difference between the total mass content (liquid + catalyst) and the initial mass of catalyst. The gas yield was therefore computed by subtracting the mass of the liquid from the initial mass of the feed.

3.6 Analytical methods – gas product analysis

The weight of the gas product obtained from experiments described in **sessions 3.3.3** and **3.4** was determined by weighing the microreactors before and after the venting gas product in the 15 mL microreactors into a 1 L gas bag. This step was done using an analytical balance with a maximum weighing limit of 620 g and a precision of 1 mg / 0.001g Sartorius Extend ED623S (Sartorius AG, Goettingen, Germany).

All the gas product obtained from all the experiments described in this thesis was analyzed on the gas chromatograph (GC) following previously described method by Asomaning et al. (2014b). 150 µL of the gas product was manually injected to detect the presence of N_2, CO, CO_2, H_2, and short-chain hydrocarbon compounds (C_1-C_7) compound on an Agilent 7890A GC system (Agilent Technologies, Santa Chara, CA, USA) coupled to a thermal conductivity detector (TCD) and flame ionization detector (FID). The injector and detector temperature were kept constant at 170 ˚C and 200 ˚C, respectively. The oven temperature program for the product analysis was set at 40 ˚C for 5 min and then increased at 20 ˚C min^{-1} to 200 ˚C and held for 4 min to achieve a total run time of 25 minutes. The carrier gas used to detect CO, CO_2, and N_2 was helium gas at a constant pressure of 20 psi (137.8 kPa). It is worth mentioning that, in the H_2 analysis, the same GC system and parameters were used, but the carrier gas used in this analysis was argon. The hydrocarbon gas analysis was conducted on the same GC system but with a flame ionization detector (FID), the run time for detecting hydrocarbon compounds was 60 minutes.

3.6.1 Analytical methods –Liquid product analysis

The microreactors were disassembled after venting the gas product. The liquid product was recovered by adding 10 mL of pentane spiked with 1 mg/mL of nonadecanoic acid methyl esters as an internal standard. The amount of the liquid product was computed by subtracting the amount

of gas and solid from the initial amount of feed. The liquid product obtained in all the experiments in this thesis was analyzed on GC-FID for quantitation and GC-MS to identify individual compounds. The method used in this analysis is the same as what was previously described by Asomaning et al. (2014b).

150 µL of the pentane extracts liquid product obtained from the experiments described in **sessions 3.3.3** and **3.4** was dispensed into a GC vial. Excess diazomethane was added to the GC vial to derivatize the fatty acids into their methyl ester derivatives. Similar sample preparation was used for the liquid product obtained from **session 3.5**, but approximately 780 mg of the crude liquid was added to 3.2 mg of nonadecanoic acid methyl ester as an internal standard in a GC vial. The liquid analysis was carried out on an Agilent 6890N GC-FID equipped with Agilent 76830 series autosampler and injector with Agilent DB-Petro column (100 m x 250 µm, film thickness 0.50 um) (Agilent Technologies, Santa Clara, CA). The GC temperature parameter was 300 ˚C for the injector and 350 ˚C for the detector. The oven temperature program was initially at 35 ˚C for 0.1 min, with 10 ˚C/min increase to 280 ˚C and held for 15.40 min for a total run time of 40 min, and the injection volume was 1 µL. The mass spectrometry (MS) analysis was also carried out on an Agilent GC 6890N coupled to an Agilent 5975B EI MS instrument. The GC parameters used were similar to the GC-FID condition, but the GC-MS interface was kept at 320 ˚C.

3.6.2 Analytical methods –FTIR analysis on liquid product

The FTIR analysis was conducted to provide evidence of the individual chemical functional groups in the liquid product. This analysis step provided additional information on residual fatty acids' deoxygenation in the liquid product obtained from **sessions 3.4** and **3.5**. The universal attenuated total reflectance (UATR) spectra were recorded in the transmission mode between 650 and 4000 cm^{-1} using a PerkinElmer Frontier FT-IR spectrometer (Perkin Elmer Inc.

Waltham. MA, USA). A background scan was initially done to ascertain no residual sample on the diamond crystal sample holder. The liquid product was subsequently analyzed on the FTIR spectrometer.

3.6.3. Analytical methods –Total acid number (TAN) determination on crude liquid product

The total acid number (TAN) titration analysis was performed to provide additional information to detect residual fatty acids after catalytic deoxygenation of residual fatty acids in a 1 L scale-up experiment. The TAN was determined using an auto titrator 848 Titrino plus instrument (Metrohm AG, lonenstrasse, Switzerland) following ASTM standard method D664. The quantity of base used to neutralize the acidic constituent in 0.7 g of crude pyrolysis liquid sample was expressed in milligrams of potassium hydroxide.

3.8 Statistical Analysis

All the experiments conducted in this project were done in triplicates, and all the results obtained were reported as averages ± standard deviation. The statistical test performed on the data was one-way ANOVA with Tukey test to determine the significant difference in data at the 95 % confidence level. The statistical package used in this project was R software version 3.6.

Chapter 4

4.0 Results and Discussion

4.1 Microwave-assisted pyrolysis of model fatty acids

The group's previous work showed that the reaction temperature of 430 ˚C demonstrated decarboxylation as the main reaction pathway. They also reported that increasing reaction time could result in over cracking and the occurrence of other secondary reaction pathways (Asomaning et al., 2014c; Maher et al., 2008; Omidghane et al., 2017b). Based on this evidence, a reaction temperature of 430 ˚C and 1 hour was selected as the reaction condition in this study on the 2.45 GHz system at 50 % power (1000 W). Approximately 50 grams of stearic was mixed with 180 grams of silicon carbide (SiC) was used, as described in **session 3.6.** Following, similar protocol, the study was repeated using 100 grams of oleic acid and 500 grams of SiC.

The stearic acid temperature profile showed rapid heating to achieve the set temperature within 1 minute of microwave irradiation, as shown in **Figure 4-1A**. The possible explanation for the sudden rise in the process temperature to attain the set temperature is attributed to the SiC absorbing the transmitting microwave energy directed into the cavity and converted it into thermal energy. The heat generated within the SiC is transferred via conduction to the stearic acid in the reactor cavity. Also, the pressure in the microwave-assisted pyrolysis of stearic acid increased from 100 to 210 psi, indicating the formation of volatiles staying in the gas phase throughout the reaction. The observation from this study was similar to the finding of Wang et al. (2013), as they demonstrated the importance of incorporating heating aids to heat model fatty acids.

In the case of the oleic acid study, the set reaction temperature was not reached throughout the reaction time, as shown in **Figure 4-1B**. However, the pressure kept increasing even though

the set temperature was not attained throughout the reaction time tested. This outcome from the oleic acid study was unexpected and could not be explained as this was not investigated further.

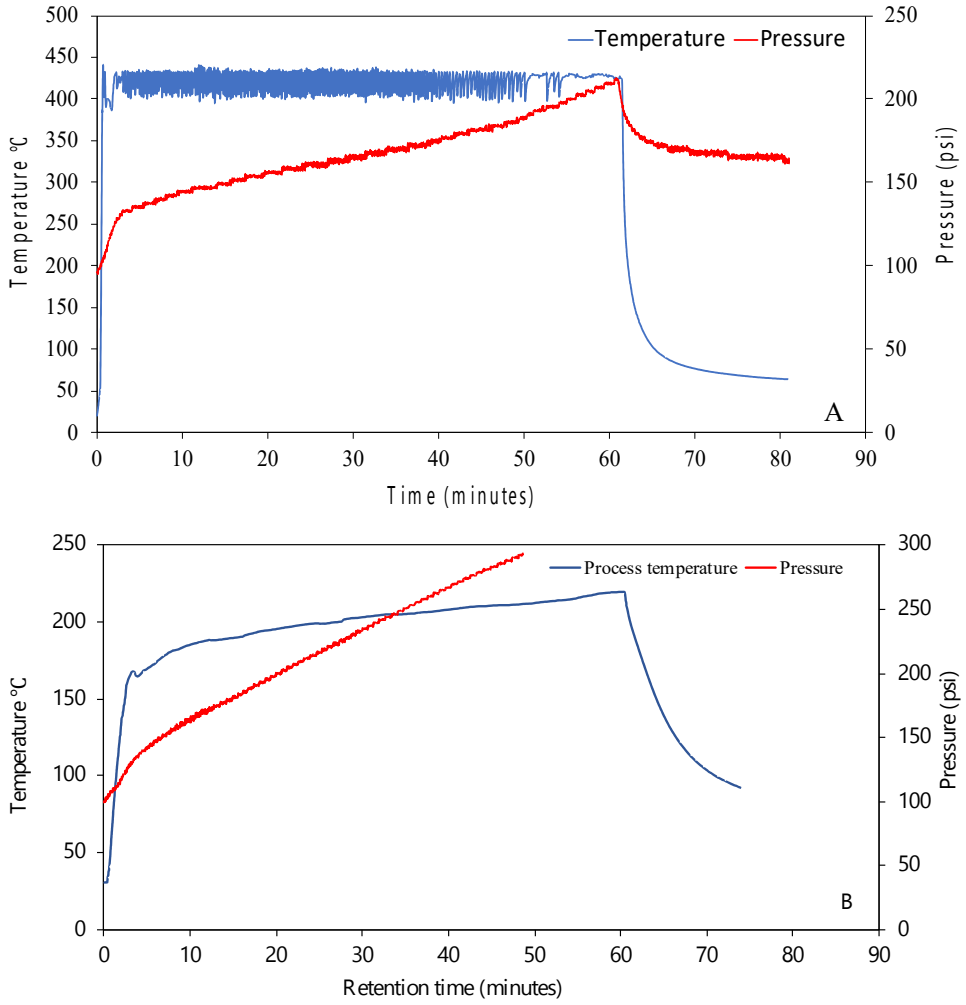

Figure 4-1: The temperature and pressure profiles during reaction of (A) stearic acid and (B) oleic acid with SiC as heating aid. Reaction was carried out on the 2.45GHz system at 50% power (1000W) and using nitrogen gas at an initial pressure was 100 psi.

4.1.2 Deoxygenation and hydrogen formation

Figure 4-2 shows carbon dioxide (CO_2) and carbon monoxide (CO) in the gas fraction obtained from the microwave-assisted pyrolysis of model fatty acids (oleic and stearic). The presence of CO and CO_2 provided evidence of decarbonylation and decarboxylation reaction

pathways that occurred in the microwave-assisted pyrolysis of stearic and oleic acid. This observation agrees with findings from previous studies, which reported that CO_2, CO, and water vapor were linked with deoxygenation of fatty acids (Asomaning et al., 2014b; Maher et al., 2008; Omidghane et al., 2017b).

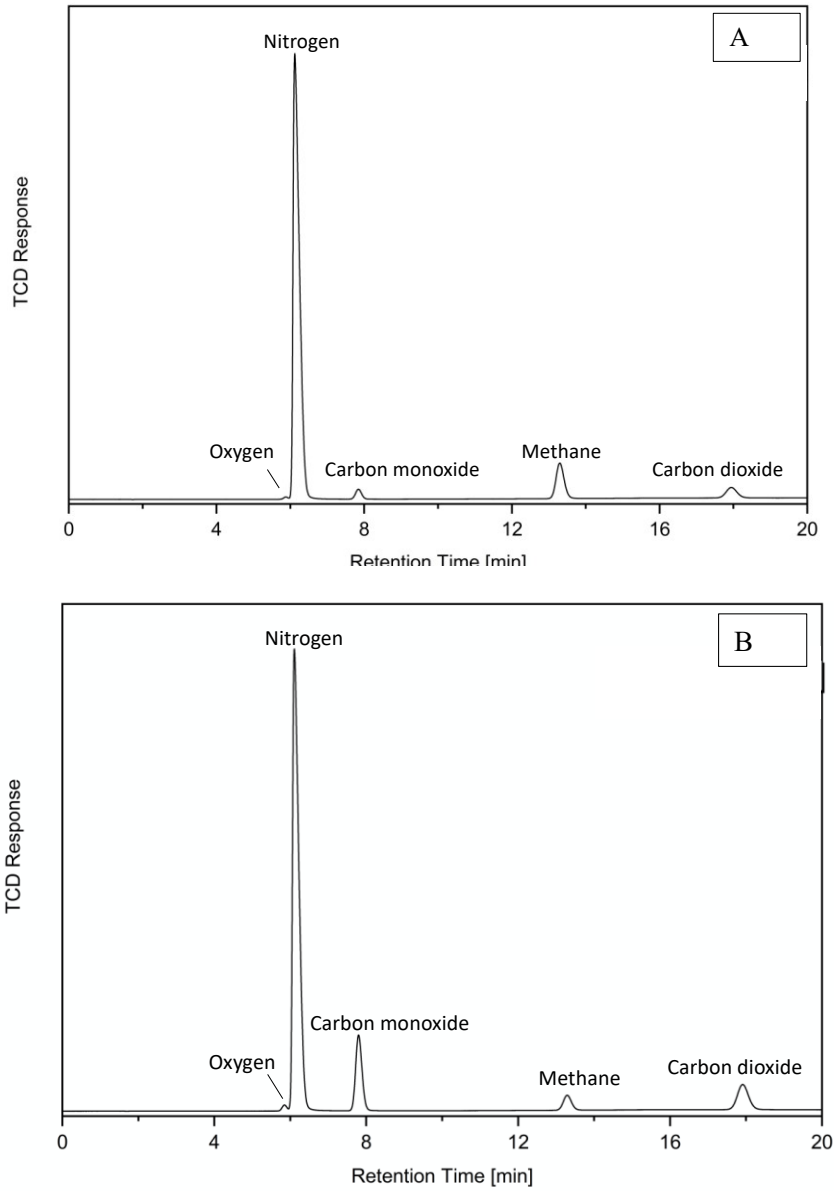

Figure 4-2: The GC-TCD chromatogram of the non-condensable gas fraction (A) stearic acid and (B) oleic acid with silicon carbide (SiC) as heating aid. The reaction was carried out on the 2.45 GHz system at 50% power level (1000 W) and using nitrogen gas at an initial pressure was 100 psi.

Figure 4-3 revealed hydrogen (H_2) in the gas fraction obtained from all the reaction conditions tested. A possible explanation for the observed hydrogen is attributed to the dehydrogenation of 6-carbon cyclic compounds to generate aromatic compounds (Macquarrie et al., 2012). Furthermore, the decarbonylation reaction pathway of the fatty acids results in CO and H_2O compounds. These compounds formed can undergo a forward reaction of the water gas shift to yield CO_2 and H_2. Therefore, this phenomenon can also be used to explain the presence of hydrogen found in the pyrolysis of stearic and oleic acid.

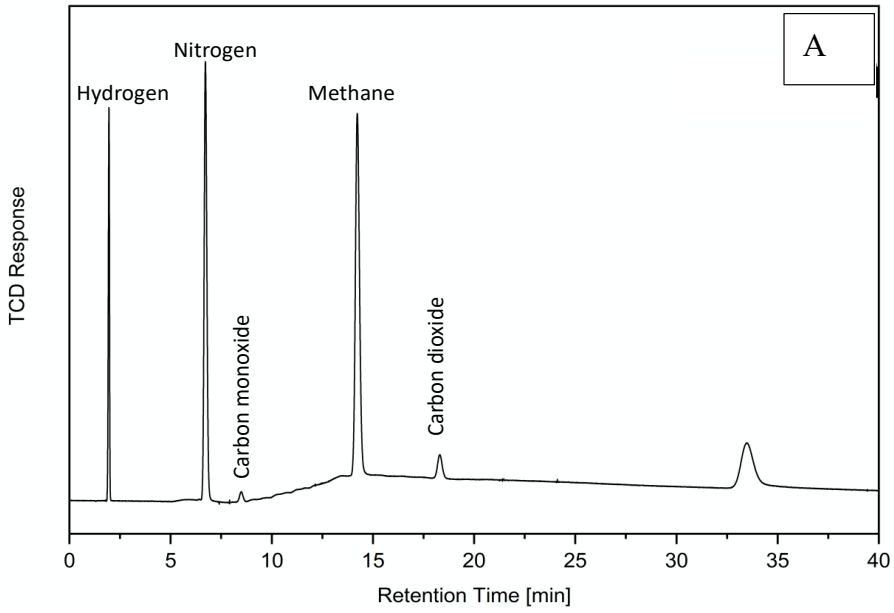

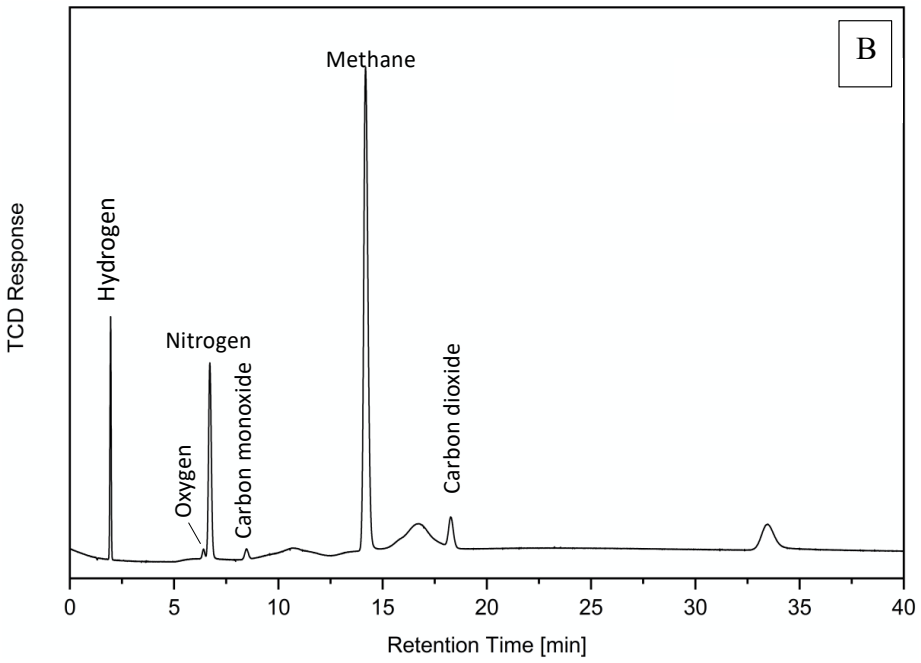

Figure 4-3: The GC-TCD chromatogram shows hydrogen gas present in the non-condensable gas fraction of (A) stearic acid and (B) oleic acid with silicon carbide (SiC) as heating aid. The reaction was carried out on the 2.45 GHz system at 50% power level (1000 W) and using nitrogen gas at an initial pressure was 100 psi. Argon gas was used as the carrier gas in the GC analysis.

4.1.3 Gas hydrocarbon products

Short-chain hydrocarbons ranging from C1 (methane) to C7 (heptane) were found in the gas fraction obtained from the microwave-assisted pyrolysis of stearic acid (A) and oleic acid (B), as shown in **Figure 4-4**. The observed short-chain hydrocarbons are attributed to the cracking effect that occurred during the microwave-assisted pyrolysis of stearic and oleic acid. The cracking effect is due to the breaking of long-chain hydrocarbons to short-chain hydrocarbons. Another plausible explanation is attributed to the direct cracking of fatty acids during the microwave-assisted pyrolysis reaction. In all the conditions tested, the gas product constituents for both oleic and stearic acids were similar. It is worth mentioning that the individual compounds in the gas

product were not quantified as the study sought to provide evidence of deoxygenation and cracking resulting from using microwave-assisted heating in the pyrolysis reaction of model fatty acids (stearic and oleic acids).

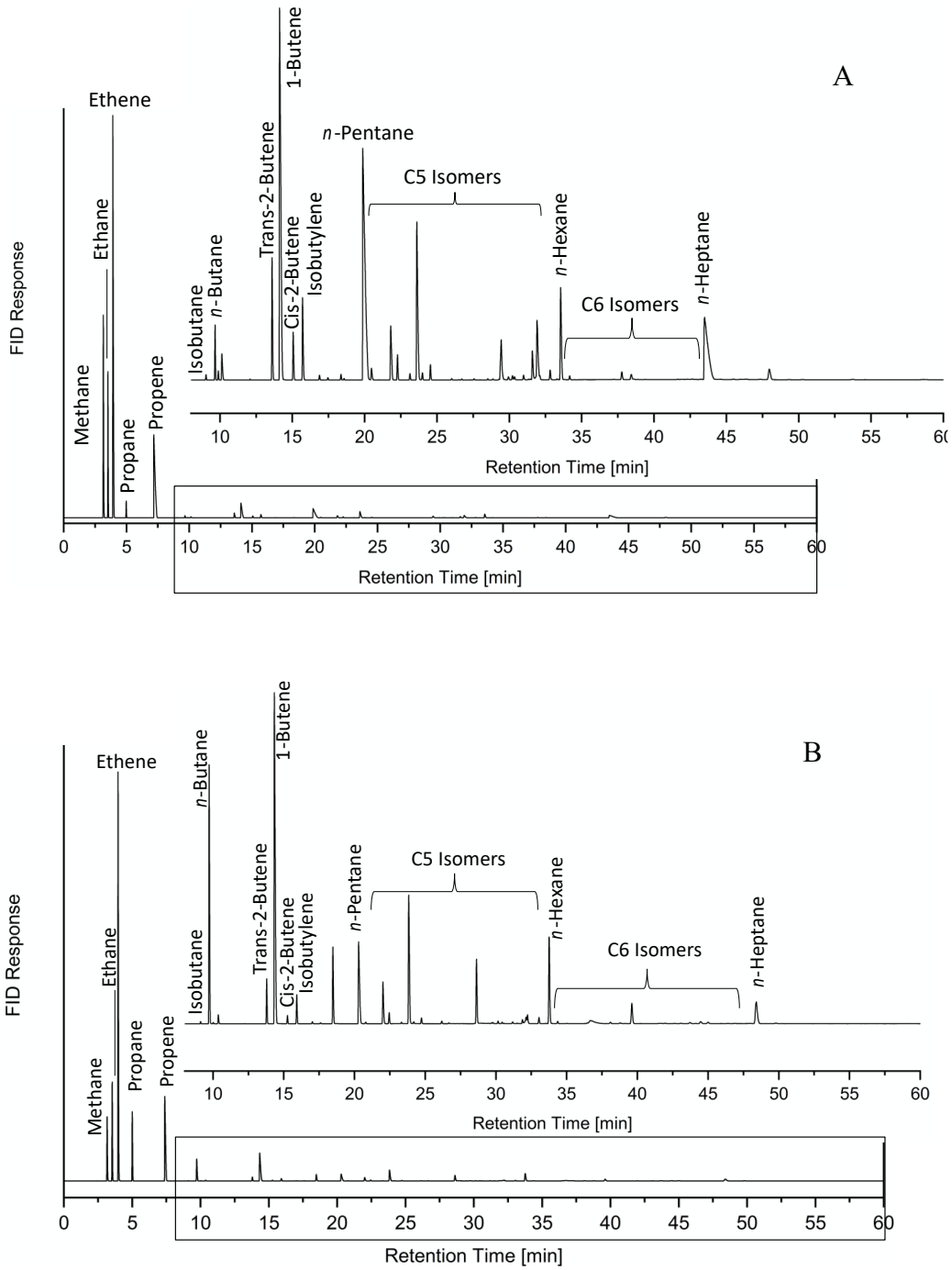

Figure 4-4: The GC-FID chromatogram shows hydrocarbon gases present in the non-condensable gas fractions of (A) stearic acid and (B) oleic acid with silicon carbide (SiC) as heating aid. The Reaction was carried out on the 2.45 GHz system at 50% power level (1000 W) and using nitrogen gas at an initial pressure was 100 psi.

4.1.4 Identification of products in the liquid fraction

The following class of compounds, such as alkenes, alkanes, aromatics, and fatty acids, were identified in the liquid fraction, as shown in **Figure 4.5**. The presence of *n*-heptadecane (C_{17}) observed from the GC analysis for both stearic acid and oleic acid provided additional evidence of fatty acid deoxygenation in the microwave-assisted pyrolysis reaction (Asomaning et al., 2014c; Maher et al., 2008). It is imperative to note that the reaction mechanisms for these model fatty acids (stearic acid and oleic acid) were different.

In a saturated fatty acid reaction mechanism, the deoxygenation reaction pathway precedes the cleavage of the C-C bond of a deoxygenated hydrocarbon into a short-chain hydrocarbon. Whereas, in the unsaturated fatty acid, deoxygenation and cracking of the allylic C-C bond yielding short-chain hydrocarbon and short-chain fatty acid simultaneously occurred. This observation is attributed to the lower bond dissociation energy of the allylic C-C bond compared to the C-C bond next to the carboxyl group (Asomaning et al., 2014a). The double bonds present in the feedstock can influence the pathways of the reaction mechanism.

The short-chain fatty acids seen in the chromatogram are attributed to the long-chain fatty acid feedstock cracking. Also, under the conditions tested, limited conversion was achieved. This was inferred from the presence of stearic and oleic acid as the main components in the liquid product chromatogram, as shown in **Figure 4.5 A** and **Figure 4.5 B**. It is worth mentioning that the individual compounds in the liquid fraction were not quantified, but the goal was to provide

evidence of deoxygenation occurring in a microwave-assisted pyrolysis reaction of model fatty acids (stearic and oleic acids).

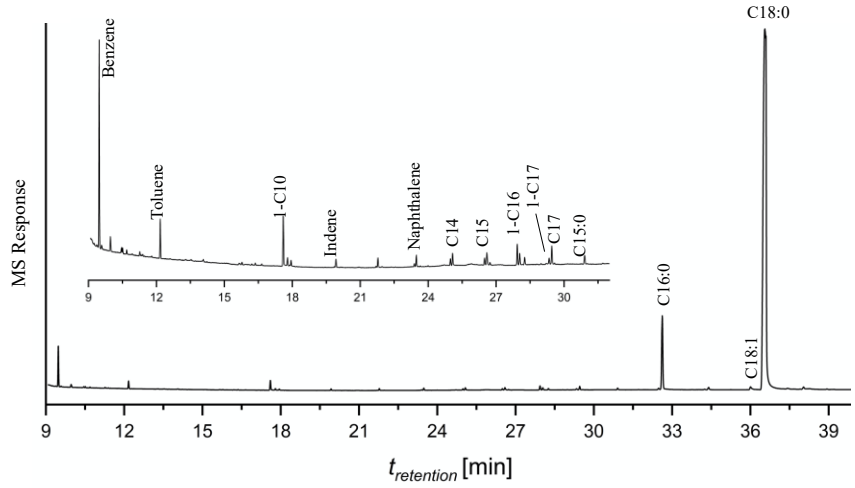

Figure 4-5A: GC-MS chromatogram of stearic acid condensable product. Reaction was carried out on the 2.45 GHz system at 50% power (1000W) with SiC as heating aid.

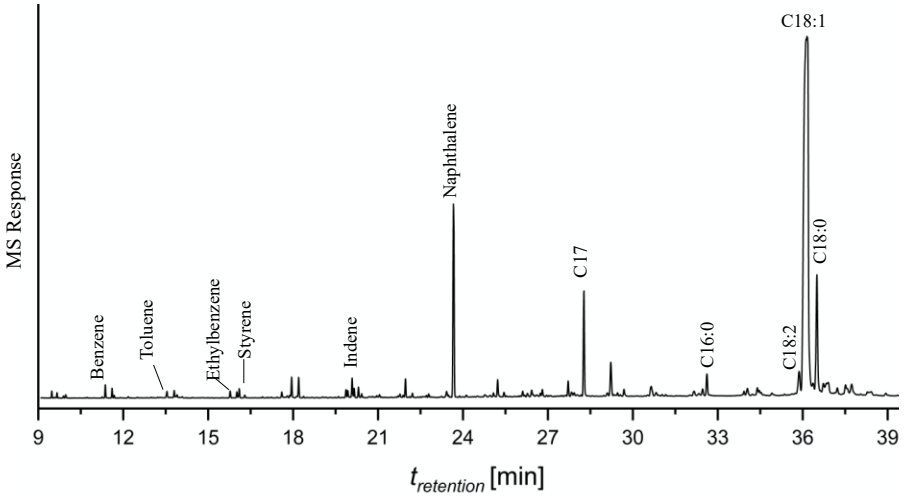

Figure 4-5B: GC-MS chromatogram of oleic acid condensable product. Reaction was carried out on the 2.45 GHz system at 50% power (1000W) with SiC as heating aid.

As shown in **Figure 4-5A** and **Figure 4-5B**, most of the peaks identified were aromatic compounds. Thus, generating some interest in what could be influencing the generation of more aromatic compounds at the reaction condition employed in the microwave-assisted pyrolysis of stearic and oleic acid. As previous studies from the Bressler lab group have demonstrated that increasing reaction temperature favors the yield of aromatic compounds and subsequently resulting in the formation of polyaromatic compounds. A possible explanation for this observation in this study is attributed to the non-uniform microwave distribution, generating hotspots regions in the reactor cavity. The hotspot region tends to have higher temperatures than other regions in the reactor cavity, thus influencing the generation of aromatics compounds and subsequent polyaromatic compounds formation through polymerization. As a result of this, a study was carried out to investigate the heating distribution in the reactor cavity.

4.1.5 Microwave heating distribution with thermal paper at the center of the cavity

This study was conducted to understand the distribution of microwaves transmitted into the reactor cavity using a wet thermal paper and was carried out on the 2.45 GHz system at full power (2000 W) for 8 minutes. The thermal paper was immersed in a beaker of water to act as a microwave absorbing agent. The water molecules on the thermal paper absorbed the microwave energy, and through realigning, collision, and friction, heat was generated within the water molecules. The heat is transferred via conduction to the thermal paper, activating the heat-sensitive dye, which manifested as dark spots on the paper (Kharkovsky and Hasar, 2003). **Figure 4-6** shows the dark spots on the thermal paper as the key finding from this experiment. An explanation for this observation is attributed to the localization of heat (hot spots) on the thermal paper, which indicates that the microwave energy transmitted into the reactor cavity was not uniformly

distributed. In addition, the dark spot indicated regions in the reactor cavity where maximum standing waves are positioned, suggesting the non-uniform microwaves distribution in the cavity.

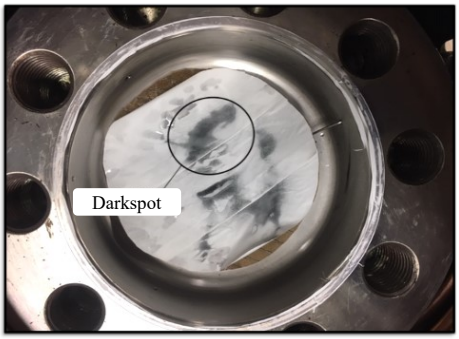

Figure 4-6. The darkspot on the thermal paper represents the regions where hotspots can be found in the reactor vessel.

In conclusion, the preliminary data from the microwave study revealed some critical concerns of the microwave technology as a heat source in the fatty acids conversion process to yield hydrocarbon fuel precursors. The concerns include the fatty acids feedstock used in the pyrolysis process was not absorbing the microwave energy. As a result of this, the need to incorporate silicon carbide (SiC) as a heating aid in the pyrolysis process was essential to absorb the microwave energy. However, the heating aid employed absorbed the microwave more rapidly, and the poor heat transfer of the heating aid to the fatty acids feedstock resulted in hotspots in the reactor. Thus, influencing the formation of aromatic compounds and incomplete conversion of the fatty acids to yield hydrocarbon fuel precursors. Because of this, the microwave-assisted pyrolysis project was not studied in detail. Nevertheless, further investigations to improve the uniform distribution of microwave energy in the reactor and the heat transfer between the heating aid and fatty acids feedstock would be essential to successfully incorporate microwave heating into the existing fatty acids conversion technology. Therefore, given the state of the microwave system,

the second phase of this thesis was initiated, incorporating a catalyst to upgrade crude pyrolysis liquid product to yield liquid hydrocarbon fuel.

4.2. Pyrolysis of oleic acid in the presence of stainless-steel mesh

Before the incorporation of deoxygenation catalysts to remove residual fatty acid in crude pyrolysis liquid product to yield liquid hydrocarbon fuel, this study was conducted to investigate the catalytic effect of the stainless-steel materials of the microreactor used in oleic acid pyrolysis, focusing on the liquid product composition. This stainless-steel study is important because metals such as nickel, aluminum, iron, and chromium, used as an alloy in making stainless steel, have been employed as active sites on catalytic support for catalytic deoxygenation reactions. Therefore, understanding the inert nature of the stainless steel microreactors is important. In this study, a disc-shaped stainless-steel mesh was incorporated into the pyrolysis of oleic acid at a set temperature of 430 ˚C for 2 hours, in an inert initial atmospheric pressure.

4.2.1 Mass balance

The product distribution obtained from the oleic acid pyrolysis in the presence of stainless-steel mesh were solid, liquid, and gaseous products. The liquid product was the dominant product, followed by the gas and the solid product. The outcome from this study revealed that the various treatments applied to the stainless-steel mesh when compared to each other were statistically similar for the product distribution. It is worth mentioning that the comparison was made within each product category obtained from the oleic acid pyrolysis reaction, as shown in **Figure 4-7.**

The gas product is a non-condensable volatile formed from the pyrolysis reaction of oleic acids under the presence of stainless-steel mesh. The gas product yield was determined by the difference in the microreactors' weight before and after venting the gas. Conversely, the liquid

product was determined using the difference of the gas and solid product from the initial feed weight. The polymerization of aromatic compounds to yield polyaromatic compounds, a precursor for coke formation, was used to explain the presence of solid products obtained from the pyrolysis of oleic acid (Asomaning et al., 2014b).

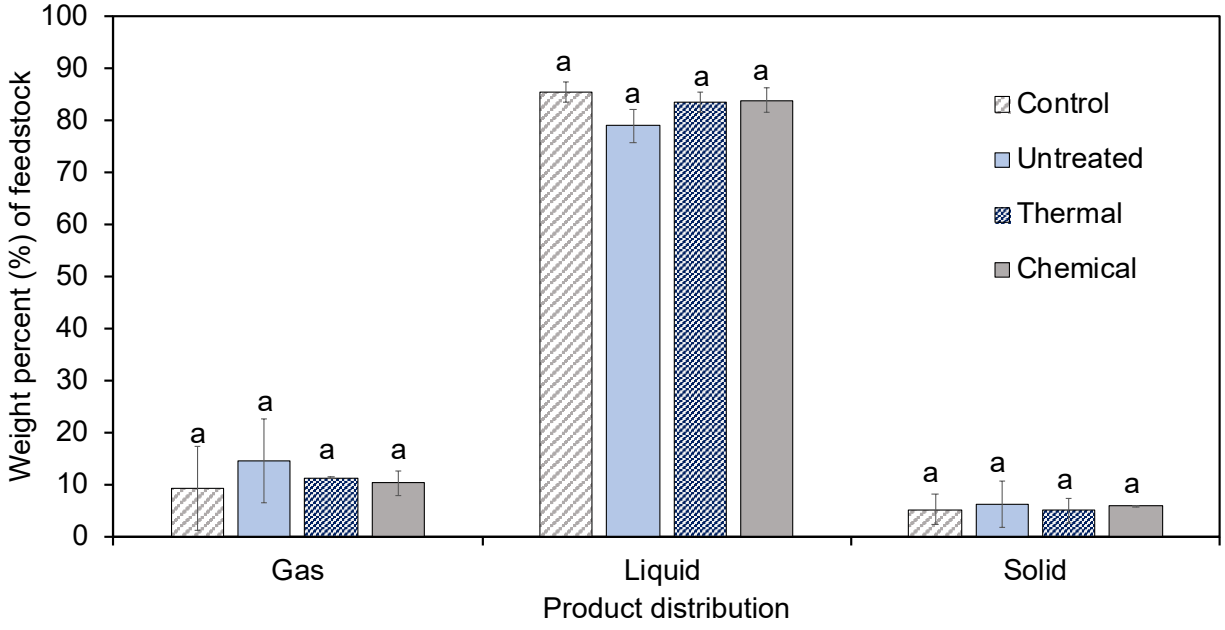

Figure 4.7. The distribution of the pyrolysis product obtained from oleic acid pyrolysis conducted at 430 ˚C for 2 hours using different treatments on stainless-steel mesh. Bar chart represents mean ± standard deviation with n =3. Bars with the same letter within a product category are statistically similar using Tukey test at 95% confidence level.

4.2.2 Gas Composition

The gaseous product was analyzed using a suite of gas chromatograph (GC) instruments equipped with FID and TCD detectors to determine the individual constituents. The GC-TCD analysis showed the presence of carbon dioxide (CO_2), and carbon monoxide (CO) compounds in the gas fraction obtained from all the reaction conditions tested, as shown in **Figure 4.8**.

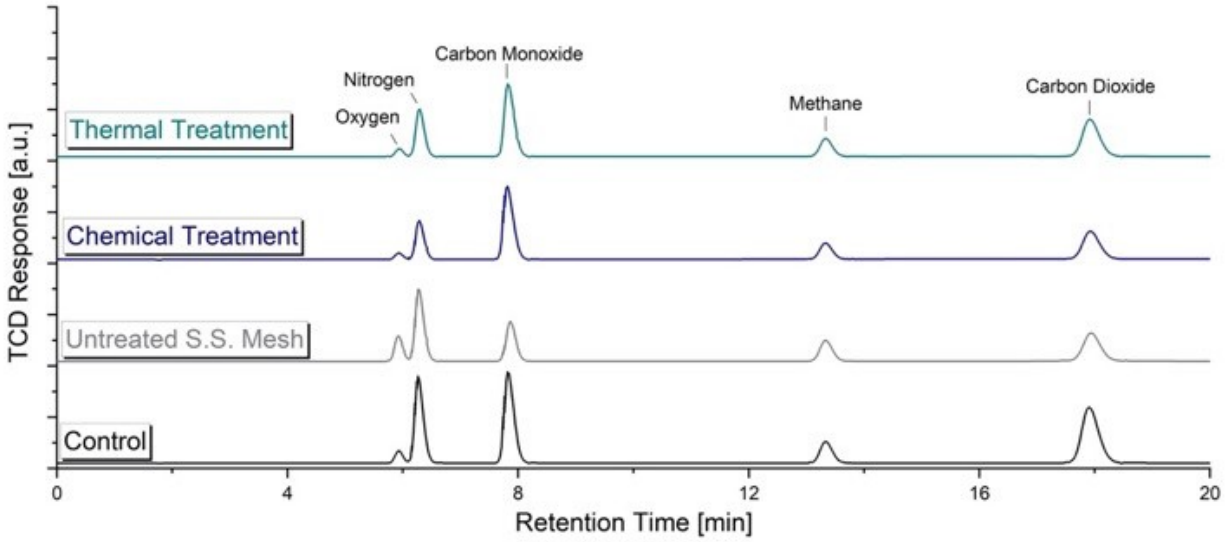

Figure 4.8. GC-TCD chromatogram obtained from the oleic pyrolysis. Chromatogram shows the presence of CO and CO_2 deoxygenation compounds in the gas product from the pyrolysis reaction carried out at 430 ˚C for 2 hours. NB. Control (no mesh used), Untreated (mesh used as received).

The presence of CO_2 and CO, as shown in **Figure 4-8**, provided evidence of deoxygenation reaction pathway occurring from the oleic acid pyrolysis in the presence of stainless-steel mesh. The formation of CO_2, a product of decarboxylation, resulted from the cleavage of the carboxyl group in the oleic acid, which removed two oxygen molecules with a carbon atom present in the carboxyl group of the oleic acid. At the same time, the CO, a product of decarbonylation, is formed from the removal of one oxygen from the carboxyl group. This observation agrees with the previous research findings (Asomaning et al., 2014b; Na et al., 2010; Stefanidis et al., 2016) as they found CO_2 and CO in the gas phase as evidence of deoxygenation reaction occurring. The mole ratio of the CO and CO_2 obtained from all the treatments tested were statistically similar, as shown in **Figure 4-9.**

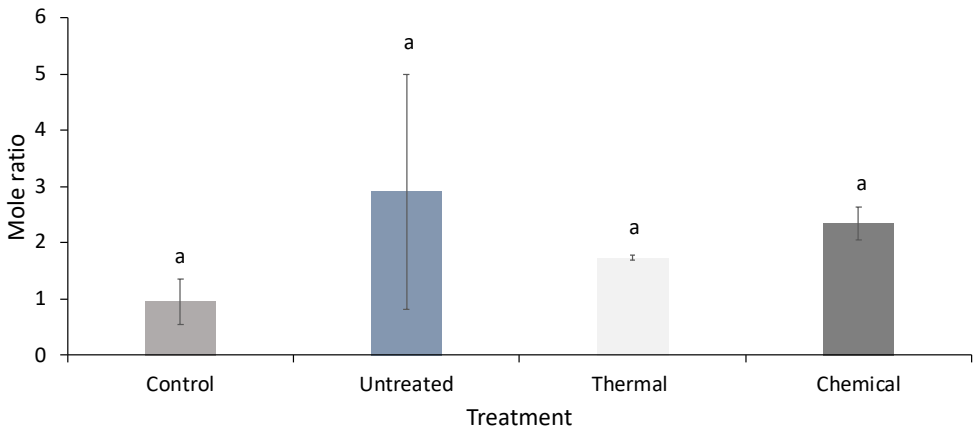

Figure 4-9. Mole ratio of CO and CO_2 in the gaseous product. The mole ratio of carbon monoxide to carbon dioxide of the gaseous product obtained from oleic acid pyrolysis in the presence of stainless-steel mesh at a reaction condition of 430 ˚C for 2 hours. Data represent mean ± standard deviation with n = 3. Bars with the same letter are statistically similar using Tukey test at 95% confidence level is no significant difference at 95% confidence level.

In addition, the GC-TCD analysis showed the presence of hydrogen in the gas product obtained from all the reaction conditions tested, as shown in **Figure 4-10.** The presence of hydrogen can be attributed to the dehydrogenation of 6-carbon number cyclic hydrocarbons to yield aromatic compounds (Omidghane et al., 2017a). Also, the hydrogen observed in the gas product can further be explained from the forward reaction of the water-gas shift reaction (WGSR). During this reaction, carbon monoxide reacts with water vapor to yield carbon dioxide and hydrogen. Cracking long-chain compound results from the breaking of C-H bonds can liberate hydrogen (Dupain et al., 2007).

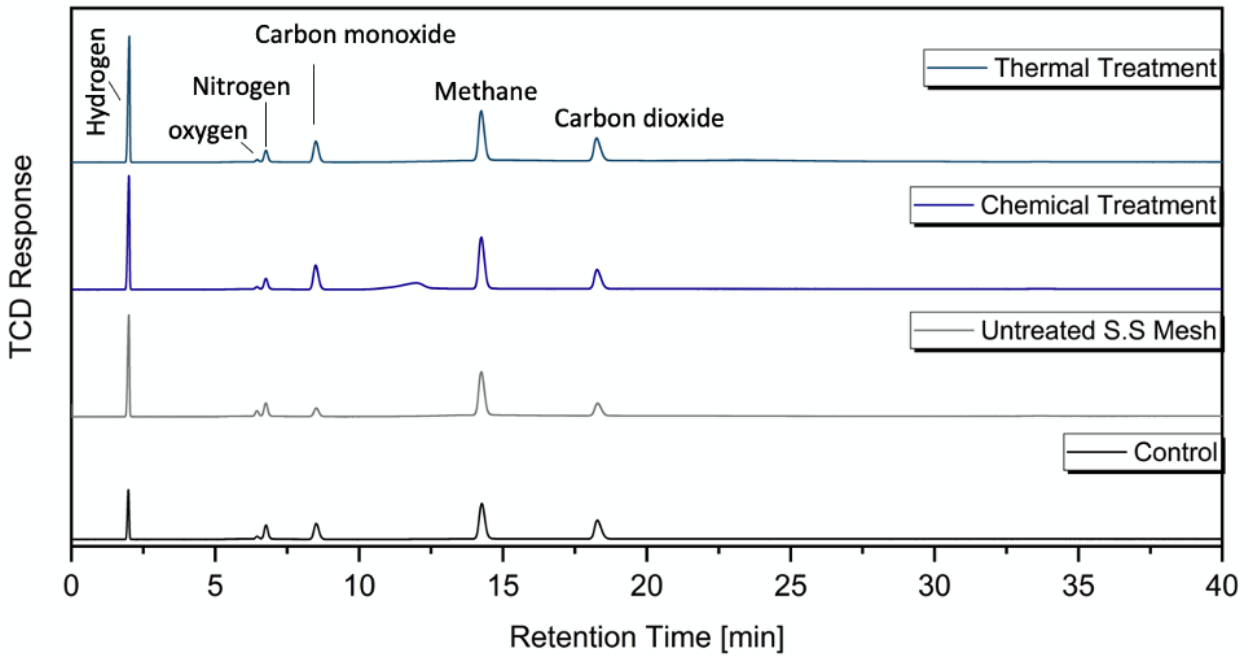

Figure 4-10. GC-TCD chromatogram showing hydrogen gas presence. The oleic acid stainless-steel mesh pyrolysis at a reaction condition of 430 ˚C for 2 hours. Yielded the formation of hydrogen gas. NB. Control (no mesh used), Untreated (mesh used as received).

The gas analysis confirmed the presence of hydrocarbons ranging from C1 to C7 in the gas product obtained from the pyrolysis of oleic acid, as shown in **Figure 4-11**. The hydrocarbon compound observed from the gas analysis were present in all treatments tested. Long-chain hydrocarbon cracking can be used to explain the presence of short-chain hydrocarbons (Maher et al. 2008). Also, the direct cracking of fatty acids resulting in short-chain hydrocarbons and fatty acids during oleic acid pyrolysis can be used to explain the presence of hydrocarbons in the gas product.

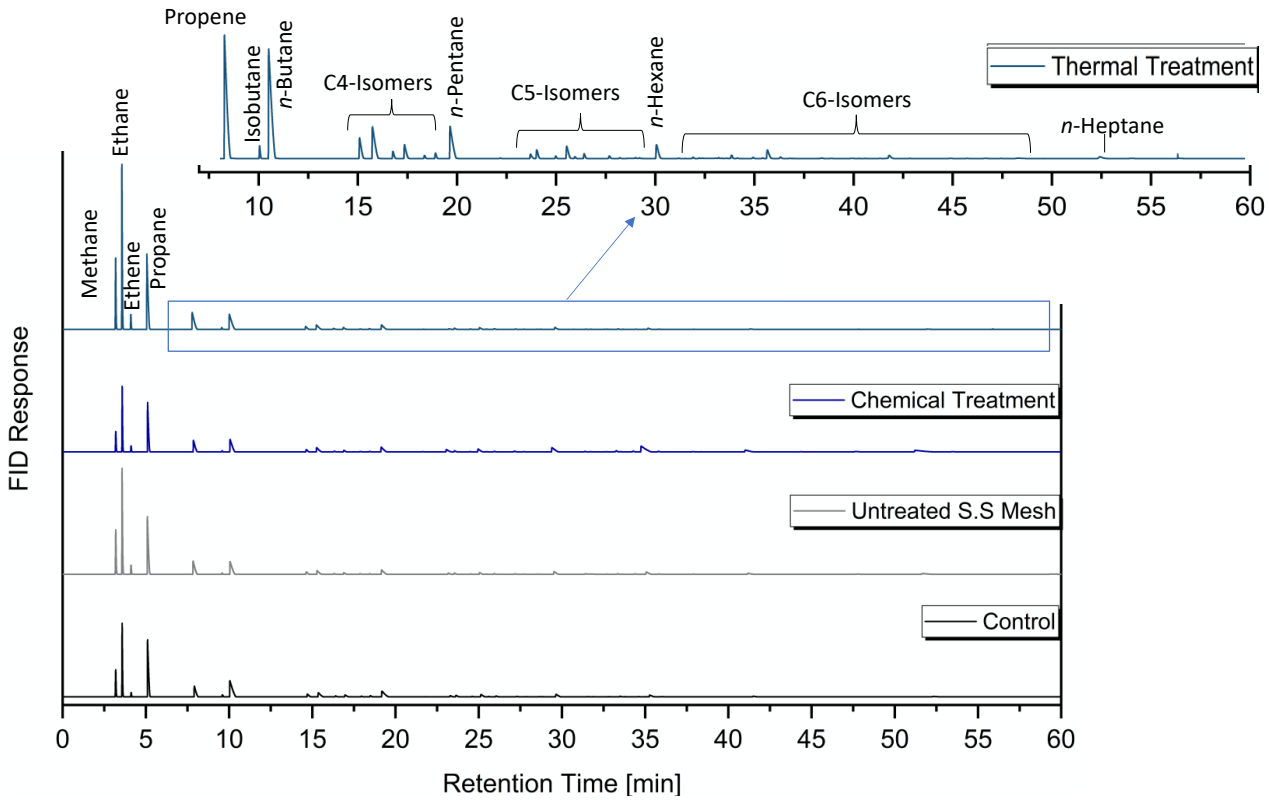

Figure 4-11. GC-FID chromatogram showing hydrocarbon gases. The oleic pyrolysis under the presence of stainless-steel mesh showing the presence short-chain hydrocarbon compounds in the gas product indicating cracking mechanism of long-chain hydrocarbon compounds from the pyrolysis reaction carried out at 430 ˚C for 2 hours. NB. Control (no mesh used), Untreated (mesh used as received).

4.2.3 Components in the liquid product

As mentioned in **session 4.2.1**, the liquid product obtained was analyzed using GC-MS and GC-FID to identify and quantify the individual compound classes. It is worth indicating that due to the high unidentified fraction observed from the GC-MS analysis of the liquid product obtained from all the treatments studied. The discussion of the liquid constituents was based on the identified compound class in the liquid product. The identified compound classes found in the liquid product were alkanes, alkenes, aromatics, branched and cyclic hydrocarbon, and residual

fatty acid. The quantification results from the GC-FID analysis in all the reaction conditions tested showed that the stainless-steel mesh treatments were statistically similar in each compound class.

Figure 4-12 showed that *n*-alkanes were the most abundant in the liquid product among the class of compounds identified. A plausible explanation for the presence of *n*-alkanes is attributed to the cracking of long-chain fatty acids and hydrocarbons through a free radical mechanism. Also, the saturation of alkenes could be one of the plausible reasons for the formation of alkanes in the liquid product obtained from the pyrolysis of oleic in the presence of a stainless-steel mesh. These results agree with the research findings of (Asomaning et al., 2014b; Omidghane et al., 2017b).

The total yield of aromatic compounds was statistically similar in the liquid product obtained in all treatment tested, as shown in **Figure 4-12**. An explanation for this observation is due to the dehydrogenation of cyclic alkanes and alkenes with a six-carbon number to yield aromatic compounds. The amount of residual fatty acids in the crude pyrolysis liquid product found in all the treatments tested were statistically similar. A possible reason for the presence of residual fatty acids is attributed to long-chain fatty acids cracking into short-chain fatty acids that did not undergo deoxygenation (Asomaning et al., 2014b; Maher et al., 2008). Furthermore, unreacted feedstock in the liquid product was accounted to be part of the total residual fatty acids in the liquid product.

The cyclic hydrocarbon predominantly found in the liquid product for all the treatment tested were C5 (cyclopentanes and cyclopentenes) and C6 (cyclohexanes and cyclohexenes). The amount of cyclic hydrocarbon in the liquid product was statistically similar for all the treatments tested.

In summary, the semi-quantitation analysis of the liquid product constituents revealed that the presence of the stainless-steel mesh and the stainless-steel reactor material used in the oleic acid

pyrolysis reaction was inert and had no catalytic effect on the product distribution and liquid product composition.

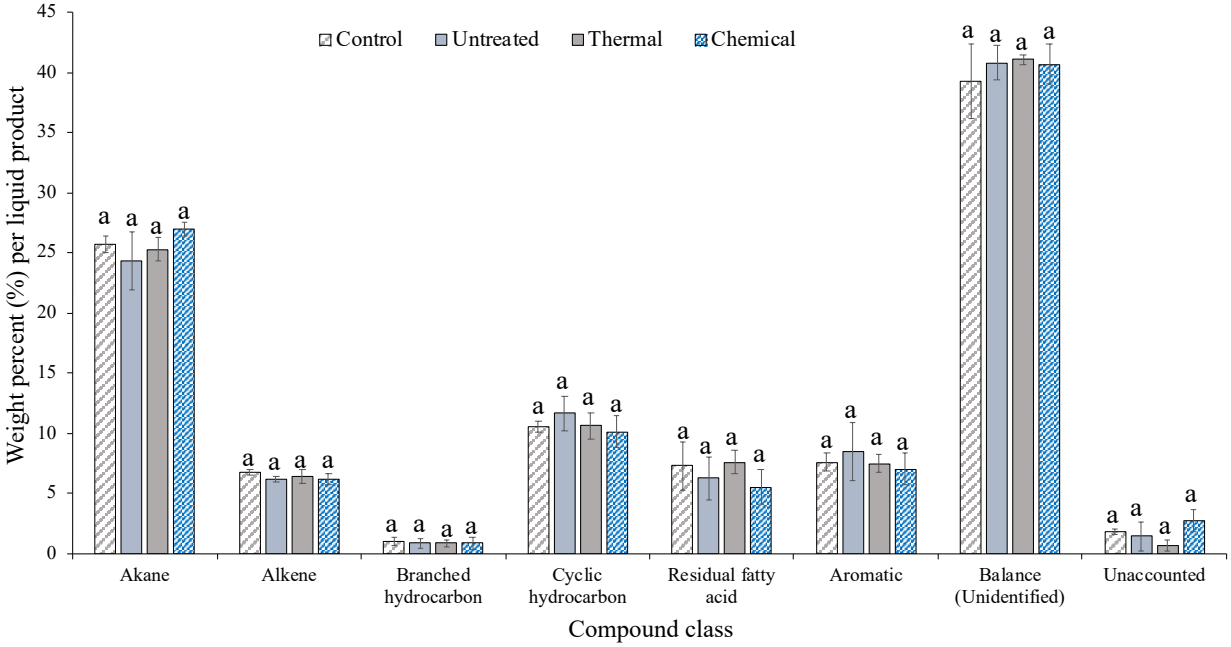

Figure 4-12. The compound classes in the liquid product. The oleic acid pyrolysis in the presence of stainless-steel mesh. At a reaction condition of 430 ˚C for 2 hours at an atmospheric inert pressure yielded liquid product. Data represent mean ± standard deviation with n = 3. Bars with the same letter within a compound class are statistically similar using Tukey test at 95% confidence level. NB. Control means no stainless-steel mesh was used; untreated (stainless-steel mesh was used without any further treatment).

4.3 Catalytic deoxygenation of acids in crude pyrolysis liquid in a 15 mL batch microreactor

The evaluation of the study described in **section 4.2** showed that the incorporation of stainless-steel mesh and the stainless-steel microreactor had no catalytic effect on the product distribution and liquid product composition. However, the presence of residual fatty acid in the crude pyrolysis liquid product may limit the direct utilization in petroleum infrastructures if not

removed. Therefore, commercially available catalysts such as nickel on silica-alumina, platinum on silica, silica support, and silica-alumina support were incorporated into the existing fatty acid conversion technology in the Bressler lab to deoxygenate the residual fatty acids in crude pyrolysis liquid product to yield liquid hydrocarbon fuel. In this study, 1 gram of crude pyrolysis liquid product was treated with 0.2 grams of each catalyst at different reaction times, such as 0.5, 1, and 2 hours and at a set temperature of 350 ˚C.

4.3.1 Product distribution

The following products such as gas, liquid and solid fractions were found in catalytic deoxygenation of residual fatty acids in the crude liquid product. As shown in **Figure 4-13,** the gas yield obtained at 2 hours reaction time for the two catalysts treatment (platinum on silica and nickel on silica-alumina catalyst) significantly increased compared to other treatments subjected to the crude pyrolysis liquid product. At the same time, the gas product yield from the catalytic supports and the uncatalyzed treatment were statistically similar. Interestingly, at 0.5 and 1 hour treatment, the gas yield of the nickel on silica-alumina catalyst significantly increased compared to other catalytic treatments, suggesting that the nickel on silica-alumina catalyst influenced the yield of the gas fraction in the reaction conditions tested. A possible explanation for this observation is attributed to the fact that increasing reaction time from 0.5 to 2 hours extended the interaction time of the crude pyrolysis liquid product with the catalyst's active site, thus increasing the gas product yield.

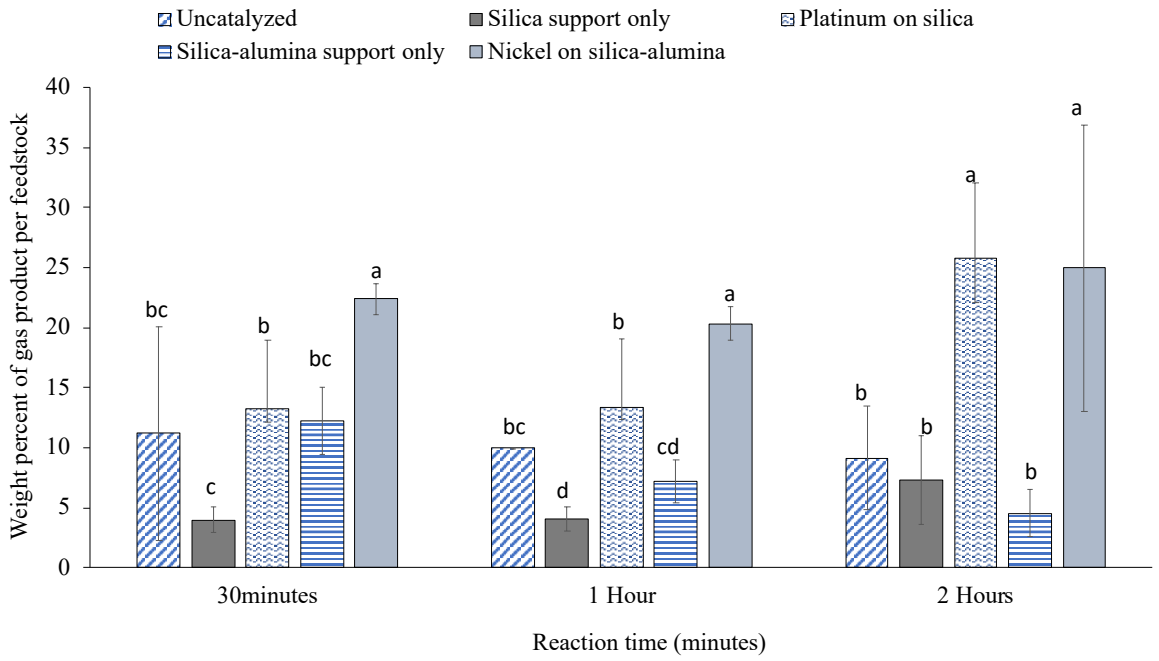

Figure 4-13. Gas product distribution for varying reaction times. The gas yield obtained from catalytic pyrolysis of crude pyrolysis liquid product to remove residual fatty acid present at reaction temperature of 350 ˚C and with different reaction times (0.5 to 2 hours). The bar chart represents the mean ± standard deviation with n = 3. Treatment bars with the same letter within each reaction time are statistically similar using Tukey test at 95% confidence level.

Figure 4-14 shows the liquid product obtained in all the reaction condition tested. At 2 hours of reaction time, the liquid yield obtained from the platinum on silica and nickel on silica-alumina catalyst substantially decreased, compared with other treatments such as uncatalyzed, silica support, and silica-alumina support.

Interestingly, the yield of liquid product generated from the nickel on silica-alumina treatment at 1 – hour significantly decreased compared to the liquid product obtained from other treatments (platinum on silica, catalytic supports, and uncatalyzed). At 30 minutes, the yield of the liquid product obtained in all the treatment tested were statistically similar.

The decrease in the yield of the liquid product obtained from the nickel on silica-alumina catalyst can be linked to the increasing gas product as the reaction time increased from 30 minutes to 2 hours.

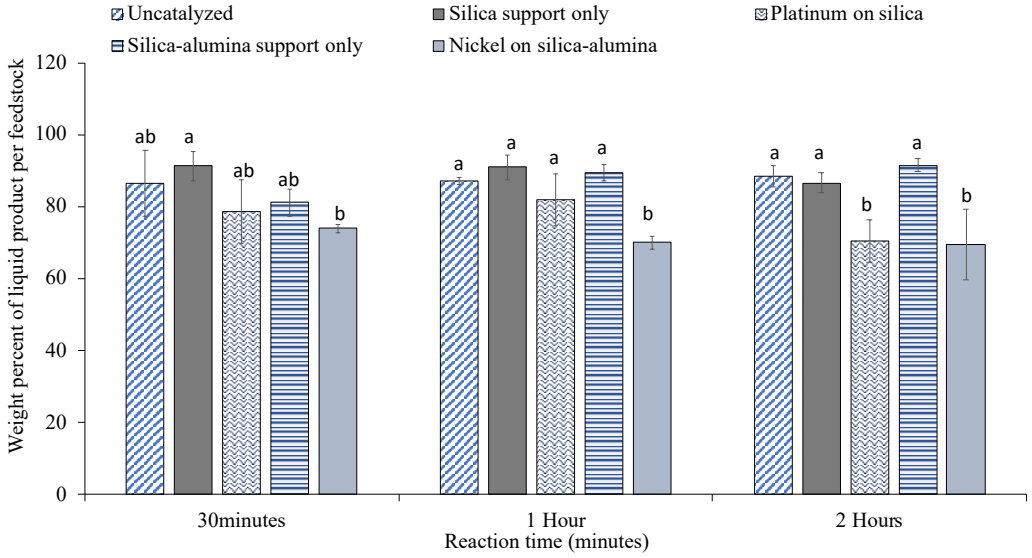

Figure 4-14. Liquid product distribution for varying reaction times. The liquid yield obtained from the catalytic pyrolysis of crude pyrolysis liquid product to remove residual fatty acid at a reaction temperature of 350 ˚C and with different reaction times (0.5 to 2 hours). The bar chart represents the mean ± standard deviation with n = 3. Treatment bars with the same letter within each reaction time are statistically similar using Tukey test at 95% confidence level.

The product distribution of the catalytic pyrolysis reaction resulted in solids in all the reaction conditions tested. It is worth mentioning that pentane-insoluble were accounted as part of the solid yield from the catalytic deoxygenation of crude pyrolysis liquid products. The formation of the solid from the catalytic upgrading of crude pyrolysis liquid products is due to the polymerization of aromatics compounds (Iliopoulou et al., 2019). A similar result reported elsewhere showed that the incorporation of catalyst in deoxygenation reaction decreases the liquid

yield product while increasing the gas and solid product yield (Lopez-Urionabarrenechea et al., 2012; Syamsiro et al., 2014).

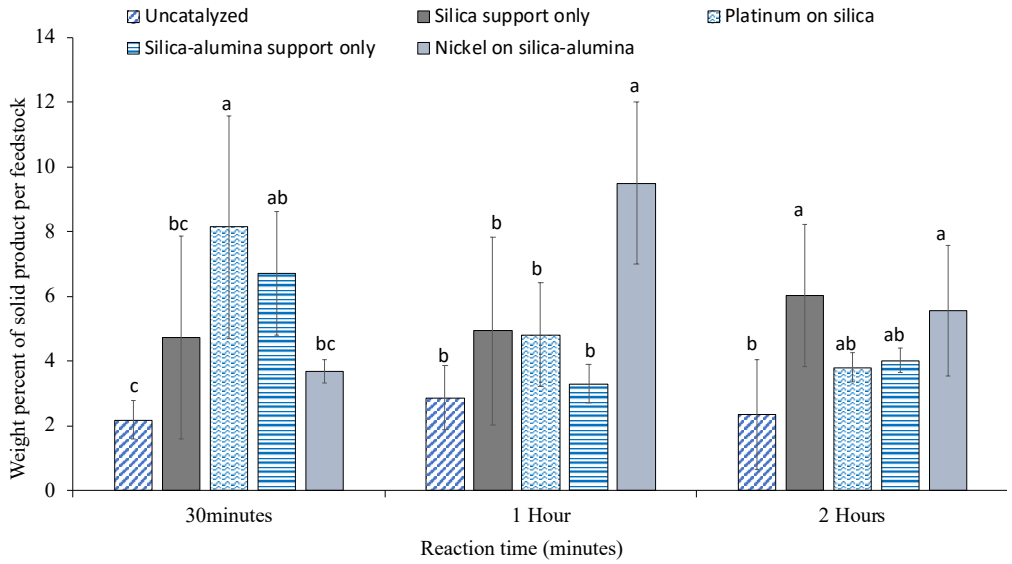

Figure 4-15. The solid yield distribution for varying reaction times. The solid yield obtained from the catalytic pyrolysis of crude pyrolysis liquid product to remove residual fatty acid at a reaction temperature of 350 ºC and with different reaction times (0.5 to 2 hours). The bar chart represents the mean ± standard deviation with n = 3. Treatment bars with the same letter within a reaction time were statistically similar using Tukey test at 95% confidence level.

The liquid product obtained from this study was the product of interest. Therefore, the following analysis, such as GC-MS, GC-FID, and FTIR, was conducted on the pentane-dissolved liquid product to understand the removal of residual fatty in the crude pyrolysis liquid product using deoxygenation catalyst. Also, this step of the study was important to provide the needed information on the functional groups and the individual compound classes in the pentane-dissolved liquid product.

4.3.2 Characterization of pentane-soluble liquid product using FT-IR and GC-FID/ GC-MS

FTIR analysis was performed on the pentane-dissolved liquid product obtained from all the reaction conditions tested to provide evidence on removing residual fatty acid in the crude pyrolysis liquid product to yield hydrocarbon fuel.

As shown in **Figures 4-16**, **4-17,** and **4-18**, all the bands in the pentane-dissolved liquid product was between 650 to 2956 cm^{-1} wavenumbers. In all the reaction conditions tested, the peak position was similar, with some minor exceptions in some peak intensities. It should be noted that the FTIR spectra generated from the pentane-dissolved liquid product were compared to the FTIR spectra generated from a caustic washed pyrolysis liquid product.

The FTIR spectra can be classified into two regions as the diagnostic region and the fingerprint region. The diagnostic region lies above the 1500 cm^{-1} wavenumber, whereas the fingerprint region lies below the 1500 cm^{-1} wavenumber. The sample FT-IR peaks characterization was done by matching them with standard characteristic IR absorption peaks (Richardson, 2011). The most substantial sharp peaks found at 2854, 2922, and 2956 cm^{-1} were attributed to the sp^3 C-H stretch corresponding to the alkanes in the pentane dissolved liquid product. A medium peak found at 1712 cm^{-1}, which lies within the wavenumber range of 1760-1690 cm^{-1}, corresponds to the C=O stretch for the carbonyl group in a carboxylic acid. Another medium peak was observed at 1458 cm^{-1}, which lies within 1500-1400 cm^{-1} wavenumber corresponds to C=C stretch for aromatic hydrocarbon. The peak found at 1378 cm^{-1} was assigned to the C-H bend in alkanes. Peaks found at 965 cm^{-1} wavenumbers corresponding to =C-H bend in alkenes compound.

The FTIR spectra obtained from this study were similar to peak patterns reported elsewhere (Rehan et al., 2017; Siddiqui et al., 2009).

Increasing reaction time from 0.5 to 2 hours saw a variation in the carbonyl (C=O) peak intensities in all the catalysts used in the deoxygenation reaction. As shown in figure 4-16, the absence of the C=O peaks in the FTIR spectra of the nickel on silica-alumina catalyst treatment indicated the successful removal of residual fatty in the crude pyrolysis liquid product. Whereas, in the platinum on silica and the catalytic support used (silica and silica-alumina) treatments, the C=O peak was present in the FTIR spectra, denoting that the removal of residual fatty acids was not complete.

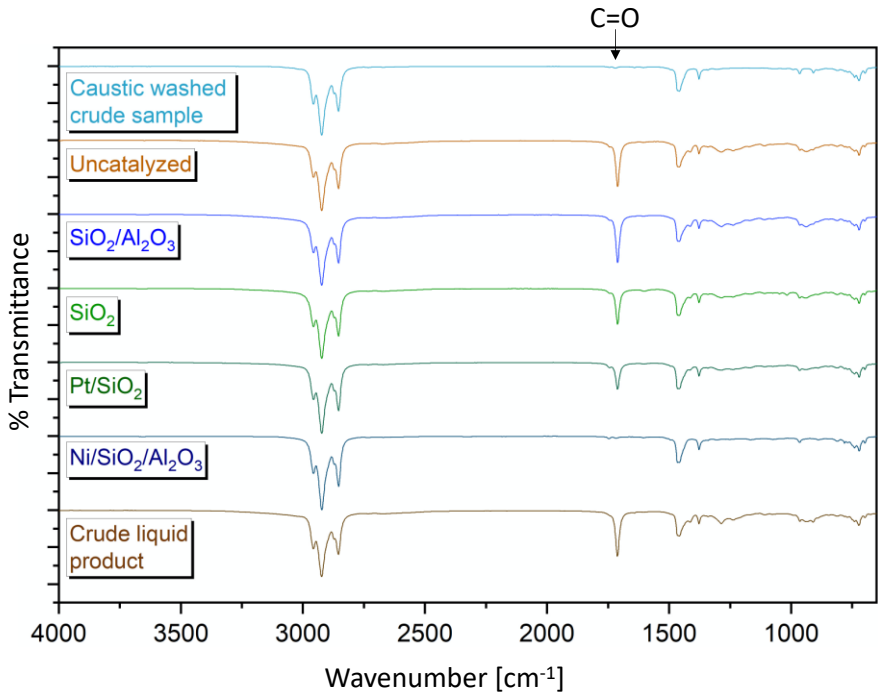

Figure 4-16. FTIR spectra for liquid product collected after 2 hours catalytic deoxygenation reaction. The C = O carbonyl stretching vibrations indicate the residual fatty acids present in the liquid product after the deoxygenation of crude pyrolysis liquid product in all reaction conditions tested.

Conversely, in the 0.5- and 1-hour FTIR spectra, the carbonyl (C=O) peak was present in the liquid fraction obtained in all the treatments tested, as shown in **Figures 4-17** and **4-18**. The different C=O peak intensities in the FTIR spectra displayed the progress of residual fatty acids removal via catalytic deoxygenation reaction. This observation suggests that decreasing reaction time reduced the interaction of the reactant with the catalyst's active sites, which resulted in an unsuccessful removal of residual fatty acids in the crude pyrolysis liquid product.

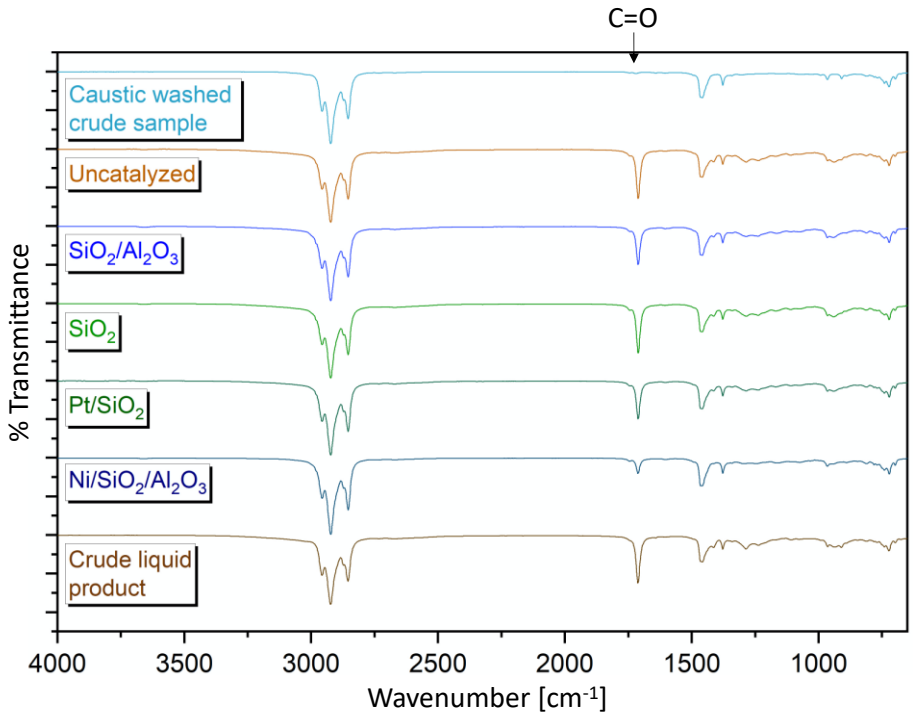

Figure 4-17. FTIR spectra for liquid product collected after 1-hour catalytic deoxygenation reaction. The C = O carbonyl stretching vibrations indicate the residual fatty acids present in the liquid product after the deoxygenation of crude pyrolysis liquid product in all reaction conditions tested**.**

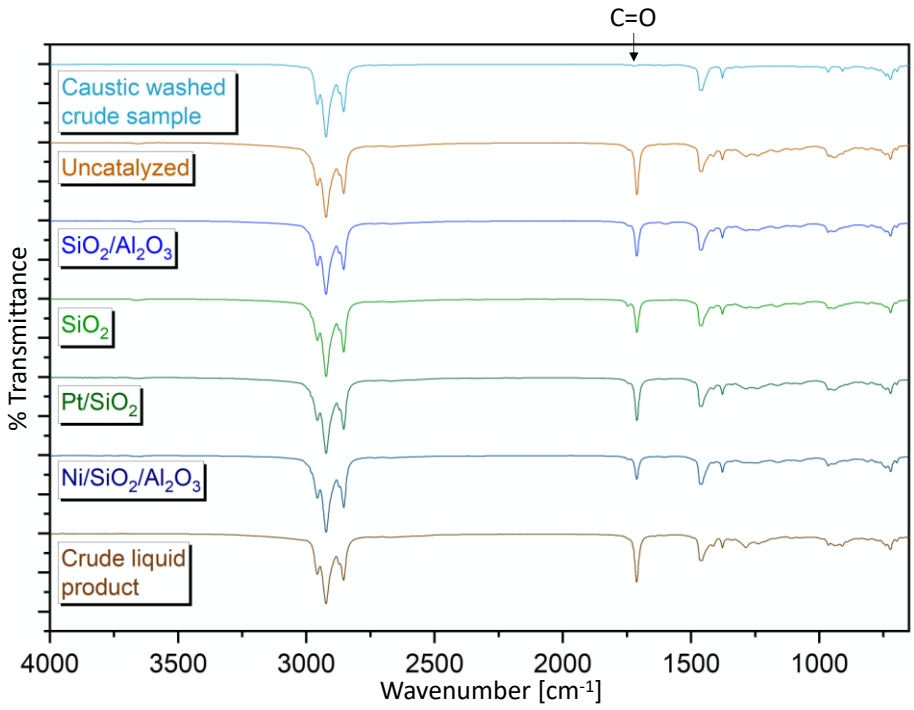

Figure 4-18. FTIR spectra for liquid product collected after 30 minutes of catalytic deoxygenation reaction. The C = O carbonyl stretching vibrations indicate the residual fatty acids present in the liquid product after the deoxygenation of crude pyrolysis liquid product in all reaction conditions tested.

Interestingly, the intensity of the C=O peak in the liquid fraction of the uncatalyzed treatment was similar to the untreated crude pyrolysis liquid product obtained in the 0.5- and 1-hour reaction times tested. However, in the case of the platinum on silica and the nickel on silica-alumina catalysts, the C=O peak was present but significantly decreased, suggesting that the removal of residual in the crude pyrolysis liquid was not successful at the 0.5- and 1-hour reaction time.

In summary, the FTIR analysis step performed in this study revealed that the nickel on silica catalyst at 2 hours treatment resulted in the successful removal of residual fatty acids in the crude pyrolysis liquid product yielding liquid hydrocarbon fuel.

4.3.3 Identification of constituents in the liquid product

The individual compounds in the liquid product were identified using procedures described in **session 3.5.1.** Most of the identified peaks in all the treatments employed were *n*-alkanes, 1-alkenes, and internal alkene, and a fatty acid. It is worth stating that the distribution of the individual compound in the liquid product was dependent on the reaction conditions such as time and the type of catalyst used in the deoxygenation of residual fatty acids in crude pyrolysis liquid products.

As shown in **Figure 4-18**, the main *n*-alkane peak patterns observed was similar in all the reaction conditions tested. Fatty acids peaks was seen in the platinum on silica catalyst, and the catalytic supports tested. Whereas in the nickel on silica-alumina ($Ni/SiO_2/Al_2O_3$) catalyst treatment, the fatty acids peaks was absent, suggesting successful removal of residual fatty acids in the crude pyrolysis liquid product. This observation confirmed the disappearance of the carbonyl peak in the FTIR spectra, as discussed in session **4.3.2.**

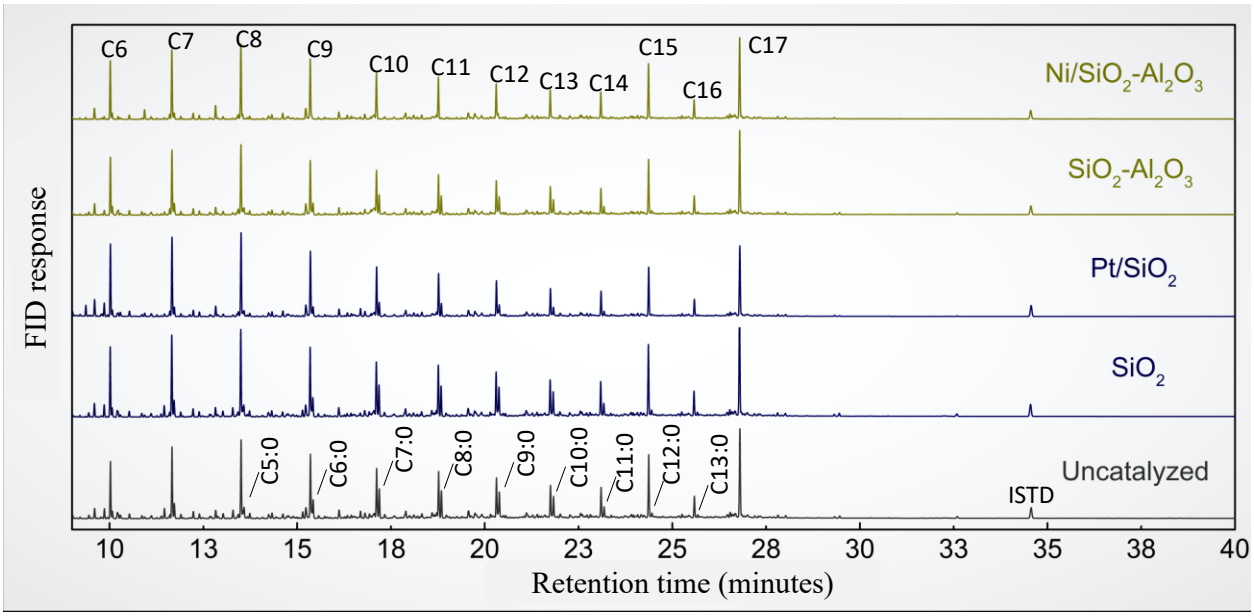

Figure 4-18. The 2 hours GC-FID chromatogram shows the individual constituents in the liquid product. The deoxygenation of crude pyrolysis liquid product at a reaction time of 2 hours

using different commercially available catalyst and their respective supports. NB. ISTD refers to the internal standard used in quantification. Also, the C_6 to C_{17} refers to the carbon number of compounds identified.

4.4.4 Alkane product

The *n*-alkane compounds were targeted to be the product of interest in the catalytic deoxygenation of residual fatty acids in a crude pyrolysis liquid product. The *n*-alkanes with carbon numbers ranging from $C_6 - C_{17}$ were identified. It should be noted that the feed used in this study already contained the *n*-alkanes.

As shown in **Figure 4-19**, *n*-alkanes obtained from the nickel on silica-alumina treatment increased from 41.7 to 46.6 wt.% as the reaction time increased from 0.5 to 2 hours. A similar trend was observed in the platinum on silica treatment, with the *n*-alkanes increasing from 39.8 to 44.3 wt.%. An explanation for this observation is that as reaction time increases, the catalytic activity is enhanced, resulting in a longer contact time of the reactants and the catalyst's active sites resulting in the decarboxylation of the residual fatty acids into liquid hydrocarbons (Yang and Carreon, 2017b).

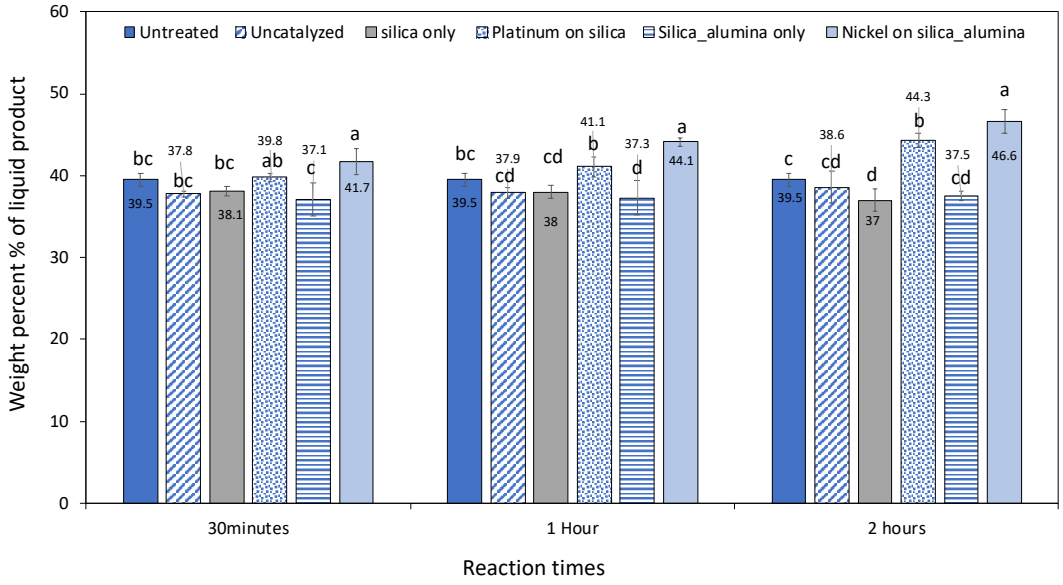

Figure 4-19. The C6 – C20 alkanes composition of pentane-soluble liquid pyrolysis product. Alkanes present in the pentane-soluble liquid product as a function of time using nickel on silica-alumina, silica-alumina support only, platinum silica, silica support only and uncatalyzed treatment. The bars represent the mean ± standard deviation with n = 3. Treatments within each reaction time with the same letter are statistically similar using Tukey test at 95% confidence level.

4.4.5 Alkene product

The amount of alkenes significantly decreased compared with the untreated crude pyrolysis liquid product, as shown in **Figure 4-20**. This is because the alkene generated from this study further acts as a precursor for generating aromatic compounds via the Diel-Alder and aromatization reaction. In this reaction, dienes and alkenes react to produce cyclohexenes, and upon dehydrogenation, aromatic compounds are formed. The increase in aromatic compounds, as shown in **Figure 4-22,** can explain the decrease in alkene in the conditions tested. In addition, the in situ hydrogen generated from dehydrogenation reaction can result in the saturation of alkene (Krobkrong et al., 2018; Pillay et al., 2009). Therefore, these mechanisms can be used to explain the decrease in the alkenes observed.

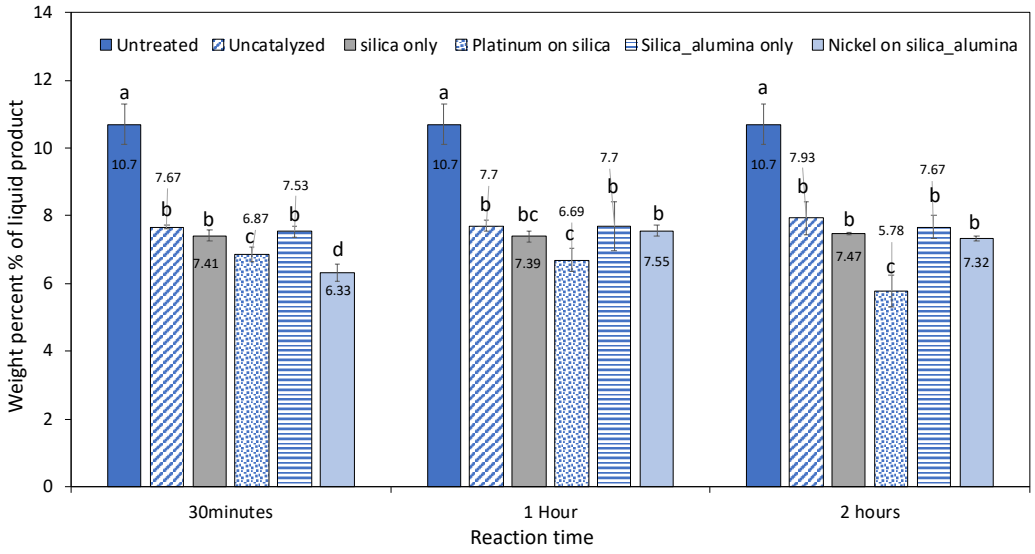

Figure 4-20. The 1-alkenes and internal alkenes composition of pentane-soluble liquid pyrolysis product. The alkenes present in the pentane-soluble liquid product as a function of time using nickel on silica-alumina, silica-alumina support only, platinum silica, silica support only and uncatalyzed treatment. The bars represent the mean ± standard deviation with n = 3. Treatments within each reaction time with the same letter are statistically similar using Tukey test at 95% confidence level.

4.4.6 Cyclic and aromatic compounds

The results obtained from the catalytic treatment on the crude pyrolysis liquid product showed cyclic and aromatic compounds in the pentane-dissolved liquid product. The total amount of cyclic alkanes in the pentane recovered liquid product is shown in **Figure 4-21A**. As reaction time increases from 0.5 to 2 hours, a significant increase in cyclic alkanes was observed compared to the untreated crude liquid product. On the other hand, the cyclic alkenes amount, as shown in **Figure 4-21B**, stabilized as the reaction time increased from 0.5 to 2 hours. However, the nickel on silica-alumina catalyst treatment was an exception, where a significant decrease in the cyclic alkenes was observed compared to the untreated crude liquid product at 2 hours.

The presence of cyclic hydrocarbons found in the liquid product is attributed to be formed from the Diel-Alder reaction, which involves the dienes and dienophile compounds (Asomaning et al., 2014a). Furthermore, intramolecular cyclization of alkenyl radicals with terminal bonds has been proposed as a new pathway for forming cyclic hydrocarbon compounds (Kubátová et al., 2012).

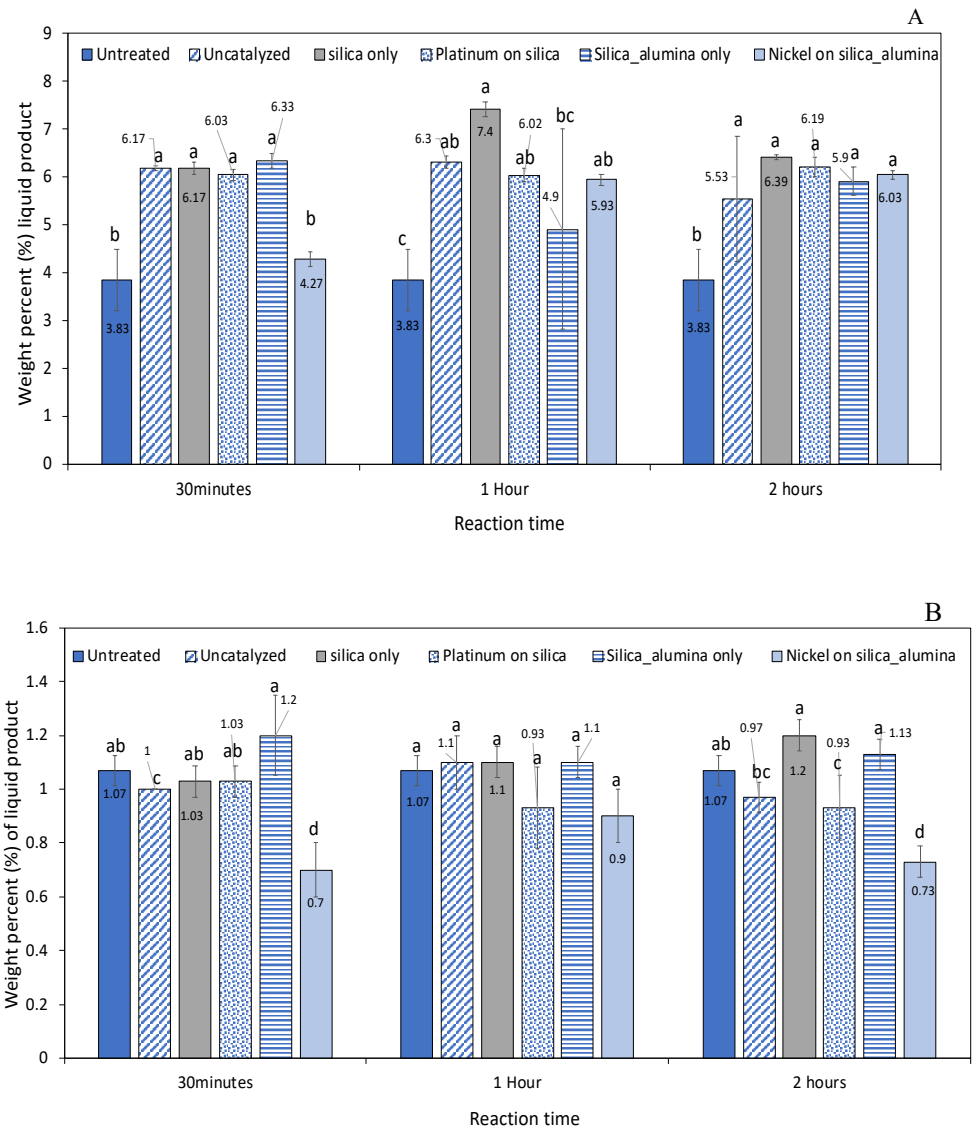

Figure 4-21. The weight percent of cyclic alkanes (A) and cyclic alkene (B) compounds the pentane-soluble liquid pyrolysis product. The cyclic compound in the pentane-soluble liquid product as a function of time using nickel on silica-alumina, silica-alumina support only, platinum silica, silica support only and uncatalyzed treatment. The bars represent the mean ± standard deviation with n = 3. Treatments within each reaction time with the same letter are statistically similar using Tukey test at 95% confidence level.

Figure 4-22 showed an increasing trend in the aromatic compounds found in the liquid product obtained in the catalysts and supports tested. The aromatic compounds obtained from the

catalysts and support treatment ranged from 7.57 ± 0.12 at 0.5 hours to 8.8 ± 0.36 wt.% at 2 hours. Under all the conditions tested, the amount of aromatic compounds in the liquid product of the uncatalyzed treatment was statistically different from the catalyst and the supports treatments. This suggests that incorporating catalysts and supports in all the reaction conditions tested further increased the aromatization reaction.

In all the reaction conditions tested, mono-aromatic compounds such as benzene, toluene, and xylenes were observed. Mono-aromatic compounds found in the liquid product are attributed to the dehydrogenation reaction pathway occurring on the cyclic alkanes and alkenes with a six-carbon number (Kubátová et al., 2012; Melero et al., 2010). In addition, the constituent in the liquid product showed polyaromatic compounds such as indanes, indenes, and naphthalene. The occurrence of polyaromatic compounds is due to polymerization and dehydrogenation of mono-aromatics compounds (Kubátová et al., 2012; M. Snåre et al., 2008).

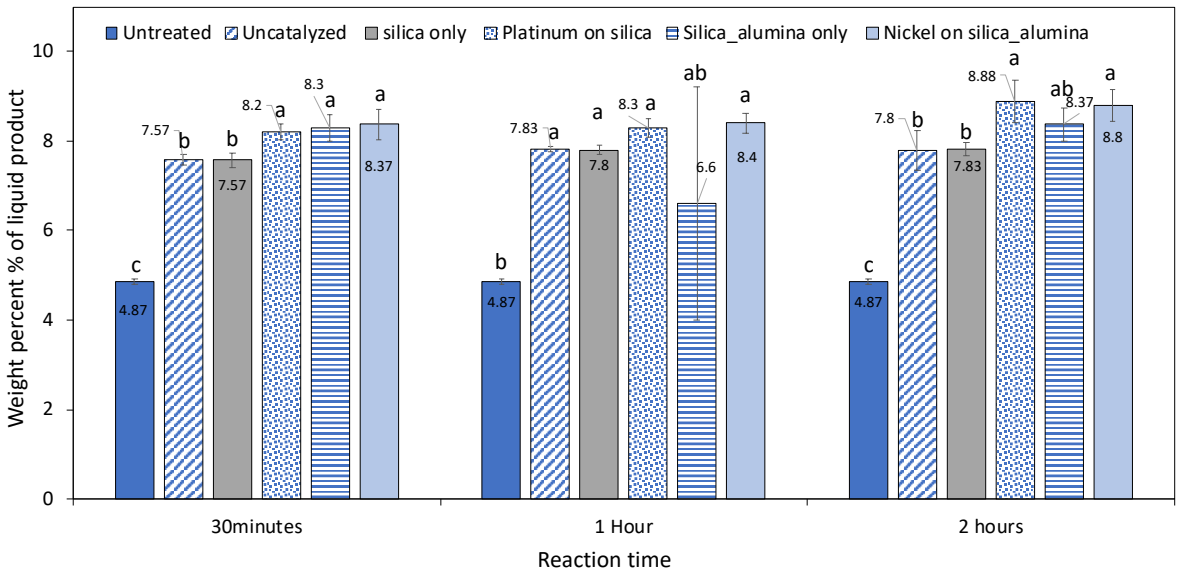

Figure 4-22. The weight percent of aromatic compounds in pentane-soluble liquid pyrolysis product. Aromatic compound in pentane-soluble liquid product as a function of time using nickel

on silica-alumina, silica-alumina support only, platinum silica, silica support only and uncatalyzed treatment. The bars represent the mean ± standard deviation with n = 3. Treatments within each reaction time with the same letter are statistically similar using Tukey test at 95% confidence level.

4.4.6 Branched hydrocarbon

The GC-MS identification analysis revealed the presence of branched hydrocarbon compounds in the pentane recovered liquid product obtained from all the conditions tested, as shown in **Figure 4-23**. A significant decrease in the amount of branched hydrocarbon compounds was observed compared to the untreated crude liquid product as the reaction time increased from 0.5 to 2 hours.

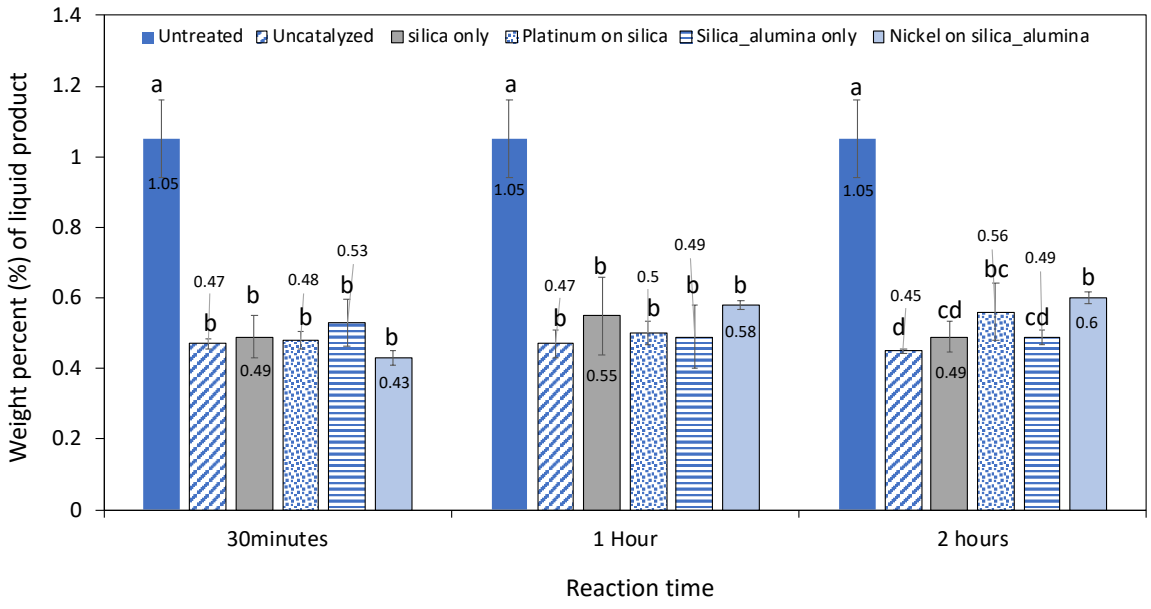

Figure 4-23. Weight percent of branched hydrocarbon compounds in the pentane-soluble liquid pyrolysis product. Branched hydrocarbon compound in pentane-soluble liquid product as a function of time using nickel on silica-alumina, silica-alumina support only, platinum silica, silica support only and uncatalyzed treatment. The bars represent the mean ± standard deviation

with n = 3. Treatments within each reaction time with the same letter are statistically similar using Tukey test at 95% confidence level.

As shown in **Figure 4-23**, the total branched compounds in the liquid product obtained from the catalyzed treatments and the uncatalyzed treatment was statistically similar at reaction times from 0.5 to 1 hour. However, at 2 hours, the nickel on silica-alumina catalyst treatment resulted in a considerably higher total branched hydrocarbon representing 0.6 % of the liquid product compared to the 0.45 % of the uncatalyzed treatment. An explanation for this outcome is that increasing reaction time to 2 hours promoted branching through radical addition in the catalytic deoxygenation of residual fatty acids in crude pyrolysis liquid product. It is worth noting that the total branched compound in all the catalytic treatments significantly decreased compared to the untreated crude liquid product. This observation is because the catalysts employed did not significantly improve the isomerization reaction.

4.4.7 Residual Fatty acids

As shown in **Figure 4-24**, the total fatty acids weight percentage in the liquid product obtained from the platinum on silica catalyst treatment significantly decreased from 9.28 % to 5.48 %, with increasing reaction time from 0.5 to 2 hours. In the case of the nickel on silica-alumina catalyst, the fatty acids significantly decreased from 3.72 % to a complete acid removal as the reaction time increased from 0.5 to 2 hours. The results indicated that increasing reaction time enhanced the removal of residual fatty acids in the crude liquid product. The catalytic treatment that showed the presence of residual fatty acids in the liquid product suggested that deoxygenation was not complete.

Consequently, the nickel on silica-alumina catalyst treatment at 2 hours resulted in successful removal of residual fatty acid in the crude pyrolysis liquid product. One possible explanation for this outcome is due to the fact that as reaction time increases, the interaction of the reactant and the active sites of the catalyst increases, resulting in residual fatty acids removal. Therefore, based on the results shown, it was concluded that the incorporation of nickel on silica-alumina at 2 hours was necessary to achieve complete fatty acids removal to yield liquid hydrocarbon fuel.

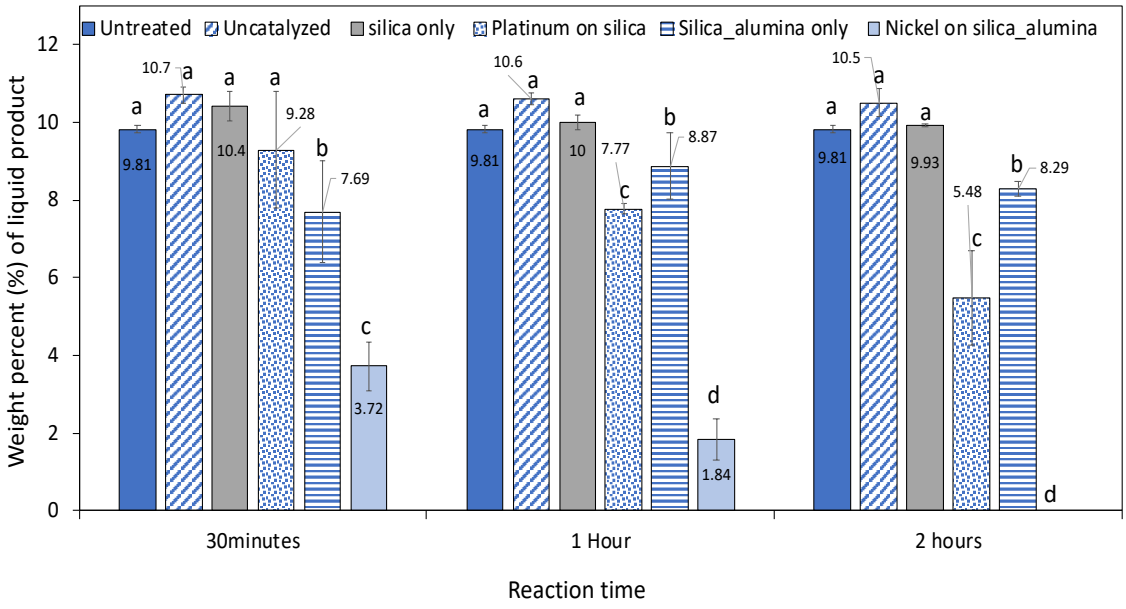

Figure 4-24. Weight percent of residual fatty acid compounds in the pentane-soluble liquid pyrolysis product. The residual fatty acids in pentane soluble liquid product as a function of time using nickel on silica-alumina, silica-alumina support only, platinum silica, silica support only and uncatalyzed treatment. The bars represent the mean ± standard deviation with n = 3. Treatments within each reaction time with the same letter are statistically similar using Tukey test at 95% confidence level.

4.5 The gas fraction product and the extent of deoxygenation

The gas product obtained was analyzed on the GC-TCD and GC-FID to provide additional information to support the deoxygenation mechanism, as explained in **section 4.4.6.1**. The GC-TCD chromatogram, as shown in **Figure 4-25,** revealed CO and CO_2 compounds in the gas product obtained in all the reaction conditions tested. This demonstrated that the deoxygenation reaction occurred via decarbonylation and decarboxylation (Asomaning et al., 2014; Crawford et al., 2020; Kubátová et al., 2011). Interestingly, when the crude liquid product was treated with nickel on silica-alumina catalyst at 2 hours, complete disappearance of CO and a profound CO_2 peak was observed, as shown in **Figure 4-25C**. This outcome suggests that decarboxylation of the residual fatty acids in the crude pyrolysis liquid product was favoured in the catalytic deoxygenation reaction. The presence of high electronegativity oxygen molecule in the carboxyl group of the residual fatty acid in the crude pyrolysis liquid product reduces the bond dissociation energy of the C-C bond closer to the carboxylic group, which breaks and gets adsorb unto the nickel on the silica-alumina support, resulting in the O-H bond's cleavage favouring the decarboxylation reaction (Berenblyum et al., 2011; Jenab et al., 2014).

Furthermore, the water-gas shift reaction can be used as a possible mechanism to explain the presence of hydrogen, and the disappearance of carbon monoxide, as this reaction involves carbon monoxide and water to yield hydrogen and carbon dioxide (Lestari et al., 2009). The decarbonylation reaction of fatty acids results in the formation of carbon monoxide and water molecules. Therefore, the forward reaction of the water-gas shift is a plausible explanation for the carbon dioxide and hydrogen peaks seen in all the reaction conditions tested. In addition, dehydrogenation reaction can be used to explain the presence of hydrogen observed in the GC-TCD chromatogram.

A

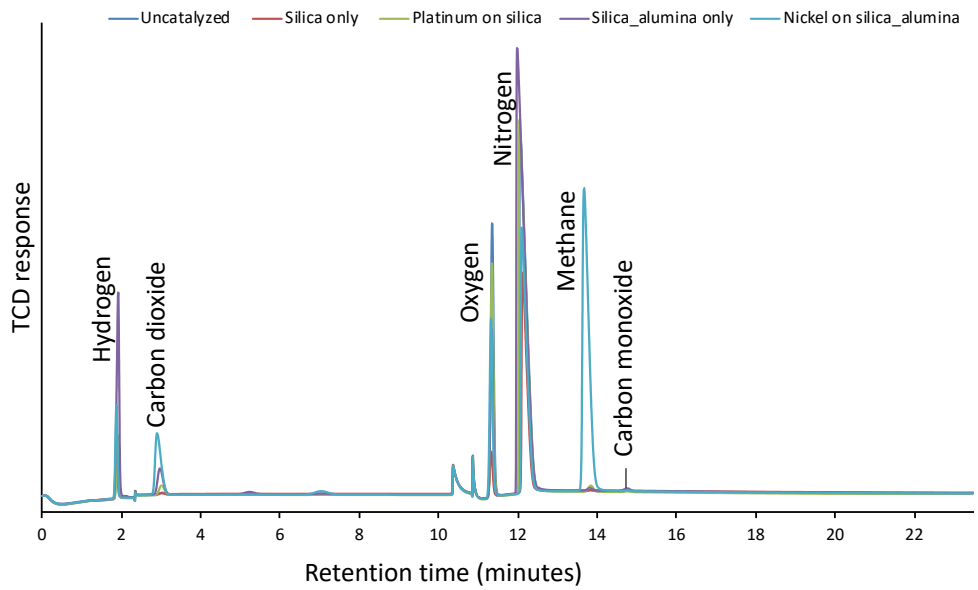
Uncatalyzed
Silica only
Platinum on silica
Silica_alumina only
Nickel on silica_alumina
TCD response
Hydrogen
Carbon dioxide
Oxygen
Nitrogen
Methane
Carbon monoxide
0
2
4
6
8
10
12
14
16
18
20
22
Retention time (minutes)

B

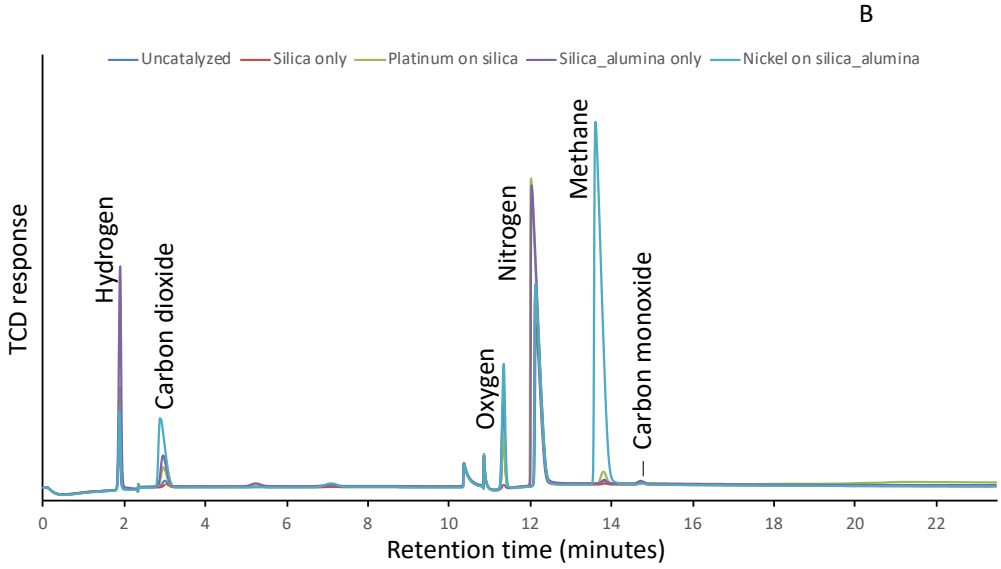
Uncatalyzed
Silica only
Platinum on silica
Silica_alumina only
Nickel on silica_alumina
TCD response
Hydrogen
Carbon dioxide
Oxygen
Nitrogen
Methane
Carbon monoxide
0
2
4
6
8
10
12
14
16
18
20
22
Retention time (minutes)

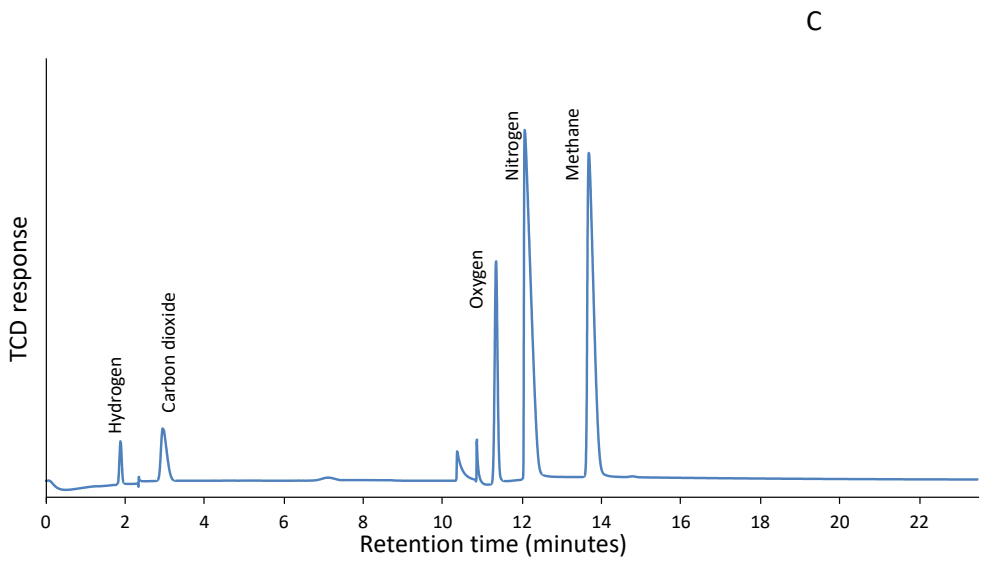

Figure 4-25. Typical GC-TCD chromatogram displaying carbon monoxide, carbon dioxide and hydrogen compounds in the gas product. The gas-phase chromatograms for (A) 30 minutes catalyst treatment (B) 1-hour catalyst treatment (C) Nickel on silica-alumina catalyst treatment at 2 hours on crude pyrolysis liquid product at a reaction temperature of 350 ˚C.

Short-chain hydrocarbons with carbon numbers ranging from C_1-C_6 were found in the gas fraction obtained in all the reaction conditions tested, as shown in **Figure 4-26.** Hydrocarbon compounds in the gas fraction reveal the cracking of the long-chain hydrocarbons into non-condensable short-chain hydrocarbons (Lestari et al., 2009). The high methane peak observed from the nickel on silica-alumina catalyst treatment, as shown in **Figure 4-26,** can be attributed to the cracking of hydrocarbon compounds and methanation reaction (Ren et al., 2015). In a methanation reaction, carbon oxides react with in situ hydrogen to generate methane and water (Borgschulte et al., 2013). Therefore, this mechanism can be used to explain the methane observed in the gas fraction. In addition, the short-chain hydrocarbons in the gas fraction are attributed to the cracking of long-chain hydrocarbons into short hydrocarbons in all the reaction conditions tested.

A

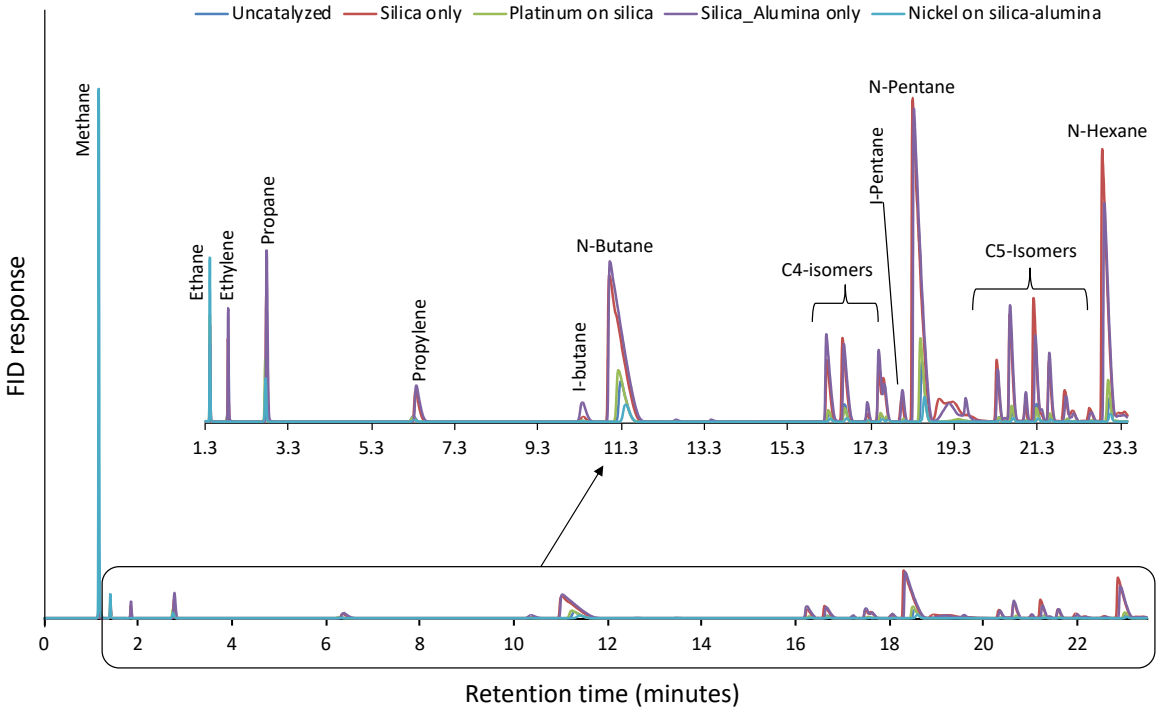
Uncatalyzed
Silica only
Platinum on silica
Silica_Alumina only
Nickel on silica-alumina
FID response
Methane
Ethane
Ethylene
Propane
Propylene
I-butane
N-Butane
C4-isomers
I-Pentane
N-Pentane
C5-Isomers
N-Hexane
1.3
3.3
5.3
7.3
9.3
11.3
13.3
15.3
17.3
19.3
21.3
23.3
0
2
4
6
8
10
12
14
16
18
20
22
Retention time (minutes)

B

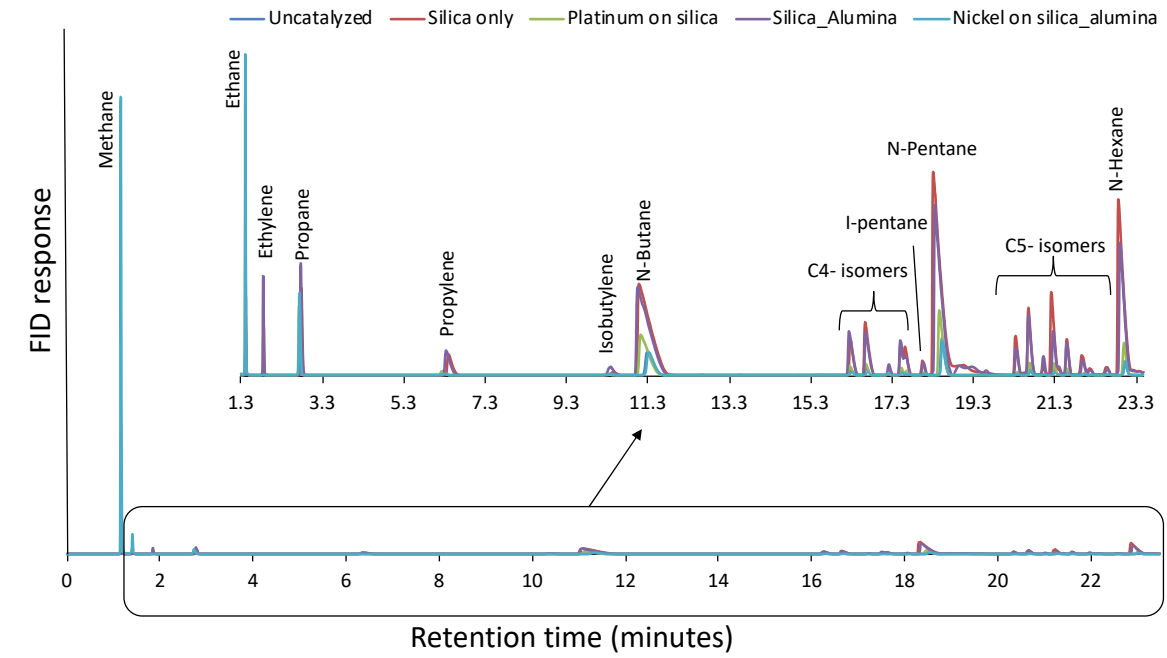
Uncatalyzed
Silica only
Platinum on silica
Silica_Alumina
Nickel on silica_alumina
FID response
Methane
Ethane
Ethylene
Propane
Propylene
Isobutylene
N-Butane
C4- isomers
I-pentane
N-Pentane
C5- isomers
N-Hexane
1.3
3.3
5.3
7.3
9.3
11.3
13.3
15.3
17.3
19.3
21.3
23.3
0
2
4
6
8
10
12
14
16
18
20
22
Retention time (minutes)

C

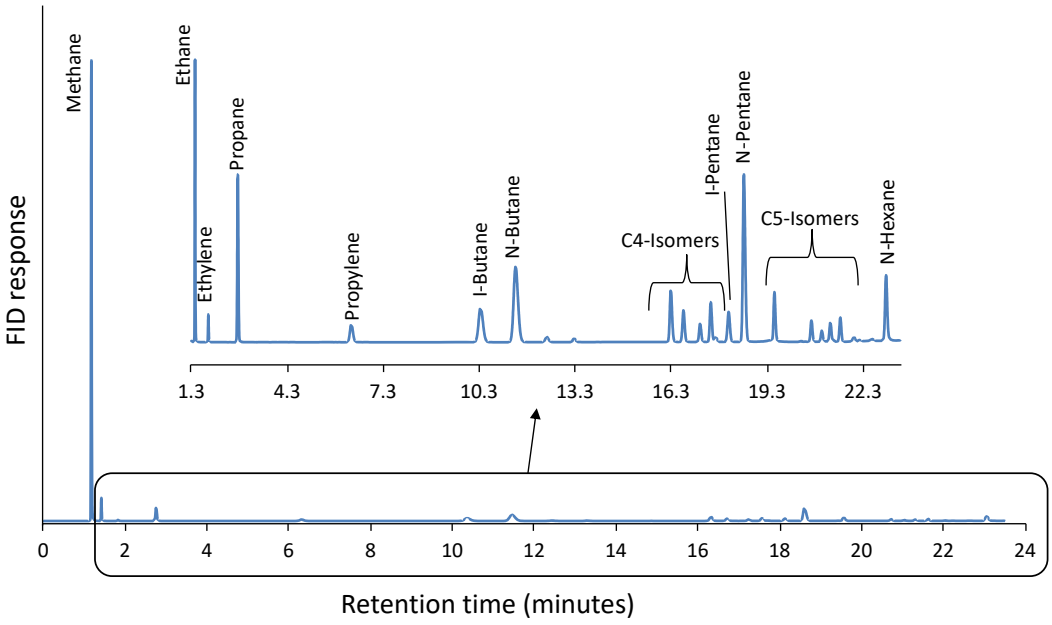

Figure 4-26. Typical GC-FID chromatogram displaying hydrocarbon compound in the gas product. The gas-phase chromatogram for (A) 30 minutes catalyst treatment (B) 1-hour catalyst treatment (C) Nickel on silica-alumina catalyst treatment at 2 hours on crude pyrolysis liquid product at a reaction temperature of 350 ˚C.

4.6 A scale-up experiment using nickel on silica-alumina catalyst to deoxygenate residual fatty acids in a crude pyrolysis liquid product

The evaluation of the results explained in **section 4.3,** revealed that the nickel on silica-alumina catalyst at 2 hours reaction time in a 15 mL microreactor resulted in complete removal of residual fatty acids to yield liquid hydrocarbon fuel. Based on this, a scale-up experiment was conducted using the nickel on silica-alumina catalyst to remove residual fatty acids. This experiment provided understanding on the mass balance of the product distributions, and the regeneration and reuse of the spent nickel on silica-alumina catalyst. In this experiment, reaction temperatures of 300 ˚C and 350 ˚C was tested at 1.5 hours using approximately 100 grams of crude

liquid product and 20 grams of nickel on silica-alumina catalyst in a 1 L continuously stirred tank reactor. The product characterization was determined using the same analytical techniques as in the microreactor studies.

4.6.1 Product distribution

The catalytic deoxygenation of residual fatty acids in a crude pyrolysis liquid product in all conditions tested resulted in gaseous and liquid product, as shown in **Figure 4.27.** The fine powder nature of the nickel on silica-alumina catalyst made isolating the liquid product from the catalyst challenging. Therefore, the solid product was not reported in this study.

The gas product yield obtained from the 300 ˚C, 350 ˚C, and the recycled catalyst at 300 ˚C temperature treatment were 18.8 %, 26.2 %, and 12.6 %, respectively. The observed increase in the gas product yield at 350 ˚C can be explained in terms of further deoxygenation of residual fatty acids as well as a decrease in the liquid product. The gas product yield obtained from all the treatments tested were significantly different from each other. Increasing the reaction temperature resulted in a decrease in the liquid product yield. The yield of liquid product obtained from the recycled nickel catalyst at the 300 ˚C temperature treatment significantly increased as shown in **Figure 4-27,** compared to the liquid yield obtained from the fresh nickel catalyst at 300 ˚C and 350 ˚C temperature treatment. No residual fatty acids were identified in the liquid product obtained from the fresh nickel catalyst at 300 ˚C and 350 ˚C temperature treatments, but in the recycled nickel catalyst at 300 ˚C temperature treatment, residual fatty acids were identified, indicating that deoxygenation was not complete.

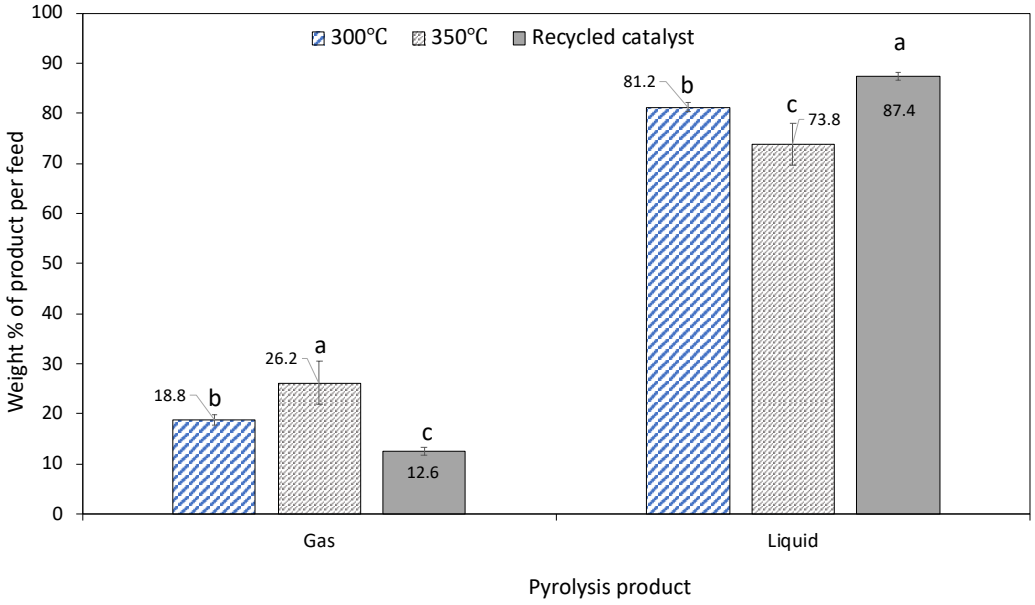

Figure 4-27. The pyrolysis product distribution in a 1 L batch reactor. The pyrolysis product distribution was obtained from the nickel on silica-alumina catalyst treatment used to deoxygenate residual fatty acids in a crude pyrolysis liquid product. The bar represents the mean ± standard deviation with n=3. Treatments within each product category with the same letter are statistically similar using Tukey test at 95% confidence level. Recycled catalyst refers to a used catalyst that was washed with a pentane solvent.

4.6.2 Liquid product analysis and deoxygenation performance of the catalysts using FT-IR and GC-FID/ GC-MS

The constituents in the crude liquid product obtained from the study was analyzed using similar analytical approach used in the microreactor study explained in **session 4.3**. The following compound classes, *n*-alkanes, alkenes, cyclic hydrocarbons, branched hydrocarbons, aromatics, and fatty acid was found in the liquid product obtained from the recycled nickel on silica-alumina catalyst treatment at 300 ˚C. Whereas, in the case of the fresh nickel on silica-alumina catalyst at 300 ˚C and 350 ˚C treatment, fatty acids peak was absent, indicating successful removal of residual

acids in the liquid product obtained at these conditions. The fatty acids observed in the liquid product from the recycled nickel on silica-alumina catalyst treatment suggest that the removal of residual fatty acid was not complete.

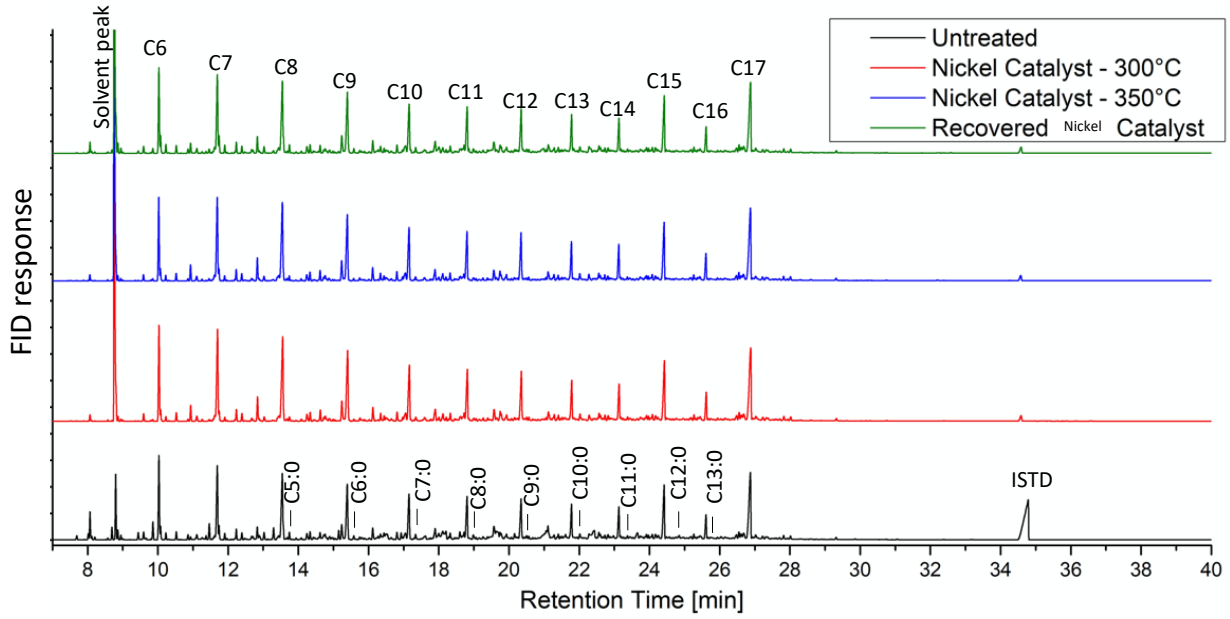

Figure 4-28. A representative GC-FID chromatogram of liquid pyrolysis product. Chromatogram of crude liquid product obtained from fresh nickel on silica-alumina catalyst at 300 ˚C and 350 ˚C and the recycled nickel on silica-alumina catalyst at 300 ˚C treatment at 1.5 hours, under inert reaction atmosphere at 1 atm. Note. ISTD is the Internal standard used in the quantification of the individual compounds. Untreated refers to the crude pyrolysis liquid product received from an industrial partner. Recycled catalyst refers to a used catalyst that was washed with pentane solvent. *The internal standard (ISTD) peak in the untreated chromatogram is higher than the ISTD peak of other treatments. A higher amount of nonadecanoic acid methyl ester (ISTD) was used in compound characterization.

4.6.2.1 The liquid composition

The constituents in the liquid product was dependent on the reaction temperature employed in the scale-up experiment. It is worth mentioning that the crude pyrolysis liquid product used in

this study predominantly contained *n*-alkanes. However, an increase in *n*-alkanes was observed after treating the crude pyrolysis liquid product with the fresh nickel on silica-alumina catalyst at 300 ˚C and 350 ˚C temperature treatment. This observation can be attributed to the deoxygenation of residual fatty acid via the decarboxylation pathway to increase the *n*-alkanes (Nozawa et al., 2014). In addition, saturation of alkenes in the liquid with in-situ hydrogen can be used to explain the increase in *n*- alkanes (Berenblyum et al., 2010; Matsumoto et al., 1970). In the case of the recycled spent nickel on silica-alumina catalyst at 300 ˚C treatment, the amount of *n*-alkanes was statistically similar to the untreated crude liquid product indicating no increase in *n*-alkanes.

Interestingly, a decrease in alkenes content was observed in the liquid product obtained from all the reaction conditions tested, as shown in **Figure 4-29**. An explanation for this observation is the utilization of the in-situ hydrogen generated from dehydrogenation and cracking resulting in the saturation of the alkenes bound to the active sites of the catalyst.

The following compounds: cyclopentanes, cyclopentenes, cyclohexanes, and cyclohexenes, were the primary cyclic compounds found in the liquid product. As shown in **Figure 4-29**, the weight percent of cyclic compounds significantly increased as a function of the temperature treatment applied to the catalytic deoxygenation reaction compared to the untreated sample. The formation of cyclic compounds has been reported in literature through a reaction pathway known as intermolecular radical cyclization (Kubátová et al., 2012). The 6-carbon cyclic compounds observed are attributed to the Diel-Alder reaction, which occurs between dienes and dienophiles (Asomaning et al., 2014c; Immer et al., 2010). The cyclic alkanes in all the reaction conditions tested significantly increased compared to the untreated liquid sample. This observation is due to the hydrogenation of the cyclic alkenes, hence increasing the amount of cyclic alkanes compounds

in the fresh catalyst. However, the amount of the cyclic alkanes for the fresh and recycled nickel on silica-alumina catalyst were statistically similar in all the reaction conditions tested.

As shown in **Figure 4-29**, residual fatty acids were observed in the liquid product obtained from the recycled nickel on silica-alumina catalyst treated at 300 ˚C reaction temperature. This observation indicates that the catalytic activity decreased, and the regeneration method employed was not successful. The fresh nickel on silica-alumina catalyst showed complete deoxygenation at 300 ˚C and 350 ˚C treatments evidenced by the absence of acids.

Therefore, the increase in alkane in the liquid product obtained from the fresh nickel on silica-alumina catalyst at 300 ˚C and 350 ˚C treatment and the absence of a carbon monoxide peak, as shown in the gas chromatogram, provided evidence for decarboxylation reaction pathway being dominant.

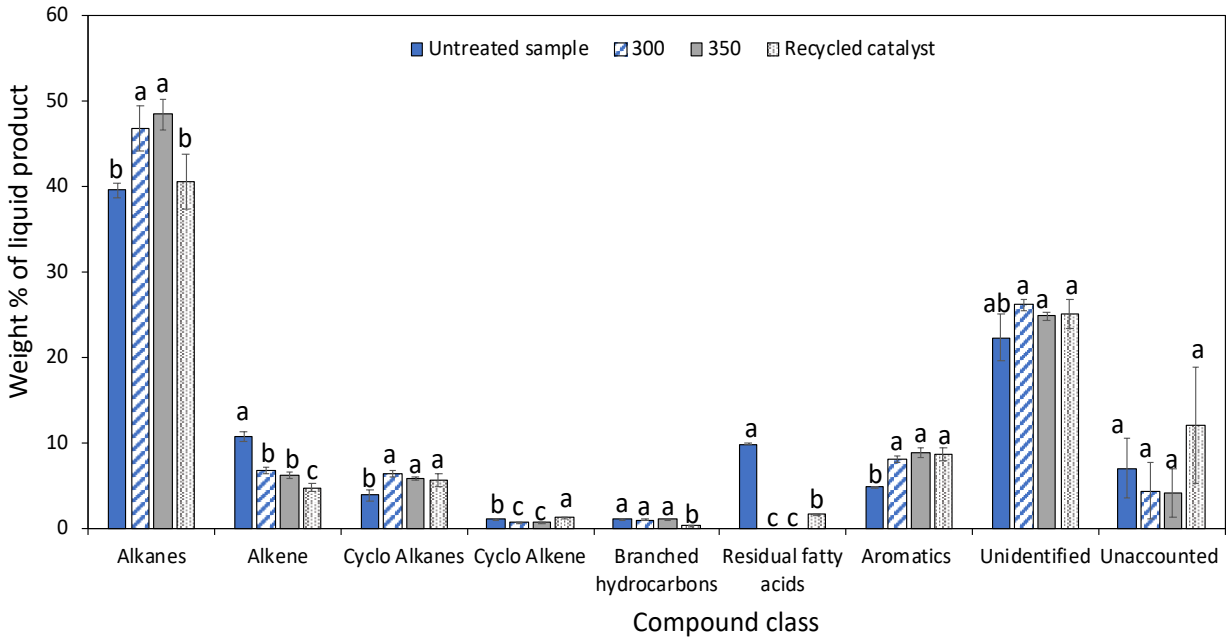

Figure 4-29; The compound classes in the crude liquid product from the 1 L batch reactor. Composition of the liquid product obtained from the catalytic deoxygenation of residual fatty acids using nickel on silica-alumina at 300 ˚C and 350 ˚C, respectively. The recycled catalyst reaction temperature used was 300 ˚C. The bar represents the mean ± standard deviation with n = 3.

Treatments within each compound class with the same letter are statistically similar using Tukey test at 95% confidence level. NB. Untreated sample refers to the received crude pyrolysis liquid product; recycled catalyst refers to a used catalyst that was cleaned with a pentane solvent.

4.6.3. Characterization of liquid product using FTIR

To obtain further evidence on the deoxygenation of residual fatty acid in the crude pyrolysis liquid product. An FTIR analysis was done to understand the different kinds of functional groups in the liquid product obtained after the nickel on silica-alumina catalyst treatment. The FTIR spectra of the crude liquid product obtained from catalytic deoxygenation of fatty acids are shown in **Figure 4-30**.

All the spectra obtained from the catalytic run were compared with the FTIR spectra of the caustic-washed crude liquid product. This comparison was made to understand the similarity of using deoxygenation catalyst and the caustic washing approach to remove residual fatty acids from crude pyrolysis liquid product. In the caustic washing approach, the hydrocarbon liquid fraction was separated using a caustic (NaOH) solution to extract the residual fatty acid in the crude pyrolysis liquid product. The hydrocarbon liquid fraction obtained was then used in the FTIR analysis to generate the spectra.

The interpretation of the various bands in the individual liquid product's spectra is based on the literature (Haug et al., 2011; Socrates, 2001). The spectrum for all the conditions tested shows strong absorption bands in the region 2800-2900 cm^{-1}, which is assigned to the presence of aliphatic C-H stretching. Bands occurring at 1700 cm^{-1} correspond to the carbonyl group of the carboxylic acid in the liquid product obtained in all the reaction conditions.

The comparison of the FTIR spectra at the 1700 cm^{-1} wavenumber showed significant changes in the C=O band when the conditions tested were compared in **Figure 4-30**. The observed

disappearance of the C=O band in the fresh nickel on silica-alumina catalyst at 350 ˚C revealed the successful removal of residual fatty acids in the crude liquid product. Interestingly, the FTIR spectra for the fresh and the recycled nickel on silica-alumina catalyst at 300 ˚C treatment showed a small bump of the C=O band, which corresponds to residual fatty acids in the crude liquid product, suggesting incomplete residual fatty acids removal.

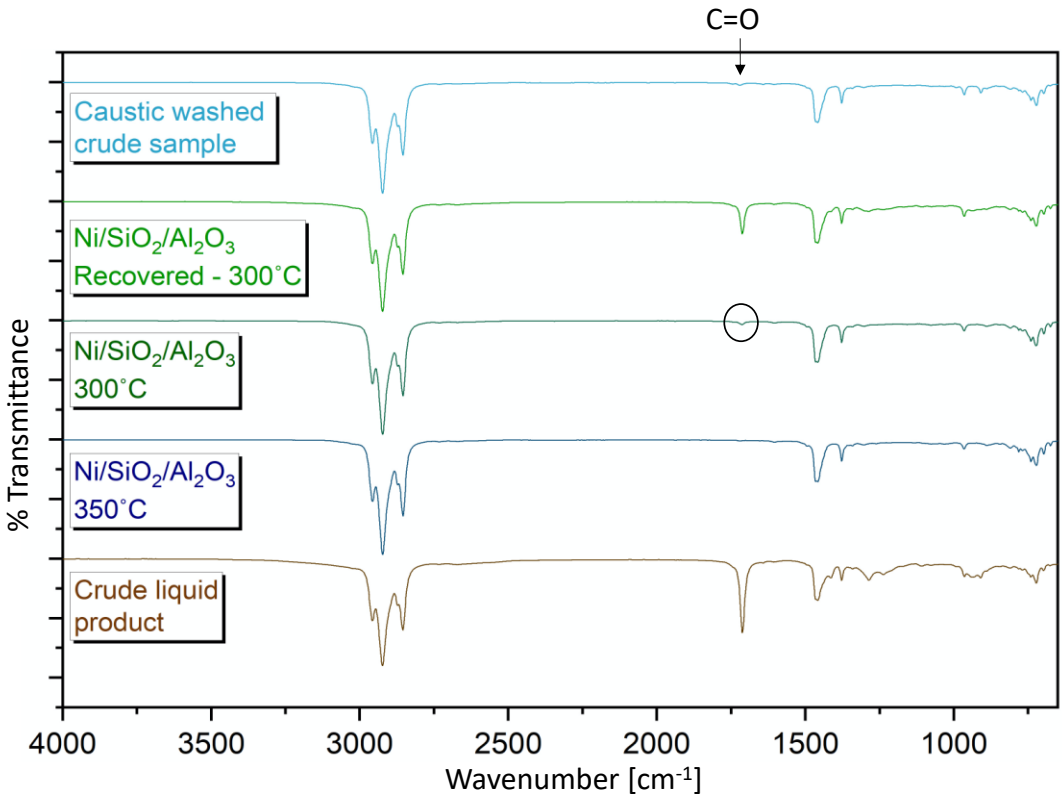

Figure 4-30. FTIR spectra of the crude liquid product from the 1 L batch reactor. FTIR spectra of the crude liquid product obtained from the catalytic deoxygenation of residual fatty acids at a temperature of 300 ˚C and 350 ˚C, at a reaction time of 1.5 hours. The C=O stretching vibrations indicates the residual fatty acids in the liquid product after the deoxygenation of crude pyrolysis liquid product in all reaction conditions tested.

4.6.4 Acid number determination

Given the FTIR spectra in **Figure 4-30**, the fresh nickel on silica-alumina at 300 ˚C temperature treatment spectra showed a small bump of C=O band, which corresponds to the carboxylic acid in the liquid product. Therefore, a further test was conducted to determine the total acid number in all the liquid products obtained in this study. This step provided additional information to support the FTIR spectra and GC analysis data by establishing the total acid number in the liquid product collected during the deoxygenation reaction.

Table 4 shows the total acid number in the untreated crude pyrolysis liquid product and the catalyzed liquid product. The total acid number in the liquid product obtained from the 350 ˚C temperature treatment was not detectable, signifying no residual acids in the liquid product. On the other hand, a lower amount of acid number of 1.9 mgKOH/g was detected in the liquid product for the fresh nickel on silica-alumina catalyst at 300 ˚C temperature treatment. Thus, confirming the small bump seen in the FTIR spectra in **Figure 4-30** corresponding to the residual fatty acid in the liquid product. The solvent regenerated spent nickel on silica-alumina catalyst gave an acid number of 28.6 mgKOH/g in the liquid product, suggesting that the performance of the recycled nickel on silica-alumina catalyst to remove the residual fatty acid in the crude pyrolysis liquid product decreased. Therefore, the total acid number determination confirmed the presence and absence of residual fatty acids in the liquid product obtained from the catalytic removal of residual fatty acids in crude pyrolysis liquid product.

Table 4.0 Total acid number in the sample and the catalyst treated liquid product

Sample (Liquid product)	Acid number TAN mgKOH/g
Untreated (Crude pyrolysis liquid)	68.9 ± 0.89
300 ˚C Temperature treatment	1.94 ± 0.027
350 ˚C Temperature treatment	ND
Solvent cleaned catalyst of 300 ℃ treatment	28.6 ± 0.13

*ND not detected by the instrument.

4.6.5. Gas fraction

The catalytic deoxygenation of residual fatty acids in a crude pyrolysis liquid product resulted in a gas fraction in all the reaction conditions. The gas fraction provides further evidence of deoxygenation and cracking that resulted from the catalytic deoxygenation reaction on the residual fatty acid present in the crude liquid product.

The gas analyzed on the GC-TCD showed CO, CO_2, and H_2 compounds, as shown in **Figure 4-31**, which suggests the presence of deoxygenation of residual fatty acid in the crude pyrolysis liquid product. A plausible explanation for the occurrence of in situ hydrogen is attributed to the dehydrogenation of cyclic compounds, which results in the formation of aromatic compounds present in the liquid product (Hermida et al., 2015). On the other hand, the presence of short-chain hydrocarbon compounds provides evidence of cracking during the catalytic deoxygenation of residual fatty acids in the crude pyrolysis liquid product.

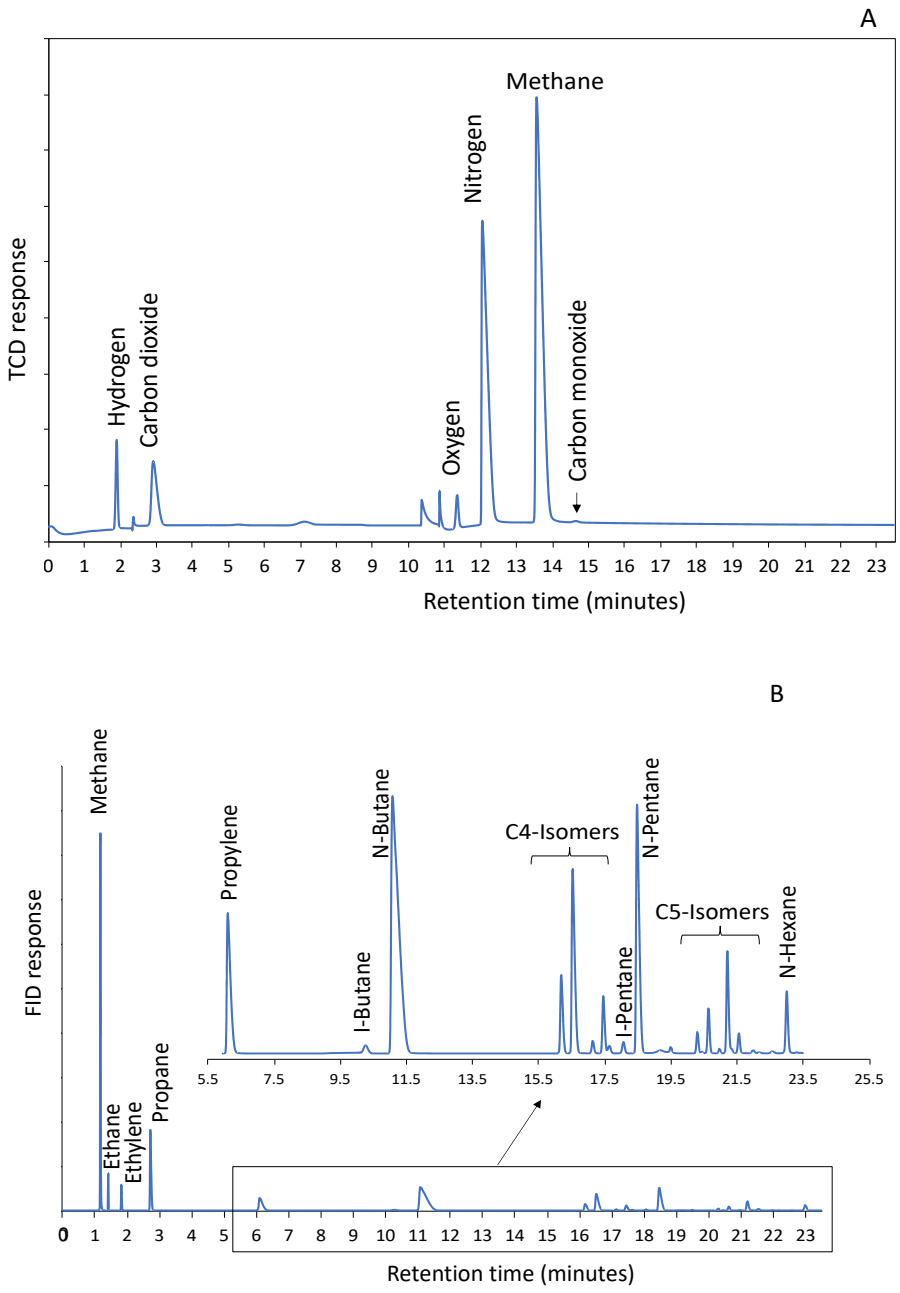

Figure 4-31. The representative GC-FID and GC-TCD chromatogram. Gas-phase chromatogram showing (A) the presence of CO, CO_2 and H_2 compounds, (B) the occurrence of hydrocarbon compounds in the gas yield of the catalytic deoxygenation of residual fatty acids in crude pyrolysis liquid product.

Chapter 5

5.0. Conclusion

In summary, this thesis demonstrated an alternative approach to improve fatty acid conversion to yield liquid hydrocarbon fuel. The preliminary data from the microwave study revealed some critical concerns of the microwave technology as the fatty acids feedstock used did not absorb the microwave energy and the heating aid used to absorb the microwave generated hotspot in the reactor thus, influencing the formation of aromatic compounds. This thesis also demonstrated the feasibility of using nickel on silica-alumina catalyst to deoxygenate residual fatty acid in the crude pyrolysis liquid product into liquid hydrocarbon fuel.

The main conclusions from this work are:

(1) The microwave-assisted heating of stearic acid and silicon carbide mixture resulted in rapid heating to attain the set temperature of 430 ˚C within 1 minute. In the case of the oleic acid run, the set temperature was not reached. The microwave-assisted pyrolysis of stearic and oleic acid with SiC as heating aid demonstrated the presence of deoxygenation products and cracking products in the non-condensable gas product and hydrocarbons and aromatic compounds in the condensable product.

(2) The dark spots observed on the wet thermal paper demonstrated the non-uniform distribution of microwaves in the reactor cavity. The dark spot indicated the hotspot regions in the reactor cavity, which tends to have a high temperature gradient, thus, facilitating undesirable secondary reaction pathways. Therefore, this study provided the needed evidence to improve microwave distribution in the reactor cavity.

(3) The presence of stainless-steel mesh in oleic acid pyrolysis did not have a catalytic effect on the product yields and liquid composition. In addition, the product yields and the

chemical composition of the liquid product obtained from the individual treatments (chemical, thermal, and untreated) subjected to the stainless-steel mesh were statistically similar. Therefore, any changes observed regarding the product composition is due to the reaction condition employed in the pyrolysis reaction. However, the liquid product generated will require further upgrading to remove the residual fatty acids to yield liquid hydrocarbon fuel.

(4) The crude liquid product obtained from fatty acid pyrolysis conversion may contain residual fatty acid, limiting direct utilization in petroleum infrastructures. A catalytic upgrading approach was employed to deoxygenate residual fatty acids to yield liquid hydrocarbon fuel. The nickel on silica-alumina catalyst at 2 hours reaction time demonstrated complete removal of residual fatty acids in the crude liquid product. The result indicated that deoxygenation reaction occurred through decarboxylation, confirmed by the CO_2 in the gas fraction. This study potentially demonstrated the feasibility of using a deoxygenating catalyst to remove residual fatty acid to yield hydrocarbon fuel.

(5) Finally, the scale-up study demonstrated the viability of scaling up the nickel on silica-alumina catalyst in a 1L batch reactor to deoxygenate residual fatty acid in crude liquid product to generate a drop-in liquid hydrocarbon fuel.

The overall objective of this thesis was achieved. The microwave-assisted heating did improve the heating rate to attain the set temperature within 1 minute to enhance the deoxygenation of model fatty acids compounds. This can result in energy saving by reducing the energy consumption required for pyrolysis reaction. The feasibility of utilizing a less expensive catalyst to remove residual fatty acids to yield a drop-in hydrocarbon fuel provided an economic advantage to reduce the operational cost of the crude liquid product upgrading process. The findings from this research

will directly support the conversion of fatty acids to yield renewable hydrocarbon fuel and platform chemicals.

5.1 Recommendation for future direction

This thesis demonstrated the importance of using microwave-assisted heating to speed up the heating rate in fatty acid pyrolysis and the incorporation of deoxygenation catalysts (nickel on silica-alumina catalyst) to upgrade the crude pyrolysis liquid product into drop-in hydrocarbon liquid fuel. It is worthy to mention that further studies could complement the current work and explore other reaction conditions that were not tackled in the research.

Exploring thermal regeneration of the spent nickel on silica-alumina catalyst and further reducing with hydrogen will further reduce production cost as this approach will prevent one-time use of the fresh nickel on silica-alumina catalyst. It is expected that the regenerated catalyst will behave similarly in terms of catalytic activity as that of the fresh catalyst.

In this study, a batch setup process was explored due to its easiness of use and relatively lower cost. The 15 mL and 1 L capacity batch reactor setup provided scientific evidence on the deoxygenation of residual fatty acid in the crude pyrolysis liquid product. However, at a large-scale industrial operation, the batch process application comes with some limitations. It requires a continuous cleanup and feed change after each run, which results in lower throughput and, at some points, mechanical interruption causing some downtime operation. Hence scaling up in a continuous reactor will provide insight into the number of runs needed for the catalyst to deactivate before a plausible regeneration.

Reference

Aho, A., DeMartini, N., Pranovich, A., Krogell, J., Kumar, N., Eränen, K., Murzin, D. Y. (2013). Pyrolysis of pine and gasification of pine chars - Influence of organically bound metals. *Bioresource Technology*, 128, 22-29.

Alonso, D. M., Bond, J. Q., & Dumesic, J. A. (2010). Catalytic conversion of biomass to biofuels. *Green Chemistry*, *12*(9), 1493–1513.

Alotaibi, M. A., Kozhevnikova, E. F., & Kozhevnikov, I. V. (2012). Hydrogenation of methyl isobutyl ketone over bifunctional Pt-zeolite catalyst. *Journal of Catalysis*, 293, 141-144.

Arend, M., Nonnen, T., Hoelderich, W. F., Fischer, J., & Groos, J. (2011). Catalytic deoxygenation of oleic acid in continuous gas flow for the production of diesel-like hydrocarbons. *Applied Catalysis A: General*, 399(1-2), 198-204.

Arun, N., Sharma, R. V., & Dalai, A. K. (2015). Green diesel synthesis by hydrodeoxygenation of bio-based feedstocks: Strategies for catalyst design and development. *Renewable and Sustainable Energy Reviews*, 48, 240-255.

Asikin-Mijan, N., Lee, H. V., Juan, J. C., Noorsaadah, A. R., & Taufiq-Yap, Y. H. (2017). Catalytic deoxygenation of triglycerides to green diesel over modified CaO-based catalysts. *RSC Advances*, *7*(73), 46445-46460.

Asikin-Mijan, N., Lee, H. V., Marliza, T. S., & Taufiq-Yap, Y. H. (2018). Pyrolytic-deoxygenation of triglycerides model compound and non-edible oil to hydrocarbons over SiO2-Al2O3 supported NiO-CaO catalysts. *Journal of Analytical and Applied Pyrolysis*, *129*, 221–230.

Asomaning, J., Haupt, S., Chae, M., & Bressler, D. C. (2018). Recent developments in microwave-assisted thermal conversion of biomass for fuels and chemicals. *Renewable and Sustainable Energy Reviews*, *92*(May), 642–657.

Asomaning, J., Mussone, P., & Bressler, D. C. (2014a). Pyrolysis of polyunsaturated fatty acids. *Fuel Processing Technology*, *120*, 89–95.

Asomaning, J., Mussone, P., & Bressler, D. C. (2014b). Thermal deoxygenation and pyrolysis of oleic acid. *Journal of Analytical and Applied Pyrolysis*, *105*, 1–7.

Asomaning, J., Mussone, P., & Bressler, D. C. (2014c). Two-stage thermal conversion of inedible lipid feedstocks to renewable chemicals and fuels. *Bioresource Technology*, *158*, 55–62.

Azuara, M., Baguer, B., Villacampa, J. I., Hedin, N., & Manyà, J. J. (2016). Influence of pressure and temperature on key physicochemical properties of corn stover-derived biochar. *Fuel*, *186*,

525–533.

Balat, M., Balat, M., Kirtay, E., & Balat, H. (2009). Main routes for the thermo-conversion of biomass into fuels and chemicals. Part 1: Pyrolysis systems. *Energy Conversion and Management*, *50*(12), 3147–3157.

Berenblyum, A. S., Danyushevsky, V. Y., Katsman, E. A., Podoplelova, T. A., & Flid, V. R. (2010). Production of engine fuels from inedible vegetable oils and fats. *Petroleum Chemistry*, 50(4), 305-311.

Berenblyum, A. S., Podoplelova, T. A., Shamsiev, R. S., Katsman, E. A., & Danyushevsky, V. Y. (2011). On the mechanism of catalytic conversion of fatty acids into hydrocarbons in the presence of palladium catalysts on alumina. *Petroleum Chemistry*, *51*(5), 336–341.

Bernas, H., Eränen, K., Simakova, I., Leino, A. R., Kordás, K., Myllyoja, J., … Murzin, D. Y. (2010). Deoxygenation of dodecanoic acid under inert atmosphere. *Fuel*, *89*(8), 2033–2039.

Bezergianni, S., Dimitriadis, A., Sfetsas, T., & Kalogianni, A. (2010). Hydrotreating of waste cooking oil for biodiesel production. Part II: Effect of temperature on hydrocarbon composition. *Bioresource Technology*, 101(19), 7658-7660.

Borgschulte, A., Gallandat, N., Probst, B., Suter, R., Callini, E., Ferri, D., Züttel, A. (2013). Sorption enhanced CO2 methanation. *Physical Chemistry Chemical Physics*,15(24), 9620-9625.

Bridgwater, A. V. (2003). Renewable fuels and chemicals by thermal processing of biomass. *Chemical Engineering Journal*, 91(2-3), 87-102.

Bridgwater, A. V. (2012). Review of fast pyrolysis of biomass and product upgrading. *Biomass and Bioenergy*, 38, 68-94.

Canakci, M., & Van Gerpen, J. (2001). Biodiesel Production from Oils and Fats with High Free Fatty Acids. *Transactions of the American Society of Agricultural Engineers*, *44*(6), 1429–1436.

Capodaglio, A. G., Callegari, A., & Dondi, D. (2016). Microwave-Induced Pyrolysis for Production of Sustainable Biodiesel from Waste Sludges. *Waste and Biomass Valorization*, *7*(4), 703–709.

Chang, C. C., & Wan, S. W. (1947). China's Motor Fuels from Tung Oil. *Industrial and Engineering Chemistry*, 39(12), 1543-1548.

Chen, C., Chen, G., Yang, F., Wang, H., Han, J., Ge, Q., & Zhu, X. (2015). Vapor phase

hydrodeoxygenation and hydrogenation of m-cresol on silica supported Ni, Pd and Pt catalysts. *Chemical Engineering Science*, 135, 145-154.

Chen, L., Li, Y., Zhang, X., Zhang, Q., Wang, T., & Ma, L. (2014). Mechanistic insights into the effects of support on the reaction pathway for aqueous-phase hydrogenation of carboxylic acid over the supported Ru catalysts. *Applied Catalysis A: General*, 478, 117-128.

Chen, N., Gong, S., Shirai, H., Watanabe, T., & Qian, E. W. (2013). Effects of Si/Al ratio and Pt loading on Pt/SAPO-11 catalysts in hydroconversion of Jatropha oil. *Applied Catalysis A: General*, 466, 105-115.

Cheng, S. (2017). Development of Heterogeneous Catalysts for Upgrading Biomass Pyrolysis Bio-Oils into Advanced Biofuels, 1223.

Christian, D. G. (2000). Biomass for Renewable Energy, Fuels, and Chemicals. *Journal of Environment Quality*, 29(2), 662.

Crawford, J. M., Zaccarine, S. F., Kovach, N. C., Smoljan, C. S., Lucero, J., Trewyn, B. G., … Carreon, M. A. (2020). Decarboxylation of stearic acid over Ni/MOR catalysts. *Journal of Chemical Technology and Biotechnology*, *95*(1), 102–110.

Crossley, A., Heyes, T. D., & Hudson, B. J. F. (1962). The effect of heat on pure triglycerides. *Journal of the American Oil Chemists Society*, 39, 9-14

Davda, R. R., Shabaker, J. W., Huber, G. W., Cortright, R. D., & Dumesic, J. A. (2005). A review of catalytic issues and process conditions for renewable hydrogen and alkanes by aqueous-phase reforming of oxygenated hydrocarbons over supported metal catalysts. *Applied Catalysis B: Environmental*, 56(1-2), 171-186.

Du, S., Valla, J. A., & Bollas, G. M. (2013). Characteristics and origin of char and coke from fast and slow, catalytic and thermal pyrolysis of biomass and relevant model compounds. *Green Chemistry*, 15(11), 3214-3229.

Dupain, X., Costa, D. J., Schaverien, C. J., Makkee, M., & Moulijn, J. A. (2007). Cracking of a rapeseed vegetable oil under realistic FCC conditions. *Applied Catalysis B: Environmental*, 72(1-2), 44-61.

EIA. (2016). *International Energy Outlook 2016: U.S. Energy Information Administration (EIA), Washington DC. Office of Integrated and International Energy Analysis*. https://doi.org/DOE/EIA-0383 [Assessed 14th January 2020]

EIA. (2020). *Monthly Energy Review - April 2020*. *Monthly Energy Review*.

Elvan Sari. (2013). Green diesel production via catalytic hydrogenation/decarboxylation of triglycerides and fatty acids of vegetable oil and brown grease, 128.

Energy Information Administration. (2016). *International Energy Outlook 2016-World energy demand and economc outlook*. *International Energy Outlook 2016*. https://doi.org/www.eia.gov/forecasts/ieo/pdf/0484(2016).pdf [Assessed 15th February,2020]

Epa, U., & for the Environment, D. (2015). Bisphenol A Alternatives in Thermal Paper Background on Thermal Printing Technology. https://www.epa.gov/sites/production/files/2015-09/documents/bpa_ch3.pdf [Assessed 20th January 2020].

Espinosa-Gonzalez, I., Asomaning, J., Mussone, P., & Bressler, D. C. (2014). Two-step thermal conversion of oleaginous microalgae into renewable hydrocarbons. *Bioresource Technology*, *158*, 91–97.

Fischer, C. R., Peterson, A. A., & Tester, J. W. (2011). Production of C3 Hydrocarbons from Biomass via Hydrothermal Carboxylate Reforming. *Industrial and Engineering Chemistry Research*, 50(8), 4420-4424.

Fu, J., Lu, X., & Savage, P. E. (2010). Catalytic hydrothermal deoxygenation of palmitic acid. In *Energy and Environmental Science*, 3(3), 311-317.

Furimsky, E. (2000). Catalytic hydrodeoxygenation. *Applied Catalysis A: General*, 199(2), 147-190.

Gómez, J. M., Romero, M. D., & Callejo, V. (2013). Heterogeneous basic catalysis for upgrading of biofuels. *Catalysis Today*, 218, 143-147

Goyal, H. B., Seal, D., & Saxena, R. C. (2008). Bio-fuels from thermochemical conversion of renewable resources: A review. *Renewable and Sustainable Energy Reviews*,12(2), 504-517.

Greenhalf, C. E., Nowakowski, D. J., Harms, A. B., Titiloye, J. O., & Bridgwater, A. V. (2013). A comparative study of straw, perennial grasses and hardwoods in terms of fast pyrolysis products. *Fuel*, 108, 216-230.

Guo, D., Shi, Q., He, B., & Yuan, X. (2011). Different solvents for the regeneration of the exhausted activated carbon used in the treatment of coking wastewater. *Journal of Hazardous Materials*, *186*(2–3), 1788–1793.

Haque, K. E. (1999). Microwave energy for mineral treatment processes - A brief review. *International Journal of Mineral Processing*, 57(1), 1-24.

Haug, A., Hiesgen, R., Schulze, M., Schiller, G., & Friedrich, K. A. (2011). Fourier transform infrared spectroscopy. In *PEM Fuel Cell Diagnostic Tools*.

He, Z., & Wang, X. (2013). Hydrodeoxygenation of model compounds and catalytic systems for pyrolysis bio-oils upgrading. *Catalysis for Sustainable Energy*, 1, 28-52.

Hengst, K., Arend, M., Pfützenreuter, R., & Hoelderich, W. F. (2015). Deoxygenation and cracking of free fatty acids over acidic catalysts by single step conversion for the production of diesel fuel and fuel blends. *Applied Catalysis B: Environmental*, *174–175*, 383–394.

Hermida, L., Abdullah, A. Z., & Mohamed, A. R. (2015). Deoxygenation of fatty acid to produce diesel-like hydrocarbons: A review of process conditions, reaction kinetics and mechanism. *Renewable and Sustainable Energy Reviews*, *42*, 1223–1233.

Hossan, M. R., & Dutta, P. (2012). Effects of temperature dependent properties in electromagnetic heating. International Journal of heat and mass transfer, 55(13-14), 3412-3422.

Huang, W. C., Huang, M. S., Huang, C. F., Chen, C. C., & Ou, K. L. (2010). Thermochemical conversion of polymer wastes into hydrocarbon fuels over various fluidizing cracking catalysts. *Fuel*, 89(9), 2305-2316.

Idem, R. O., Katikaneni, S. P. R., & Bakhshi, N. N. (1996). Thermal cracking of canola oil: Reaction products in the presence and absence of steam. *Energy and Fuels*, 10(6), 1150-1162.

Idem, R. O., Katikaneni, S. P. R., & Bakhshi, N. N. (1997). Catalytic conversion of canola oil to fuels and chemicals: Roles of catalyst acidity, basicity and shape selectivity on product distribution. *Fuel Processing Technology*, 51(1-2), 101-125.

IEA. (2011). Chapter 1 股関節 概念 Chapter 1 股関節. *An Automated Irrigation System Using Arduino Microcontroller*, *1908*(January), 2–6.

Iliopoulou, E. F., Triantafyllidis, K. S., & Lappas, A. A. (2019). Overview of catalytic upgrading of biomass pyrolysis vapors toward the production of fuels and high-value chemicals. *Wiley Interdisciplinary Reviews: Energy and Environment*, *8*(1), 1–29.

Immer, J. G., Kelly, M. J., & Lamb, H. H. (2010). Catalytic reaction pathways in liquid-phase deoxygenation of C18 free fatty acids. *Applied Catalysis A: General*, *375*(1), 134–139.

Immer, J. G., & Lamb, H. H. (2010). Fed-batch catalytic deoxygenation of free fatty acids. *Energy and Fuels*, 24(10), 5291-5299.

Imran, A., Bramer, E. A., Seshan, K., & Brem, G. (2018). An overview of catalysts in biomass pyrolysis for production of biofuels. *Biofuel Research Journal*, *5*(4), 872–885.

International Energy Agency. (2020). World Energy Outlook 2020 - Event - IEA. *World Energy Outlook 2020 - Event - IEA*.

Jae, J., Tompsett, G. A., Foster, A. J., Hammond, K. D., Auerbach, S. M., Lobo, R. F., & Huber, G. W. (2011). Investigation into the shape selectivity of zeolite catalysts for biomass conversion. *Journal of Catalysis*, 279(2), 257-268.

Jenab, E., Mussone, P., Nam, G., & Bressler, D. (2014). Production of renewable hydrocarbons from thermal conversion of abietic acid and tall oil fatty acids. *Energy and Fuels*, *28*(11), 6988–6994.

Jin, S., Xiao, Z., Li, C., Chen, X., Wang, L., Xing, J., Liang, C. (2014). Catalytic hydrodeoxygenation of anisole as lignin model compound over supported nickel catalysts. *Catalysis Today*, 234, 125-132.

Kabir, G., & Hameed, B. H. (2017). Recent progress on catalytic pyrolysis of lignocellulosic biomass to high-grade bio-oil and bio-chemicals. *Renewable and Sustainable Energy Reviews*, 70, 945-967.

Kappe, C. O., Stadler, A., & Dallinger, D. (2012). *Microwaves in Organic and Medicinal Chemistry*. *Microwaves in Organic and Medicinal Chemistry*.

Karim, A., Mei, D., Lebarbier, V., Liu, C., & Wang, Y. (2011). Pyrolysis vapors upgrading using metal oxides. In *11AIChE - 2011 AIChE Annual Meeting, Conference Proceedings*.

Kay Lup, A. N., Abnisa, F., Wan Daud, W. M. A., & Aroua, M. K. (2017). A review on reactivity and stability of heterogeneous metal catalysts for deoxygenation of bio-oil model compounds. *Journal of Industrial and Engineering Chemistry*, *56*, 1–34.

Khaghanikavkani, E. (2013). Microwave Pyrolysis of Plastic. *Journal of Chemical Engineering & Process Technology*,11.

Kharkovsky, S. N., & Hasar, U. C. (2003). Measurement of Mode Patterns in a High-Power Microwave Cavity. *IEEE Transactions on Instrumentation and Measurement*, 52(6), 1815-1819.

Krobkrong, N., Itthibenchapong, V., Khongpracha, P., & Faungnawakij, K. (2018). Deoxygenation of oleic acid under an inert atmosphere using molybdenum oxide-based catalysts. *Energy Conversion and Management*, *167*(March), 1–8.

Kubátová, A., Luo, Y., Šťávová, J., Sadrameli, S. M., Aulich, T., Kozliak, E., & Seames, W. (2011). New path in the thermal cracking of triacylglycerols (canola and soybean oil). *Fuel*,

90(8), 2598-2608.

Kubátová, A., Ŝávová, J., Seames, W. S., Luo, Y., Sadrameli, S. M., Linnen, M. J., … Kozliak, E. I. (2012). Triacylglyceride thermal cracking: Pathways to cyclic hydrocarbons. In *Energy and Fuels*, 26 (1), 672-685.

Kubička, D., & Kaluža, L. (2010). Deoxygenation of vegetable oils over sulfided Ni, Mo and NiMo catalysts. *Applied Catalysis A: General*, *372*(2), 199–208.

Kubičková, I., Snåre, M., Eränen, K., Mäki-Arvela, P., & Murzin, D. Y. (2005). Hydrocarbons for diesel fuel via decarboxylation of vegetable oils. In *Catalysis Today*, 106(1-4), 197-200.

Kumar, Shinde, & Gaikwad. (2014). Reactive Extraction Of Naphthenic Acid By Using. *International Journal of Advanced Engineering Technology*.

Lam, S. S., & Chase, H. A. (2012). A review on waste to energy processes using microwave pyrolysis. *Energies*, *5*(10), 4209–4232.

Lam, S. S., Wan Mahari, W. A., Cheng, C. K., Omar, R., Chong, C. T., & Chase, H. A. (2016). Recovery of diesel-like fuel from waste palm oil by pyrolysis using a microwave heated bed of activated carbon. *Energy*, 115, 791-799.

Lam, S. S., Wan Mahari, W. A., Jusoh, A., Chong, C. T., Lee, C. L., & Chase, H. A. (2017). Pyrolysis using microwave absorbents as reaction bed: An improved approach to transform used frying oil into biofuel product with desirable properties. *Journal of Cleaner Production,* 147, 263-272.

Lappas, A. A., Kalogiannis, K. G., Iliopoulou, E. F., Triantafyllidis, K. S., & Stefanidis, S. D. (2012). Catalytic pyrolysis of biomass for transportation fuels. *Wiley Interdisciplinary Reviews: Energy and Environment*, 1(3), 285-297.

Lestari, S., Mäki-Arvela, P., Beltramini, J., Lu, G. Q. M., & Murzin, D. Y. (2009). Transforming triglycerides and fatty acids into biofuels. *ChemSusChem*, 2(12), 1109-1119.

Lin, Q., Chen, G., & Liu, Y. (2012). Scale-up of microwave heating process for the production of bio-oil from sewage sludge. *Journal of Analytical and Applied Pyrolysis*, 94, 114-119.

Liu, C., Wang, H., Karim, A. M., Sun, J., & Wang, Y. (2014). Catalytic fast pyrolysis of lignocellulosic biomass. *Chemical Society Reviews*, 43(22), 7594-7623.

Lopez-Urionabarrenechea, A., De Marco, I., Caballero, B. M., Laresgoiti, M. F., & Adrados, A. (2012). Catalytic stepwise pyrolysis of packaging plastic waste. *Journal of Analytical and Applied Pyrolysis*, 96, 54-62.

Lovás, P., Hudec, P., Hadvinová, M., & Ház, A. (2015). Conversion of rapeseed oil via catalytic cracking: Effect of the ZSM-5 catalyst on the deoxygenation process. *Fuel Processing Technology*, 134, 223-230.

Lugo-José, Y. K., Monnier, J. R., Heyden, A., & Williams, C. T. (2014). Hydrodeoxygenation of propanoic acid over silica-supported palladium: Effect of metal particle size. *Catalysis Science and Technology*, 4(11), 3909-3916.

Macquarrie, D. J., Clark, J. H., & Fitzpatrick, E. (2012). The microwave pyrolysis of biomass. *Biofuels, Bioproducts and Biorefining*, 6(5), 549-560.

Madsen, A. T., Ahmed, E. H., Christensen, C. H., Fehrmann, R., & Riisager, A. (2011). Hydrodeoxygenation of waste fat for diesel production: Study on model feed with Pt/alumina catalyst. *Fuel*, 90(11), 3433-3438.

Maher, K. D., & Bressler, D. C. (2007). Pyrolysis of triglyceride materials for the production of renewable fuels and chemicals. *Bioresource Technology*, *98*(12), 2351–2368.

Maher, Kelly D., Kirkwood, K. M., Gray, M. R., & Bressler, D. C. (2008). Pyrolytic decarboxylation and cracking of stearic acid. *Industrial and Engineering Chemistry Research*, *47*(15), 5328–5336.

Maier, W. F., Roth, W., Thies, I., & Schleyer, P. V. R. (1982). Hydrogenolysis, IV. Gas phase decarboxylation of carboxylic acids. *Chemische Berichte*.

Mäki-Arvela, P., Kubickova, I., Snåre, M., Eränen, K., & Murzin, D. Y. (2007). Catalytic deoxygenation of fatty acids and their derivatives. *Energy and Fuels*, 21(1), 30-41.

Mashuri, S. I. S., Ibrahim, M. L., Kasim, M. F., Mastuli, M. S., Rashid, U., Abdullah, A. H., … Hin, T. Y. Y. (2020). Photocatalysis for organic wastewater treatment: From the basis to current challenges for society. *Catalysts*, *10*(11), 1–29.

Matsumoto, H., Saito, Y., & Yoneda, Y. (1970). Contrast between nickel and platinum catalysts in hydrogenolysis of saturated hydrocarbons. *Journal of Catalysis*, 19(2), 101.

Melero, J. A., Clavero, M. M., Calleja, G., García, A., Miravalles, R., & Galindo, T. (2010). Production of biofuels via the catalytic cracking of mixtures of crude vegetable oils and nonedible animal fats with vacuum gas oil. In *Energy and Fuels*, 24(1), 707-717.

Mingos, D. M. P., & Baghurst, D. R. (1991). Applications of microwave dielectric heating effects to synthetic problems in chemistry. *Chemical Society Reviews,* 20(1), 1-47.

Mohamed, B. A., Kim, C. S., Ellis, N., & Bi, X. (2016). Microwave-assisted catalytic pyrolysis of

switchgrass for improving bio-oil and biochar properties. *Bioresource Technology,* 201, 121-132.

Mohan, D., Pittman, C. U., & Steele, P. H. (2006). Pyrolysis of wood/biomass for bio-oil: A critical review. *Energy and Fuels*, 20(3), 848-889.

Mortensen, P. M., Grunwaldt, J. D., Jensen, P. A., & Jensen, A. D. (2016). Influence on nickel particle size on the hydrodeoxygenation of phenol over Ni/SiO2. *Catalysis Today*, 259, 277-284.

Motasemi, F., & Afzal, M. T. (2013). A review on the microwave-assisted pyrolysis technique. *Renewable and Sustainable Energy Reviews*, 28, 317-330.

Motasemi, F., & Ani, F. N. (2012). A review on microwave-assisted production of biodiesel. *Renewable and Sustainable Energy Reviews*, *16*(7), 4719–4733.

Mullen, C. A., & Boateng, A. A. (2011). Production and Analysis of Fast Pyrolysis Oils from Proteinaceous Biomass. *Bioenergy Research*, 4(4), 303-311.

Murnieks, R., Apseniece, L., Kampars, V., Shustere, Z., & Malins, K. (2016a). Investigation of Deoxygenation of Rapeseed Oil over Raney Nickel and Ni/SiO2−Al2O3 Catalysts. *Arabian Journal for Science and Engineering*, *41*(6), 2193–2198.

Mutyala, S., Fairbridge, C., Paré, J. R. J., Bélanger, J. M. R., Ng, S., & Hawkins, R. (2010). Microwave applications to oil sands and petroleum: A review. *Fuel Processing Technology*, 91(2), 127-135.

Na, J. G., Yi, B. E., Kim, J. N., Yi, K. B., Park, S. Y., Park, J. H.,Ko, C. H. (2010). Hydrocarbon production from decarboxylation of fatty acid without hydrogen. *Catalysis Today*, *156*(1–2), 44–48.

Naik, D. V., Singh, K. K., Kumar, V., Prasad, B., Behera, B., Bangwal, D. P., … Garg, M. O. (2014). Catalytic cracking of glycerol to fine chemicals over equilibrium fluid catalytic cracking catalyst. *Energy Procedia*, *54*, 593–598.

Nawar, W. W. (1969). Thermal degradation of lipids. A review. *Journal of Agricultural and Food Chemistry*, 17(1), 18.

Ng, H. S., Kee, P. E., Yim, H. S., Chen, P. T., Wei, Y. H., & Chi-Wei Lan, J. (2020). Recent advances on the sustainable approaches for conversion and reutilization of food wastes to valuable bioproducts. *Bioresource Technology*, *302*(135), 122889.

Nozawa, T., Mizukoshi, Y., Yoshida, A., & Naito, S. (2014). Aqueous phase reforming of ethanol

and acetic acid over TiO2 supported Ru catalysts. *Applied Catalysis B: Environmental*, 146, 221-226.

Nüchter, M., Ondruschka, B., Bonrath, W., & Gum, A. (2004). Microwave assisted synthesis – a critical technology overview. *Green Chemistry*, 6(3), 128-141.

Oi, L. E., Choo, M. Y., Lee, H. V., Taufiq-Yap, Y. H., Cheng, C. K., & Juan, J. C. (2020). Catalytic deoxygenation of triolein to green fuel over mesoporous TiO2 aided by in situ hydrogen production. *International Journal of Hydrogen Energy*, *45*(20), 11605–11614.

Omidghane, M., Jenab, E., Chae, M., & Bressler, D. C. (2017a). Production of Renewable Hydrocarbons by Thermal Cracking of Oleic Acid in the Presence of Water. *Energy and Fuels*, *31*(9), 9446–9454.

Ong, H. C., Mahlia, T. M. I., Masjuki, H. H., & Norhasyima, R. S. (2011). Comparison of palm oil, Jatropha curcas and Calophyllum inophyllum for biodiesel: A review. *Renewable and Sustainable Energy Reviews*, 15(8), 3501-3515.

Pan, Z., Wang, R., Li, M., Chu, Y., & Chen, J. (2015). Deoxygenation of methyl laurate to hydrocarbons on silica-supported Ni-Mo phosphides: Effect of calcination temperatures of precursor. *Journal of Energy Chemistry*, 24(1), 77-86.

Pande, M., & Bhaskarwar, A. N. (2012). Biomass conversion to energy. In *Biomass Conversion: The Interface of Biotechnology, Chemistry and Materials Science*.

Pestman, R., Koster, R. M., Van Duijne, A., Pieterse, J. A. Z., & Ponec, V. (1997). Reactions of carboxylic acids on oxides: 2. Bimolecular reaction of aliphatic acids to ketones. *Journal of Catalysis*,168(2) 265-272.

Pianroj, Y., Jumrat, S., Werapun, W., Karrila, S., & Tongurai, C. (2016). Scaled-up reactor for microwave induced pyrolysis of oil palm shell. *Chemical Engineering and Processing: Process Intensification*, *106*, 42–49.

Pillay, B., Mathebula, M. R., & Friedrich, H. B. (2009). The oxidative dehydrogenation of n-hexane over Ni-Mo-O catalysts. *Applied Catalysis A: General*, 361(1-2), 57-64.

Popov, S., & Kumar, S. (2015). Rapid hydrothermal deoxygenation of oleic acid over activated carbon in a continuous flow process. *Energy and Fuels*, 29(5), 3377-3384.

Poutsma, M. L. (2000). Fundamental reactions of free radicals relevant to pyrolysis reactions. *Journal of Analytical and Applied Pyrolysis*, 54 (1-2), 5-35.

Qian, E. W., Chen, N., & Gong, S. (2014). Role of support in deoxygenation and isomerization of

methyl stearate over nickel-molybdenum catalysts. *Journal of Molecular Catalysis A: Chemical*, 387, 76-85.

Ravikumar, C., Senthil Kumar, P., Subhashni, S. K., Tejaswini, P. V., & Varshini, V. (2017). Microwave assisted fast pyrolysis of corn cob, corn stover, saw dust and rice straw: Experimental investigation on bio-oil yield and high heating values. *Sustainable Materials and Technologies*, *11*, 19–27.

Rehan, M., Miandad, R., Barakat, M. A., Ismail, I. M. I., Almeelbi, T., Gardy, J.,Nizami, A. S. (2017). Effect of zeolite catalysts on pyrolysis liquid oil. *International Biodeterioration and Biodegradation*,119, 162-175

Ren, J., Qin, X., Yang, J. Z., Qin, Z. F., Guo, H. L., Lin, J. Y., & Li, Z. (2015). Methanation of carbon dioxide over Ni-M/ZrO2 (M = Fe, Co, Cu) catalysts: Effect of addition of a second metal. *Fuel Processing Technology*, *137*, 204–211.

Richardson, J. (2011). Table of Characteristic IR Absorptions. *University of Colorado, Boulder, Chemistry and Biochemistry Department*, *3610*(m), 1. Retrieved from http://orgchem.colorado.edu/Spectroscopy/specttutor/irchart.html

S, R., & P, B. (2019). The potential of lignocellulosic biomass precursors for biochar production: Performance, mechanism and wastewater application—A review. *Industrial Crops and Products*, *128*(November 2018), 405–423.

Santillan-Jimenez, E., & Crocker, M. (2012). Catalytic deoxygenation of fatty acids and their derivatives to hydrocarbon fuels via decarboxylation/decarbonylation. *Journal of Chemical Technology and Biotechnology*, *87*(8), 1041–1050.

Santillan-Jimenez, E., Morgan, T., Lacny, J., Mohapatra, S., & Crocker, M. (2013). Catalytic deoxygenation of triglycerides and fatty acids to hydrocarbons over carbon-supported nickel. *Fuel*, *103*, 1010–1017.

Santillan-Jimenez, E., Morgan, T., Shoup, J., Harman-Ware, A. E., & Crocker, M. (2014). Catalytic deoxygenation of triglycerides and fatty acids to hydrocarbons over Ni-Al layered double hydroxide. *Catalysis Today*, *237*, 136–144.

Serrano-Ruiz, J. C., & Dumesic, J. A. (2011). Catalytic routes for the conversion of biomass into liquid hydrocarbon transportation fuels. *Energy and Environmental Science*, 4(1), 83-99.

Sharma, A., Pareek, V., & Zhang, D. (2015). Biomass pyrolysis - A review of modelling, process parameters and catalytic studies. *Renewable and Sustainable Energy Reviews*, *50*, 1081–

1096.

Shi, Y., Xing, E., Wu, K., Wang, J., Yang, M., & Wu, Y. (2017). Recent progress on upgrading of bio-oil to hydrocarbons over metal/zeolite bifunctional catalysts. *Catalysis Science and Technology*, 7(12), 2385-2415.

Shimada, I., Kato, S., Hirazawa, N., Nakamura, Y., Ohta, H., Suzuki, K., & Takatsuka, T. (2017). Deoxygenation of triglycerides by catalytic cracking with enhanced hydrogen transfer. Industrial & Engineering Chemistry Research, 56(1), 75-86.

Siddiqui, M. N., & Redhwi, H. H. (2009). Pyrolysis of mixed plastics for the recovery of useful products. *Fuel Processing Technology*, 90(4), 545-552.

Simakova, I., Simakova, O., Mäki-Arvela, P., & Murzin, D. Y. (2010). Decarboxylation of fatty acids over Pd supported on mesoporous carbon. *Catalysis Today*, *150*(1–2), 28–31.

Simakova, I., Simakova, O., Mäki-Arvela, P., Simakov, A., Estrada, M., & Murzin, D. Y. (2009). Deoxygenation of palmitic and stearic acid over supported Pd catalysts: Effect of metal dispersion. *Applied Catalysis A: General*, *355*(1–2), 100–108.

Snåre, M., Kubičková, I., Mäki-Arvela, P., Chichova, D., Eränen, K., & Murzin, D. Y. (2008). Catalytic deoxygenation of unsaturated renewable feedstocks for production of diesel fuel hydrocarbons. *Fuel*, 87(6), 933-945.

Snåre, M., Kubičková, I., Mäki-Arvela, P., Eränen, K., Wärnå, J., & Murzin, D. Y. (2007). Production of diesel fuel from renewable feeds: Kinetics of ethyl stearate decarboxylation. *Chemical Engineering Journal*, *134*(1–3), 29–34.

Snåre, Mathias, Kubičková, I., Mäki-Arvela, P., Eränen, K., & Murzin, D. Y. (2006). Heterogeneous catalytic deoxygenation of stearic acid for production of biodiesel. *Industrial and Engineering Chemistry Research*, 45(16), 5708-5715.

Socrates, G. (2001). *Infrared and Raman characteristic group frequencies. Tables and charts*. *Journal of Raman Spectroscopy*.

Sorrell, S., Speirs, J., Bentley, R., Brandt, A., & Miller, R. (2010). Global oil depletion: A review of the evidence. *Energy Policy*, 38(9), 5290-5295.

Spring, J. A. (2014). Thermal cracking of lipids to produce renewable fuels and platform chemicals Bioresource and Food Engineering Department of Agricultural , Food and Nutritional Science.

Srifa, A., Faungnawakij, K., Itthibenchapong, V., Viriya-empikul, N., Charinpanitkul, T., &

Assabumrungrat, S. (2014). Production of bio-hydrogenated diesel by catalytic hydrotreating of palm oil over NiMoS2/γ-Al2O3 catalyst. *Bioresource Technology*, 158, 81-90.

Srifa, A., Viriya-Empikul, N., Assabumrungrat, S., & Faungnawakij, K. (2015). Catalytic behaviors of Ni/γ-Al2O3 and Co/γ-Al2O3 during the hydrodeoxygenation of palm oil. *Catalysis Science and Technology*, 5, 3693-3705.

Stefanidis, S. D., Kalogiannis, K. G., Iliopoulou, E. F., Lappas, A. A., & Pilavachi, P. A. (2011). In-situ upgrading of biomass pyrolysis vapors: Catalyst screening on a fixed bed reactor. *Bioresource Technology*, 102(17), 8261-8267.

Stefanidis, S. D., Karakoulia, S. A., Kalogiannis, K. G., Iliopoulou, E. F., Delimitis, A., Yiannoulakis, H., … Triantafyllidis, K. S. (2016). usde. *Applied Catalysis B: Environmental*, *196*, 155–173.

Suarez, P. A. Z., Santos, A. L. F., Rodrigues, J. P., & Alves, M. B. (2009). Oils and Fats Based Biofuels: Technological Chalendges. *Quimica Nova*, 32, 768.

Syamsiro, M., Saptoadi, H., Norsujianto, T., Noviasri, P., Cheng, S., Alimuddin, Z., & Yoshikawa, K. (2014). Fuel oil production from municipal plastic wastes in sequential pyrolysis and catalytic reforming reactors. In *Energy Procedia*, 47, 180-188.

Tajuddin, N. A., Lee, A. F., & Wilson, K. (2016). Production of biodiesel via catalytic upgrading and refining of sustainable oleagineous feedstocks. In *Handbook of Biofuels Production: Processes and Technologies: Second Edition* 121-164.

Taufiqurrahmi, N., & Bhatia, S. (2011). Catalytic cracking of edible and non-edible oils for the production of biofuels. *Energy and Environmental Science*, 4(4), 1087-1112

Thostenson, E. T., & Chou, T. W. (1999). Microwave processing: fundamentals and applications. *Composites Part A: Applied Science and Manufacturing*, 30(9), 1055-1071.

Tran, N. T. T., Uemura, Y., Chowdhury, S., & Ramli, A. (2016). Vapor-phase hydrodeoxygenation of guaiacol on Al-MCM-41 supported Ni and Co catalysts. *Applied Catalysis A: General*, 512, 93-100.

U.S. Energy Information Administration. (2020). Oil and petroleum products explained: Use of Oil.

Van Gerpen, J. (2005). Biodiesel processing and production. *Fuel Processing Technology*, 86(10), 1097-1107.

Velghe, I., Carleer, R., Yperman, J., & Schreurs, S. (2011). Study of the pyrolysis of municipal

solid waste for the production of valuable products. *Journal of Analytical and Applied Pyrolysis,* 92(2), 366-375.

Veriansyah, B., Han, J. Y., Kim, S. K., Hong, S. A., Kim, Y. J., Lim, J. S., … Kim, J. (2012). Production of renewable diesel by hydroprocessing of soybean oil: Effect of catalysts. *Fuel*, *94*, 578–585.

Wan, Y., Chen, P., Zhang, B., Yang, C., Liu, Y., Lin, X., & Ruan, R. (2009). Microwave-assisted pyrolysis of biomass: Catalysts to improve product selectivity. *Journal of Analytical and Applied Pyrolysis*, *86*(1), 161–167.

Wang, J., Chae, M., Bressler, D. C., & Sauvageau, D. (2020). Improved bioethanol productivity through gas flow rate-driven self-cycling fermentation. *Biotechnology for Biofuels*, 13(1), 14.

Wang, L., Weng, Y., Duan, P., Liu, X., Wang, X., Zhang, Y., Ma, L. (2019). Influence of acid pretreatment on the hydrodeoxygenation performance of carbon supported RuMo bimetallic catalysts on sorbitol conversion. *SN Applied Sciences*, 1(5), 404.

Wang, W. C., Thapaliya, N., Campos, A., Stikeleather, L. F., & Roberts, W. L. (2012). Hydrocarbon fuels from vegetable oils via hydrolysis and thermo-catalytic decarboxylation. *Fuel*, 95(1), 622-629

Wang, Y., Dai, L., Shan, S., Zeng, Q., Fan, L., Liu, Y., … Zhou, Y. (2016). Effect of unsaturation degree on microwave-assisted pyrolysis of fatty acid salts. *Journal of Analytical and Applied Pyrolysis*, *120*, 247–251.

Wang, Y., Dai, L., Wang, R., Fan, L., Liu, Y., Xie, Q., & Ruan, R. (2016). Hydrocarbon fuel production from soapstone through fast microwave-assisted pyrolysis using microwave absorbent. *Journal of Analytical and Applied Pyrolysis*, *119*, 251–258.

Wang, Y., Liu, Y., Ruan, R., Wen, P., Wan, Y., & Zhang, J. (2013). Microwave-Assisted decarboxylation of sodium oleate and renewable hydrocarbon fuel production. *China Petroleum Processing and Petrochemical Technology*, *15*(3), 19–27.

World Coal Association. (2016). Uses of Coal.

Wu, C., De Visscher, A., & Gates, I. D. (2019). On naphthenic acids removal from crude oil and oil sands process-affected water. *Fuel*, *253*(March), 1229–1246.

Wu, J., Shi, J., Fu, J., Leidl, J. A., Hou, Z., & Lu, X. (2016). Catalytic decarboxylation of fatty acids to aviation fuels over nickel supported on activated carbon. *Scientific Reports* 6, 27820.

Xu, C. C., Liao, B., Pang, S., Nazari, L., Mahmood, N., Tushar, M. S. H. K., Ray, M. B. (2018b).

Biomass Energy. *Comprehensive Energy Systems* (Vol. 1–5). Elsevier Ltd.

Yakub, M. I., Abdalla, A. Y., Feroz, K. K., Suzana, Y., Ibraheem, A., & Chin, S. A. (2015). Pyrolysis of Oil Palm Residues in a Fixed Bed Tubular Reactor. *Journal of Power and Energy Engineering*, *03*(04), 185–193.

Yang, L., & Carreon, M. A. (2017a). Deoxygenation of Palmitic and Lauric Acids over Pt/ZIF-67 Membrane/Zeolite 5A Bead Catalysts. *ACS Applied Materials and Interfaces*, 9(37),31993-32000.

Yang, L., & Carreon, M. A. (2017b). *Effect of reaction parameters on the decarboxylation of oleic acid over Pt/ZIF-67membrane/zeolite 5A bead catalysts*. *Journal of Chemical Technology and Biotechnology*, 92, 52-58

Yang, L., Tate, K. L., Jasinski, J. B., & Carreon, M. A. (2015). Decarboxylation of Oleic Acid to Heptadecane over Pt Supported on Zeolite 5A Beads. *ACS Catalysis*, *5*(11), 6497–6502.

Zanuttini, M. S., Lago, C. D., Querini, C. A., & Peralta, M. A. (2013). Deoxygenation of m-cresol on Pt/γ-Al2O3 catalysts. In *Catalysis Today*, 213, 9-17

Zhang, A., Tang, J., Lai, P., He, Y., Li, J., & Xiao, Z. (2020). Bio-hydrocarbon Fuel Preparation from Pyrolysate of Swida wilsoniana Fruit Oil by Catalytic Hydrogenation. *Chemistry and Industry of Forest Products*, *40*(5), 43–49.

Zhang, H., Lin, H., Wang, W., Zheng, Y., & Hu, P. (2014). Hydroprocessing of waste cooking oil over a dispersed nano catalyst: Kinetics study and temperature effect. *Applied Catalysis B: Environmental*, 150-151, 238-248.

Zhang, Q., Chang, J., Wang, T., & Xu, Y. (2007). Review of biomass pyrolysis oil properties and upgrading research. *Energy Conversion and Management*, 48(1), 87-92